Master Thesis, Department of Geosciences

Two marine seismic interference attenuation methods

Based on automatic detection of seismic interference moveout

Sindre Jansen

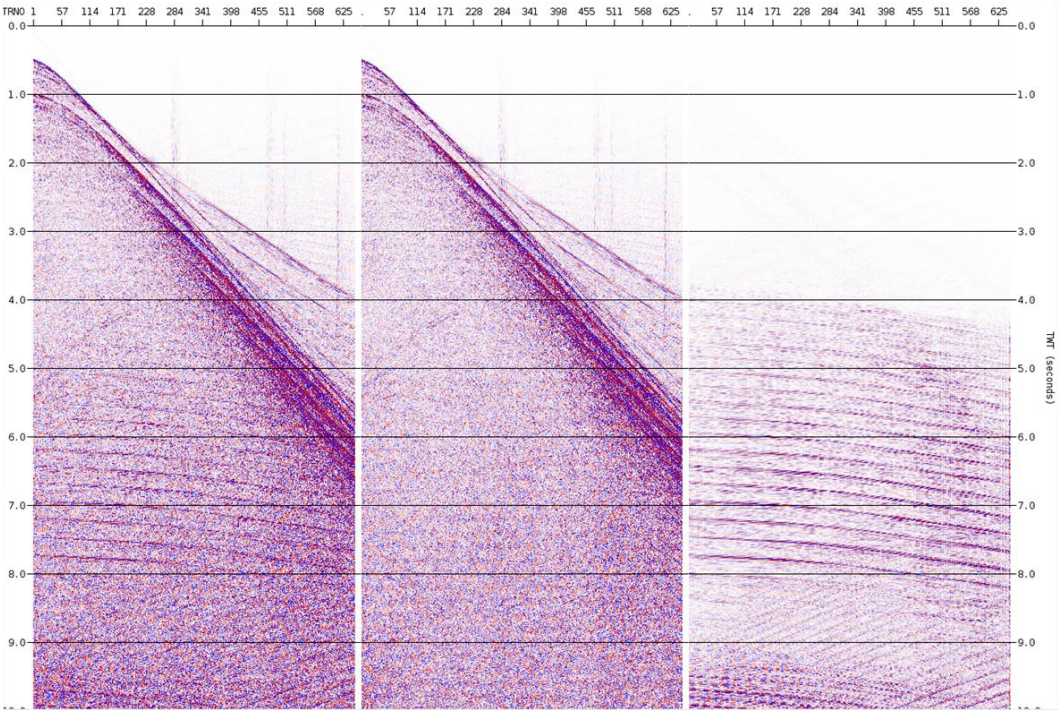

UNIVERSITY OF OSLO

FACULTY OF MATHEMATICS AND NATURAL SCIENCES

Two marine seismic interference attenuation methods

Based on automatic detection of seismic interference moveout

Sindre Jansen

Master Thesis in Geosciences

Discipline: Geophysics

Department of Geosciences

Faculty of Mathematics and Natural Sciences

University of Oslo

June, 2013

ACKNOWLEDGMENTS

This thesis work has been done in collaboration between the University of Oslo and former Fugro Geoteam AS, now CGG Veritas. Most of the work has evolved during my time at CGG Veritas' office at Skøyen. I am grateful that I have had the chance to take part in this great working environment. Specially, I would like to thank my external supervisors Dr. Thomas Elboth and Dr. Charlotte Sanchis in CGG Veritas. Daily discussions and brainstormings with Dr. Thomas Eboth have inspired many ideas during the development of this thesis. Furthermore, was the contribution by Dr. Charlotte Sanchis vital for getting our paper accepted with presentation at the EAGE conference in London'13, and furthermore getting a patent application submitted.

Second, I would like to thank my internal supervisor Prof. Valerie Maupin at the Department of Geosciences, University of Oslo. Prof. Valerie Maupin's constructive comments and ideas helped significantly during my thesis work.

Finally, I would like to thank friends, family and colleagues for their support and good company during my one year long thesis work.

Sindre Jansen
May 31, 2013

ABSTRACT

Marine Seismic Interference (SI) occurs when several seismic vessels operate in close proximity, and the interfering energy from one vessel is recorded as interfering noise by another. Generally, SI is removed by various SI removal methods. However, it is often difficult to remove SI if the arrival time, moveout and/or amplitude of the SI exceed certain limits. In this case, the vessels commence time sharing. Time sharing is expensive, and therefore something the industry wants to avoid. A strong motivation exists for developing robust and efficient SI removal methods.

The reference method for this thesis consists of sorting/transforming series of consecutive SI contaminated shot gathers to common-p domain where the SI appears random. The SI can then be removed by applying a random noise attenuation method. However, this method breaks down if the arrival time of the SI is synchronized in the consecutive shot gathers.

The aim of this thesis has been to develop a method referred to as Vector Field (VF) method. VF method works on singular shot gathers, and calculates a vector field estimate which represents the local moveout in the considered shot gather. Analysis of the vector field in three different domains allow automatic SI moveout detection. The SI moveout detection comprises two possible techniques for SI removal. First technique automatically generates τ-p mutes designed to isolate the SI in τ-p domain. This technique is the main focus of the thesis. The second technique uses the line integral convolution method and an estimate of vector fields to subtract the SI from the shot domain.

Analysis of RMS plots, shot gathers, and stacks show that the VF method in combination with τ-p muting is an efficient SI removal method. Compared to the reference τ-p to common-p method, VF method in combination with τ-p muting is able to detect and remove SI regardless of a synchronized arrival time of SI in consecutive shot gathers.

Contents

1. INTRODUCTION

This master thesis in Geophysics is about removal of marine Seismic Interference (SI). It has been done in collaboration between the University of Oslo and former Fugro Geoteam AS, now CGG Veritas. The goal has been to develop new methods for SI removal in shot domain. Most of the development and testing have been carried out in MATLAB, however the final results and comparison have been done in former Fugro's, now CGG Veritas' processing software Uniseis.

Much of the contents of this thesis have also been presented in a paper accepted by EAGE (European Association of Geoscientists & Engineers) with presentation on June 12^{th} at the 75^{th} EAGE Conference & Exhibition in London'13. The title of the abstract is "*Two seismic interference attenuation methods based on automatic detection of seismic interference moveout*".

1.1 Motivation and aim of thesis

A frequently encountered problem in seismic data is the presence of various types of coherent noise and in particular, Seismic Interference (SI). SI occurs when several seismic vessels operate in close proximity, and the seismic energy from one firing vessel is recorded as interfering noise by another.

SI reduces the quality of the seismic data. Specially, if the amplitude and/or moveout of the SI exceed certain limits, making it difficult to remove by traditional signal processing. In this case the seismic vessels often commence time sharing. This provides SI-free seismic data. However, time sharing is costly due to vessel standby, and may lead to significant delays in survey completion. Figure 1.1 is borrowed from a case study presented by Petroleum Geo-Services (PGS) at a workshop hosted by FORCE in 2012. The topic was *"How to reduce time-sharing"*. It illustrates the seismic activity in the North and Norwegian Sea during May, June and July of 2011 and 2012. The dots indicate operating seismic vessels, and the red circles indicate a radius of 40 km. Their case study showed that severe SI could be expected at distances less then 40 km.

As will be mentioned in the following chapter, the appearance of SI in shot domain varies

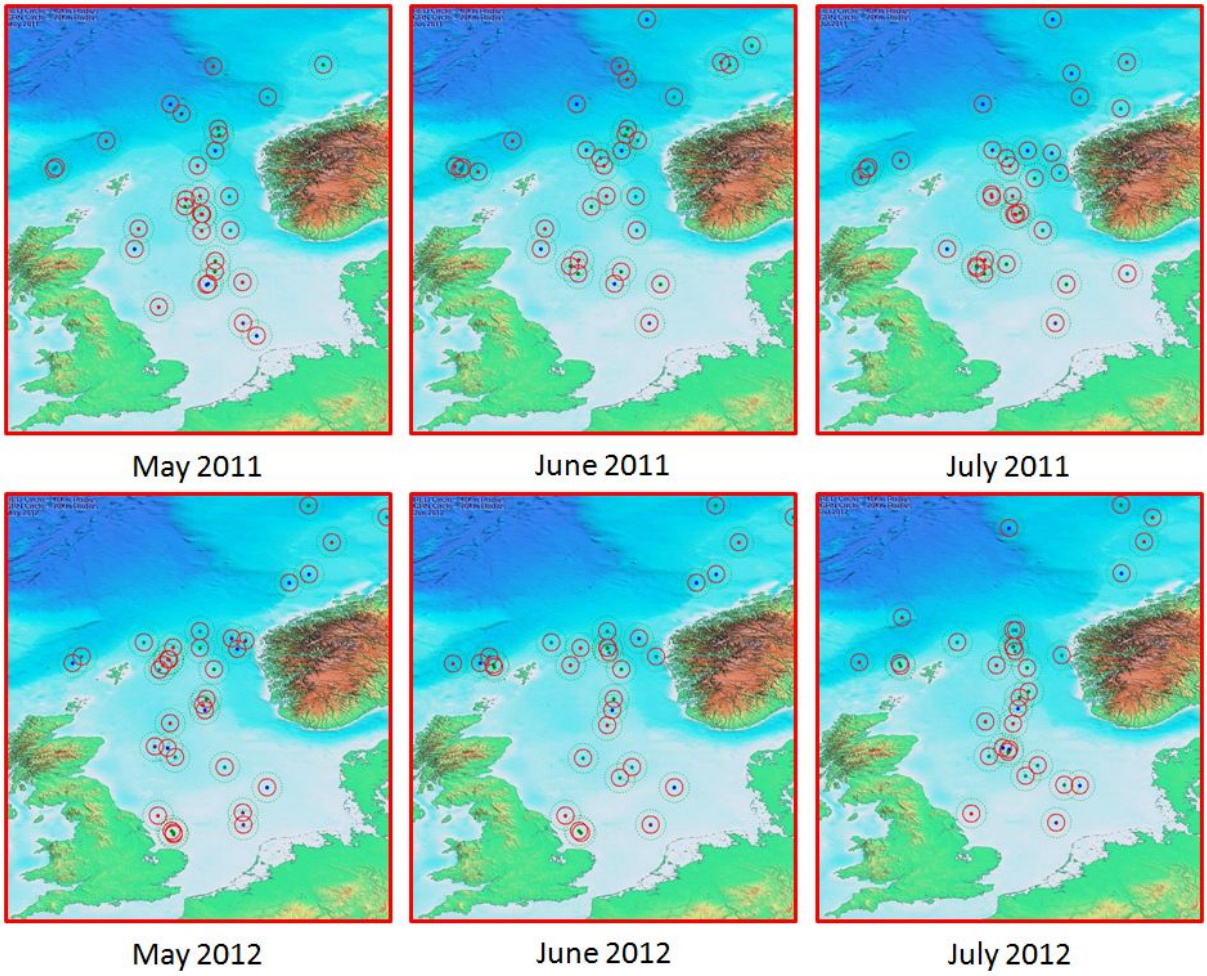

Figure 1.1: Marine seismic activity in the North and Norwegian Sea during May, June and July of 2011 and 2012. Dots indicate operating seismic vessels and red circles indicate a radius of 40 km.

considerably. Two interfering vessels may therefore not be equally affected by the interference. Few guidelines are available on when the vessels can demand time sharing. This lead to a potential source for conflict. Considering the high cost of offshore seismic acquisition, there is a strong motivation for developing efficient and robust SI attenuation methods.

The aim of this thesis has been to develop a method that automatically detect if SI is present in a shot gather, and furthermore detect the moveout. This info is then used in two methods for SI removal. The first technique consists of automatic generation of τ-p mutes, while the second technique uses the line integral convolution (LIC) and an estimate of vector fields to separate SI from reflection data.

1.2 Outline of the thesis

This thesis is made up of six parts. First the motivation and outline of the thesis is given. The second part describe attributes such as moveout, amplitude, frequency spectrum, and periodicity of SI in shot domain. This forms the basis for the third part where the most common methods for SI removal are presented. One of the methods is referred to as *"τ-p to common-p"* method, and serve as a reference method when comparing results in part five on a North Sea dataset referred to as *Lupin*.

The fourth part describes the development of the new *"Vector Field"* (VF) method. This will be the main part of this thesis. Necessary assumptions and results from testing of parameters and thresholds are discussed. VF will be applied to the Lupin dataset to obtain results presented in part five. Finally the results obtained from VF and τ-p to common-p method are discussed in part six, forming the basis for a final conclusion.

The programming related to the development of VF method has mostly been done in MATLAB, while most of the results are produced and visualized in the CGG processing package Uniseis.

2. WHAT IS SI?

This chapter gives examples of how SI appears in the shot domain with respect to moveout, shape, frequency and arrival time.

SI occurs when the seismic energy from a source vessel is recorded as interfering noise by another seismic vessel. The interfering energy travels mostly as shallow refractions and mode propagations in the water column (Calvert et al., 1984), and may be well preserved over large distances. Lie (1988) wrote that seismic vessels have been known to commence time sharing at distances up to 100 km, implying that their data was contaminated by SI at this distance.

Marine seismic noise can be divided into two groups, coherent and random (Presterud, 2009). The coherent group can be further sub-divided into linear and non-linear noise. According to Schlumberger (2013) coherent noise can be defined as following:

> *Undesirable seismic energy that shows consistent phase from trace to trace...*

Examples of coherent noise are SI, multiples, ghosts, and tugging noise. The shape and moveout of SI will be discussed further in the next section. However, a general observation is that SI commonly arrives linear in the shot domain. SI is therefore placed in the linear coherent group. Random noise lacks the consistency from trace to trace, but may in some cases have a temporal consistency. Swell noise is an example of random noise. Figure 2.1 shows two shot gathers contaminated by both SI and swell noise. The left shot gather contains SI from abeam with moveout indicated in rectangle A. The right shot gather contain SI from astern, with moveout indicated in rectangle C, and SI from the side or slightly ahead indicated in rectangle B. Some of the swell noise in both shot gathers is circled in red. Figure 2.1 illustrates the temporal consistency of swell noise in the shot domain, while more spatial consistency of SI.

2.1 The moveout of SI in marine shot gathers

It is assumed in the following that most of the SI recorded at a receiver cable has traveled through the water column. This is due to the strong sea surface reflector and the often strong sea bottom reflector. Even though some of the the interfering energy also travel through the

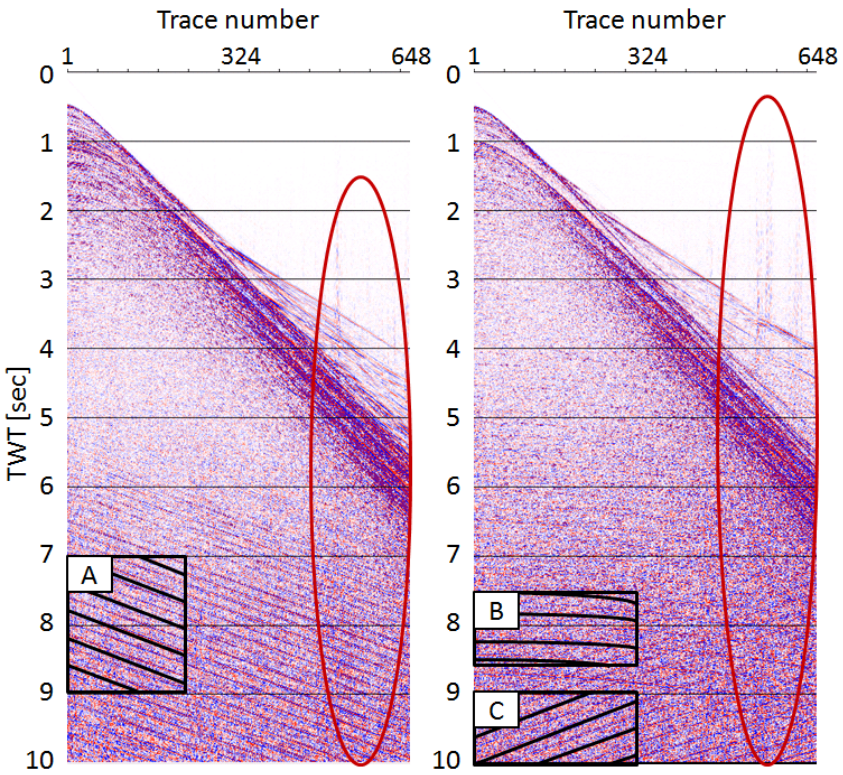

Figure 2.1: Shot gathers containing SI (moveout indicated in squares) and swell noise (red circles). Left shot gather contain SI from abeam (A), while right shot gather contain SI from astern (C) and the the side/slightly abeam (B)

.

subsurface, it is presumed that these amplitudes have been attenuated sufficiently to be neglected.

The moveout of SI in the shot domain can be decided by its velocity v, and the azimuth angle θ from which the signal arrive with when it is recorded at the receiver cable. All SI recorded at a marine receiver cable is propagating with the acoustic velocity of seawater. It varies little and may be approximated to $v_w = 1480m/s$. However, the azimuth θ of the SI may vary, depending on whether the energy arrives from abeam, astern, or at the side of the seismic cable. If we consider an θ defined as 0° at inline direction, we can combine both the velocity and the orientation of the SI in a parameter denoted as apparent velocity:

$$v_a = \frac{v_w}{\cos(\theta)} \tag{2.1}$$

The moveout in the shot domain is defined as the inverse of the apparent velocity given by:

$$p = \frac{dt}{dx} = \frac{1}{v_a} \tag{2.2}$$

From Eq. (2.1) we get the following observations when varying θ:

$$\lim_{\theta \to 0^\circ|180^\circ} v_a = \pm v_w \qquad \text{and} \qquad \lim_{\theta \to 90^\circ|270^\circ} v_a = \infty \tag{2.3}$$

Following this observation, the maximum and minimum moveout p_{max} and p_{min} of SI in the shot domain is limited by the possible arrival angles θ. p_{max} and p_{min} are found by inserting the observations from Eq. (2.3) into the moveout equation (Eq. (2.2)):

$$\lim_{\theta \to 0^\circ|180^\circ} p = \pm p_{max} = \pm \frac{1}{v_w} \qquad \text{and} \qquad \lim_{\theta \to 90^\circ|270^\circ} p_{min} = \frac{1}{\infty} = 0 \tag{2.4}$$

SI from abeam, astern, and from the side of the receiver cable are considered when calculating the moveout curves of SI in the shot domain. Furthermore, it is investigated how the shape of SI change when considering SI arriving from different distances at the side of the receiver cable.

SI from abeam and astern

First, the example of SI from abeam is considered. This example is similar to the case of the direct wave from the source. We have the arrival azimuth $\theta = 0^\circ$, which according to Eq. (2.1) gives the apparent velocity along the receiver cable $v_a = v_w$. According to Eq. (2.2) the moveout is $p = p_{max} = \frac{1}{v_w} = \frac{1}{1480} s/m$. The shape of the SI will follow a line given by the linear equation

$$t(x_n) = t(x_1) + p_{max} x_n \tag{2.5}$$

where x_n for $n = 1, 2, 3, ..., N-1, N$ is the distance along the receiver cable with N hydrophones. $t(x_1)$ is the arrival time of SI at the first hydrophone.

Now, we consider the opposite example when SI arrive from abeam. In this case we have $\theta = 180^\circ$, which gives the apparent velocity $v_a = -v_w$ of SI along the receiver cable. Eq. (2.2) gives the moveout $p = -p_{max} = -\frac{1}{1480} s/m$. The arrival time at the first hydrophone is given by $t(x_1) = t(x_N) - (-p_{max}) x_N$. The linear moveout of the SI through the receiver cable can then be expressed as Eq. (2.6):

$$t(x_n) = t(x_N) + p_{max} x_N + (-p_{max}) x_n = t(x_N) + p_{max} x_N - p_{max} x_n \tag{2.6}$$

Figure 2.2 shows a clean shot gather (left) with $N = 648$ traces and receiver spacing $12.5m$. The moveout curve of SI from abeam (*A*) and astern (*B*) is calculated and plotted (right).

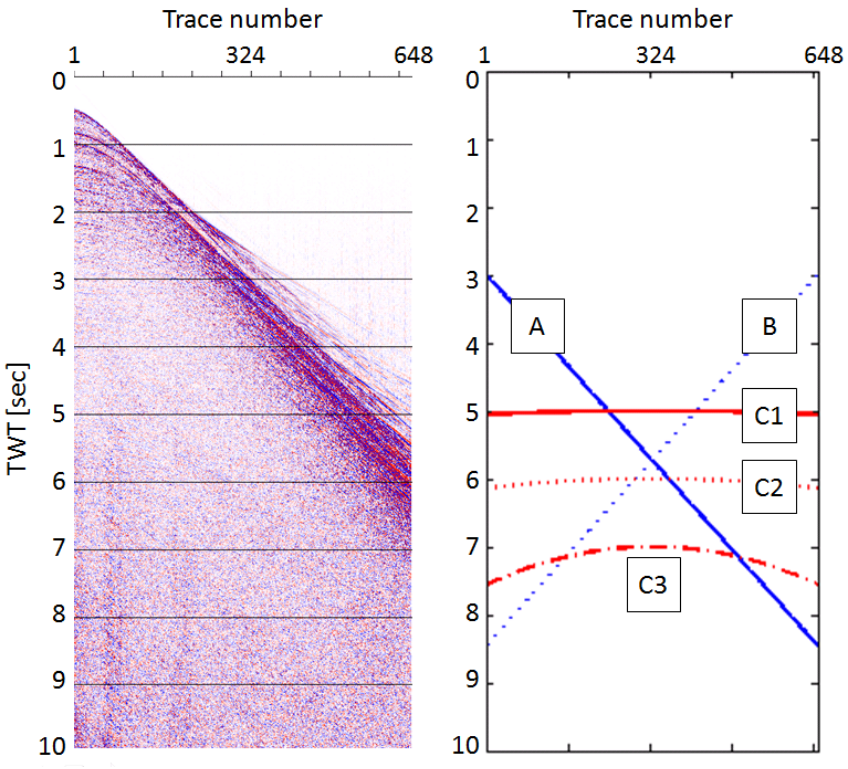

Figure 2.2: Left: A shot gather with 648 hydrophones and length of $8087.5m$. Right: Calculated moveout curves for different SI arrivals. A : SI from abeam, B : SI from astern, $C1$: SI originated a distance of $100km$ from the side, $C2$: SI originated at a distance of $40km$ from the side and $C3$: SI originated at a distance $10km$ from the side.

SI from the side

Figure 2.3 shows the geometry when the moveout of SI from the side is calculated. The interfering source is located at a distance d from the recording cable and centered perpendicular to the receiver cable at position $\frac{x_N}{2}$. As the SI spreads spherically from the interfering source and hits the receivers x_n along the recording cable, the angle θ change at every hydrophone. Following the geometry given in Figure 2.3 and using simple trigonometry, the term $\cos(\theta)$ from Eq. (2.1) can be rewritten as

$$\cos(\theta) = \frac{\frac{x_N}{2} - x_n}{d} = \frac{x_N - 2x_n}{2d} \tag{2.7}$$

By inserting Eq. (2.7) into the expression in Eq. (2.1), we can calculate the apparent velocity, and the moveout at every receiver along the recording cable. We get the following expression:

$$v_{a_n} = \frac{v_w}{\cos(\theta)} = \frac{2v_w d}{x_N - 2x_n} \tag{2.8}$$

Figure 2.2 (right) presents the calculated moveout curves ($C1$, $C2$ and $C3$) when using the setup shown in Figure 2.3 at varying distances d. Moveout curves are calculated and shown for distances $d = 10km(C3)$, $40km(C2)$ and $100km(C1)$. An increase in distance d is seen as a

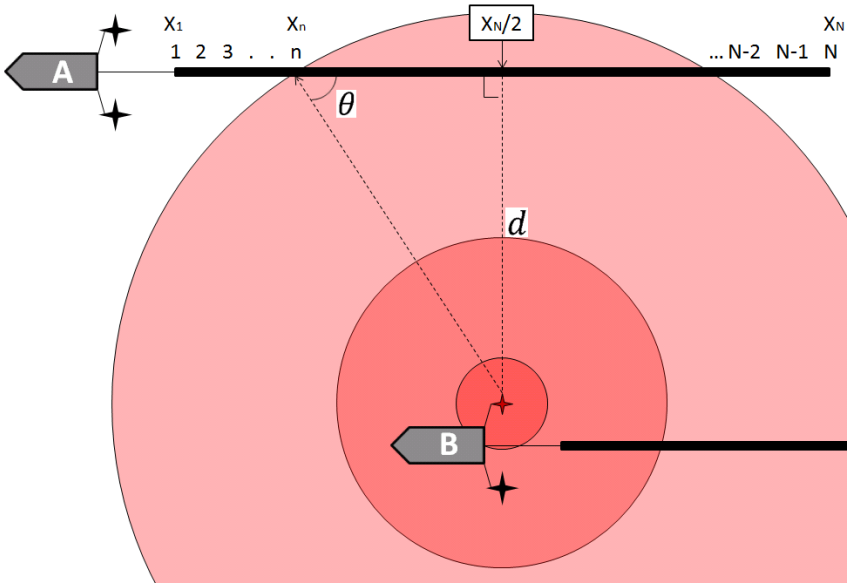

Figure 2.3: SI arriving at hydrophone x_n of vessel A, originated at firing airgun of vessel B.

decrease in curvature. The SI appears close to linear at distance $d = 40km$. The arrival times of the three curves are not related to the distances. They are simply chosen to better separate and illustrate their appearance in the plot.

2.2 Periodicity of SI in consecutive shot gathers

The periodicity of the arrival time of SI in a series of consecutive shot gathers depends on several factors. Most important are:

- Distance from the interfering vessel to the affected receiver cable
- Orientation and speed of the interfering vessel with respect to the affected receiver cable
- Shot point interval of the interfering vessel
- Recording interval for the affected receiver cable

Because of this, SI is rarely synchronized in series of consecutive shot gathers. However, the noise train of the SI often has a long time span in the shot domain. This often lead to a "semi" synchronous arrival time in consecutive shot gathers. This is the case in many of the shot gathers in the considered Lupin dataset. A varying arrival time of SI in consecutive shot gathers is the main assumption behind several existing SI removal algorithms. This is discussed in detail in Chapter 3.2.

2.3 Frequency spectrum of SI

A common way of removing noise from marine seismic data is to look at the frequency spectrum of the noise, and identify if the noise have high amplitudes at frequencies that lie outside the frequency spectrum of our desired seismic signal. If such amplitudes are identified in f-x domain, the noise can be removed by applying a *low-pass*-, *high-pass*-, or combination of the two referred to as *band-pass*-filter (Gelius and Johansen, 2010). The filters are designed to remove or damp amplitudes at unwanted frequencies.

According to modern expectations, the expected frequency band of the seismic data is roughly $2 - 150Hz$. SI is generated by a seismic source, and the source is designed to optimize the frequency band of the seismic data. SI therefore contain a broad band of frequencies. Due to the overlap in frequency content, it is impossible to remove SI by the previously mentioned filtering methods.

The shot presented in Figure 2.1 (left) is τ-p transformed and muted to isolate the SI from the shot gather. τ-p muting is considered a standard way of removing SI, and will be discussed in detail in Chapter 3.1.1. Sections of the SI free (black) shot gather and the removed SI (red) are presented in Figure 2.4. The frequency spectrum of each section are shown in the same figure with respective colors.There is a similarity in shape of the two frequency spectra. However, slightly lower amplitudes of the SI is observed at low and high frequencies. Some high amplitude low frequency temporal consistent swell noise can be seen in the SI free shot gather ($\sim 2 - 6Hz$). This is not present in the shot gather nor the frequency spectrum of the SI. High frequencies are attenuated quicker with distance then low frequencies. This may explain why lower amplitudes are observed at higher frequencies of the SI then the actual signal.

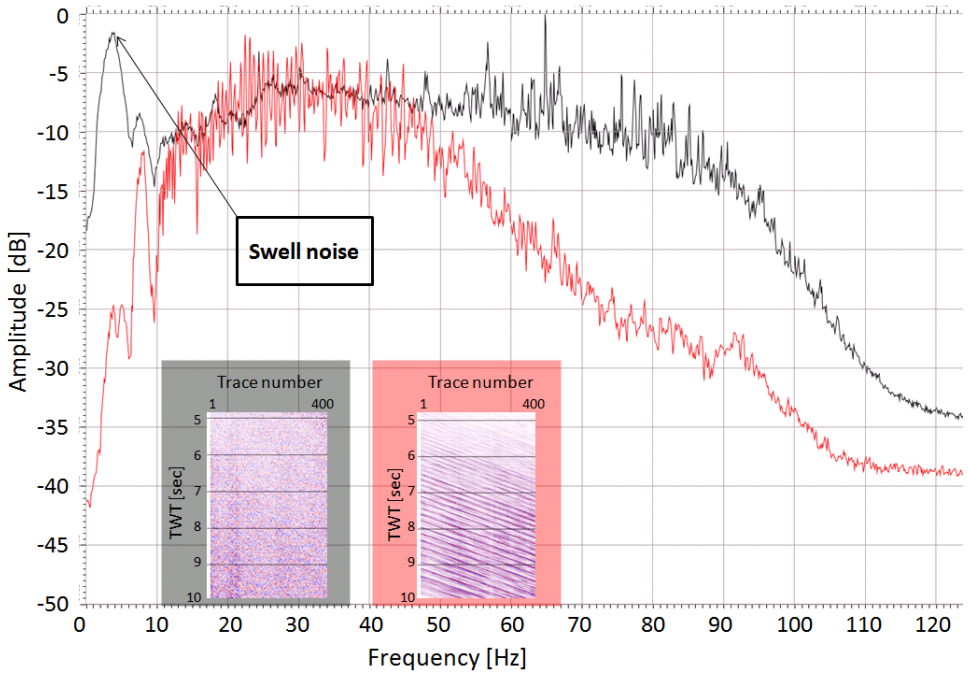

Figure 2.4: Frequency spectra of parts of SI free shot gather (black), and pure SI shot gather (red).

3. COMMONLY USED SI ATTENUATION METHODS

Generally, SI and coherent noise removal algorithms can be classified into two groups. The first group is based on the realization that coherent energy in the shot domain often appears as random noise in other domains (Larner et al., 1983). Random noise attenuation tools like f-x prediction filtering (Canales, 1984) or thresholding methods (Elboth et al., 2008) are then applied to the data, before it is sorted back to the shot domain. This SI attenuation approach has been used by Akbulut et al. (1984) and more recently by Gulunay (2008) and Elboth and Hermansen (2009).

The second group of SI removal tools is based on noise modeling and subtraction. An early example is Kirlin and Done (1990) that uses singular value decomposition to identify coherent events in the data and then subtract them. Finally, more recent approaches estimate the source position and/or firing times of the SI. The SI are then modeled and subtracted like in Brittan et al. (2008). The success of these methods strongly depends on their ability to build up an accurate model of the SI.

3.1 Transforms and sorting of the seismic data

Seismic data can be transformed or sorted by various methods. This section presents two common ways of separating the SI from the seismic data. The first method make use of a linear Radon transform (Radon, 1986) to separate SI from reflection data in τ-p domain. The second method consists of sorting data to a domain where SI appears random while reflection data is still coherent. Random noise attenuation methods are then applied to attenuate the SI.

3.1.1 Radon transform

A Radon transform consists of summing the seismic data along curves defined by the intercept time τ, and moveout p. The sum of each curve is plotted in τ-p domain. Three implementations of a Radon transform exist:

- Linear
- Hyperbolic
- Parabolic

The type determines the shape of the lines the data is summed along. As previously shown, SI often appears fairly linear in the shot domain. A linear type is therefore common when SI in the shot domain is considered. A linear Radon transform map hyperbolic events along elliptical curves, while linear events map to points. The linear Radon type is referred to as τ-p transform in the following.

Some parameters are set by a signal processor prior to a τ-p transform. The parameters determine the moveout range of which the lines are summed along, together with the moveout increments within the range. Chapter 2.1 showed that the possible minimum and maximum p values of SI in a shot gather occur when SI arrive from abeam and astern. All possible moveout curves are therefor mapped in τ-p domain if these parameters are used. However, in most cases the moveout of SI is partly known. This allow the signal processor to limit the range of p values in the τ-p transform, and therefore reducing the processing cost of the transform.

Figure 3.1 (B) illustrates a τ-p transform of a SI contaminated shot gather (A). The mapping of SI in τ-p domain is highlighted. The moveout range is determined by $DTmin$ and $DTmax$. Three examples of possible moveout curves are superimposed in the shot gather (red, green and blue). Mapping of these in τ-p domain are illustrated by crosses, with respective colors.

Muting in τ-p domain

Muting is a common way of removing SI in τ-p domain. Yu (2011) presented a multidomain $\tau - p - y$ approach for removing SI. However, a simple mute in τ-p domain is most commonly used. The general idea is to define a mute by a set of unique parameters.

Two possibilities exist once the SI is isolated. One option is to remove the SI by muting, followed by an inverse τ-p transform of the SI free τ-p gather. This result in a SI free shot gather. However, a forward/inverse τ-p transform is not considered fully signal preserving, and may lead to aliasing in the shot domain (Maroof and Gravely, 1984). This is because the signal is discretely sampled in time and space. The other option preserves the original signal by muting everything except the SI in τ-p domain. The SI model is transformed to the shot domain by an inverse τ-p transform. Finally, the SI model is adaptively subtracted in a least squares sense from the original shot gather. Figure 3.1 shows the SI free shot gather (C) after the highlighted SI in τ-p domain has been inversely transformed and subtracted. The difference plot (D) shows good preservation of reflection data.

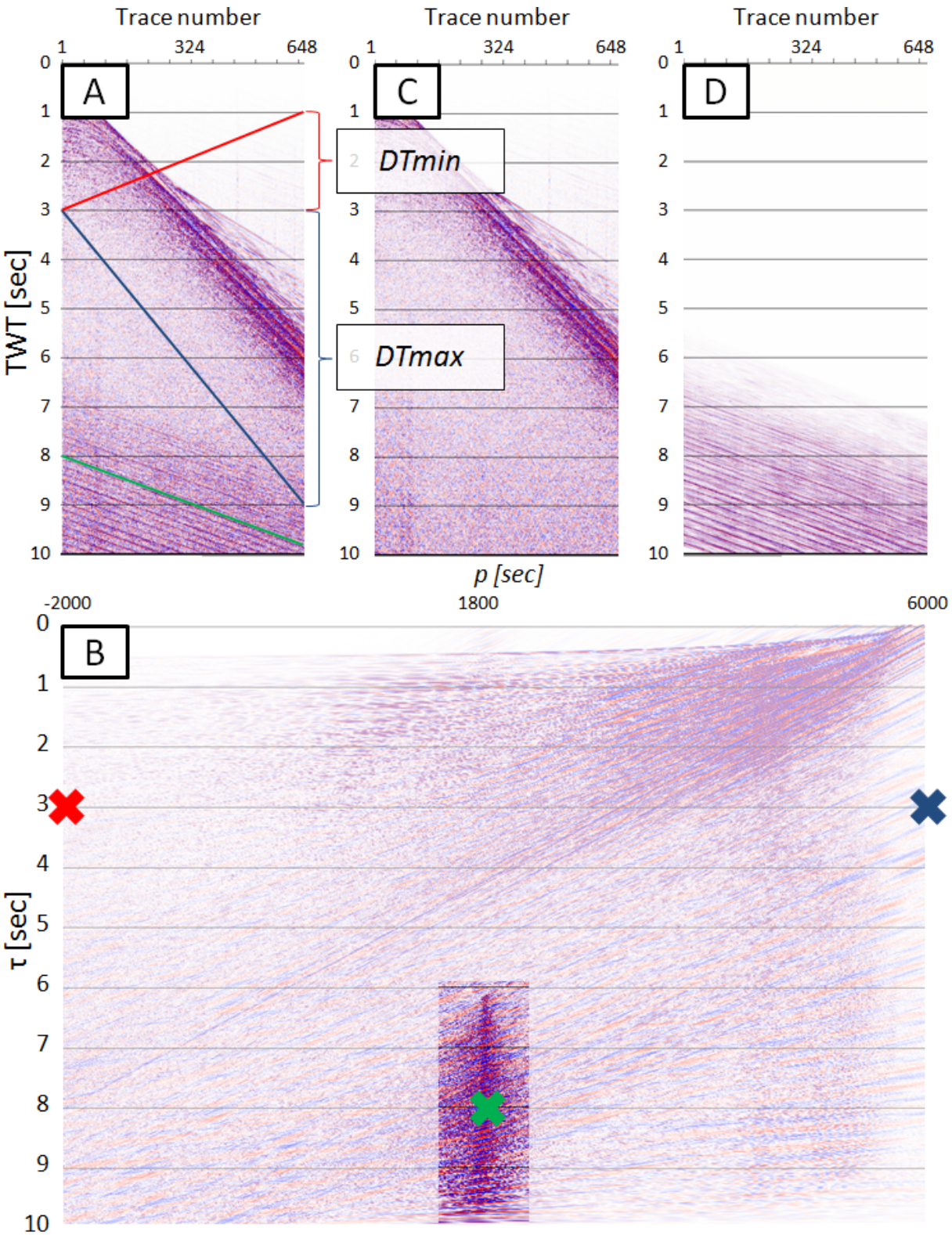

Figure 3.1: Linear Radon transform (B) of a SI contaminated shot-gather (A). Three linear lines are presented in the shot gather with colors, and mapping of these are presented as crosses in τ-p domain by respective colors. The highlighted SI in the τ-p gather is adaptively subtracted from the shot gather (C), showing the difference plot (D).

3.1.2 Randomizing the appearance of SI by sorting

As mentioned in Chapter 2, SI often appears as coherent noise in the shot domain. However, the appearance of the SI can be changed from coherent noise to random noise by sorting/transformation of the data. The general assumption is a non synchronous arrival time of the SI in the consecutive shot gathers. Three common ways of sorting a set of consecutive shot gathers to ensure random appearance of SI are presented:

- Common offset domain
- Common midpoint domain (CMP)
- Common-p domain

Once the sorting is done, SI can be removed by the random noise attenuation methods presented in Section 3.2, and SI free data can be obtained.

Common offset domain

Huaien et al. (1989) presented how a set of consecutive SI contaminated shot gathers could be sorted to common offset domain and filtered using f-x prediction filtering (Canales, 1984). The number of common offset traces in one gather is directly related to the number of sorted shot gathers. Assuming little variation in local geology, the reflections from the geology will appear fairly linear in common offset domain. The SI will arrive as random noise if the arrival time of SI is not synchronized in the consecutive shot gathers.

Common midpoint domain

A common midpoint (CMP) gather is a collection of traces from several consecutive shot gathers which reflect from a common midpoint. SI will arrive as random noise in CMP domain if a non synchronous arrival time of SI in the shot gathers is assumed. The random noise can then be removed using various random noise attenuation tools. The number of traces in one CMP gather is referred to as fold, which is calculated using the equation:

$$F = \frac{N\Delta g}{2\Delta s} \tag{3.1}$$

where N is the number of hydrophones, Δg is the group interval, and Δs is the shot point interval (in distance).

Common-p domain

Sorting to common-p domain for SI removal was first introduced by Elboth and Hermansen (2009), although it has probably been used in processing earlier. A set of consecutive shot gathers are transformed to τ-p domain by a τ-p transform. Hence, the number of obtained τ-p gathers corresponds directly to the number of τ-p transformed shot gathers.

Finally, common-p traces from the τ-p gathers are sorted together in common-p gathers. Each common-p gather will therefore contain as many traces as the number of τ-p transformed shot gathers. Furthermore, the number of common-p gathers is related to the final number of p traces contained in each τ-p gather, respectively:

$$\text{Number of common-}p\text{ gathers} = \frac{(DTmax - DTmin)}{DT} + 1 \tag{3.2}$$

where $DTmin$ and $DTmax$ represent the moveout range in each τ-p transform, and DT represents the moveout increments within the range.

Figure 3.2 illustrates the process of transforming three consecutive shot gathers (left) with variable arrival time of SI to τ-p domain (middle). Finally, three common-p traces at p values enclosing the moveout of the SI from the τ-p gathers are sorted to a common-p gather (right). The SI is seen as the high amplitudes in this specific common-p gather. The arrival time of SI changes for each p trace, starting at a late arrival for the first p trace in the common-p gather (right trace), and earlier for the two consecutive. Assuming a non synchronous arrival time of the SI in consecutive shot gathers, and a small time window which contains many common-p traces and few time samples, the SI may be considered as random noise in common-p domain. It is therefore possible to remove the SI by random noise attenuation methods.

3.2 Random noise attenuation methods

When the sorting/transforming of the seismic shot gathers have achieved to randomize the appearance of the SI, it can be filtered using various random noise attenuation methods. Two methods for such attenuation are now presented.

3.2.1 f-x Prediction Filtering (f-x PF)

The main assumption behind f-x PF is that we have some sort of linear trend in our data. By dividing our seismic data into overlapping windows, this assumption is valid in most cases. Huaien et al. (1989) presented a method for randomizing coherent noise by sorting to common offset gathers, and filter in the common offset domain using f-x PF. Gulunay and Pattberg

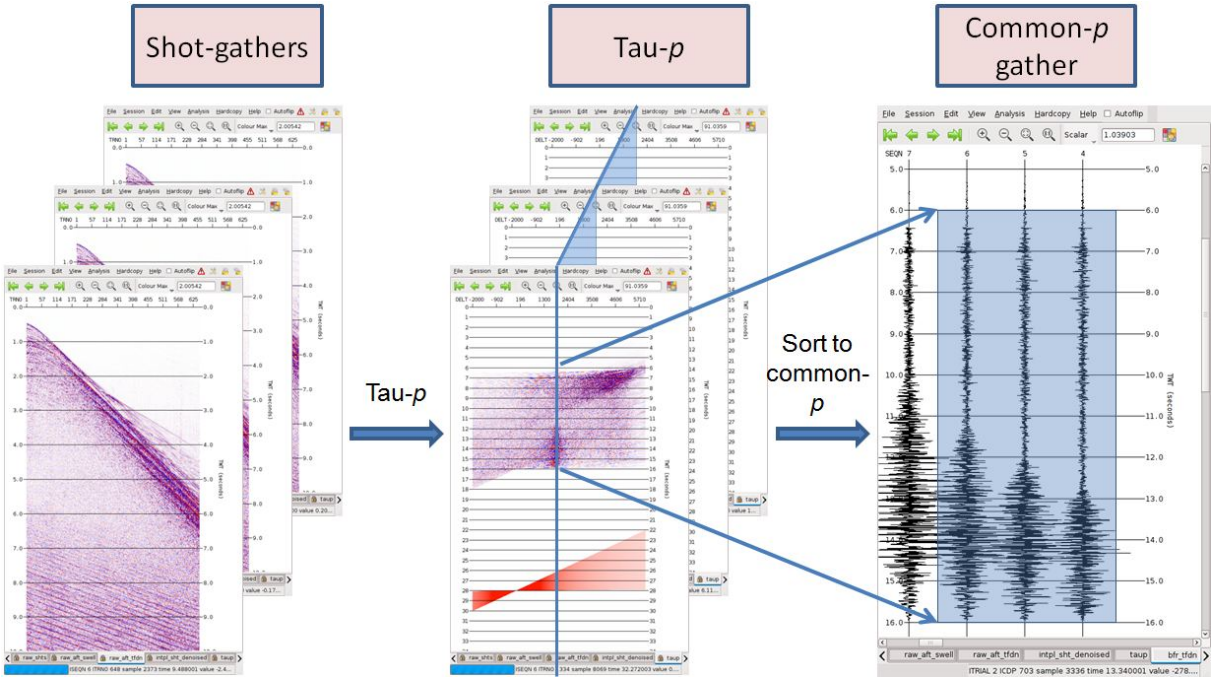

Figure 3.2: Three consecutive shot gathers (left) transformed to τ-p domain (middle), and furthermore sorted to common-p domain (right)

(2001a,2001b) proposed a method using thresholds with respect to amplitudes to detect noisy shots in frequency-shot-receiver domain. The noisy shots were filtered using f-x PF in inline direction for detection and subtraction of SI, and finally using a f-x-y PF in inline/crossline direction on frequency slices.

The following derivation of f-x PF is based on the background theory presented by Presterud (2009). First consider a linear event in space and time:

$$f(x,t) = \delta(a + bx - t) \tag{3.3}$$

where δ is the dirac-function. The Fourrier transform with respect to time gives us:

$$f(x,\omega) = e^{i\omega(a+bx)} \tag{3.4}$$

Since the signal is sampled with a spacing Δx along the x-coordinate, we have:

$$u_n = f(n\Delta x, \omega) = e^{i\omega(a+bn\Delta x)}, \qquad n = 1, 2, 3, ..., N \tag{3.5}$$

with N representing the total number of traces considered. From this it follows that

$$u_n = \alpha u_{n-1}, \qquad \alpha = e^{i\omega b\Delta x}. \tag{3.6}$$

Eq. (3.6) represents the essence of f-x PF. It says that the data point u_n can be predicted from the previous point u_{n-1}. Unpredictable values such as random noise can therefore be identified and subtracted. SI removal by f-x PF in the common offset domain is based on an underlying assumption that the amplitude of the SI is higher then the amplitude of the underlying signal (Gulunay et al., 2004). This is rarely the case in shallow parts of the data.

3.2.2 Time Frequency De-Noising

Time Frequency De-Noising (TFDN) was first presented by Vassiliou and Garossino (1998). A slightly modified version of this implementation was later presented by Elboth et al. (2008), and applied on common-p gathers to attenuate SI (Elboth and Hermansen, 2009). The latter implementation of TFDN is now presented with help from illustrations shown in Figure 3.3.

TFDN works by performing Discrete Fourier Transforms (DFT) on a set of traces within a predetermined sliding window in space and time t_n. Amplitudes $a(t_n, f, x)$ are compared at frequency slices f on the $HWIN$ traces contained in t_n. If the amplitude of the center trace in t_n at frequency f exceed a threshold $thr(t_n, f, x)$, it is reduced to the value of $thr(t_n, f, x)$.

Figure 3.3 present 5 amplitudes ($HWIN = 5$) at a certain frequency slice with center sample X (top). By sorting the $HWIN$ amplitude samples in ascending order (middle), it can be seen that the amplitude X exceed the value of the specific threshold $thr(t_n, f, x)$. Amplitude sample X is therefor muted down to the value of the threshold, and furthermore sorted back to its right position (bottom). The process is repeated for all amplitudes within a user defined frequency range.

The threshold is calculated by multiplying a user-defined time-dependent factor $fac(t)$ with the amplitude of a presumable noise-free trace. The noise-

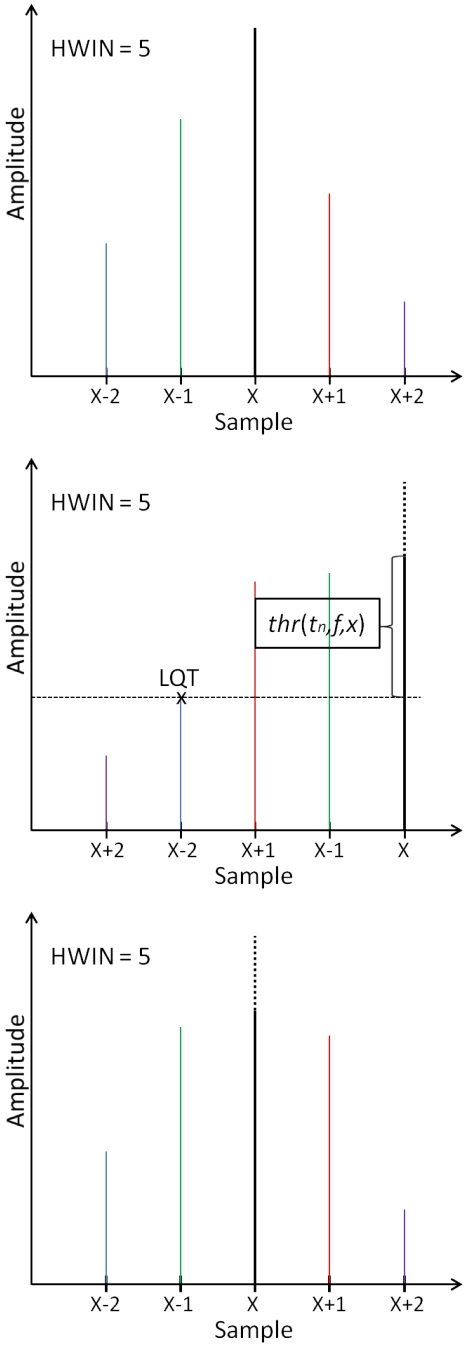

Figure 3.3: $HWIN = 5$ amplitude samples (top) with center amplitude X, sorted in ascending order (middle) and muting X according to threshold $thr(t_n, f, x)$, and finally sorting back (bottom).

free trace can be expressed as the median, the average, or the lower quartile estimation (LQT) (see Figure 3.3 (middle)) of the $HWIN$ amplitude samples at frequency f. Median is a good approximation if less then 50% of the $HWIN$ traces are affected by SI (Presterud, 2009). However, LQT can give a good approximation if more than 50% of the $HWIN$ traces are affected, thus only requiring 25% noise free traces (Presterud, 2009). If the considered $HWIN$ amplitude samples in t_n at frequency f are arranged in ascending order, the index of the median can be expressed as Eq. (3.7) and LQT as Eq. (3.8).

$$median(x) = \frac{\textit{number of values in the array} + 1}{2} \tag{3.7}$$

$$LQT(x) = (\textit{number of values in the array} + 1) * \frac{25}{100} \tag{3.8}$$

Assuming LQT is used, TFDN identify and attenuate random noise at the considered amplitude $a(t_n, f, x)$ at frequency f in $HWIN$ according to the relation given in Eq. (3.9):

$$a(t_n, f, x) = \begin{cases} thr(t_n, f, x) & \text{if} \quad a(t_n, f, x) > thr(t_n, f, x) \\ a(t_n, f, x) & \text{if} \quad a(t_n, f, x) \leq thr(t_n, f, x) \end{cases} \tag{3.9}$$

with $thr(t_n, f, c) = LQT(x) * fac(t)$. This process is repeated for all frequencies specified by the user. The modified frequency samples are finally transformed back to time domain through a inverse DFT. The process is repeated for each sliding window.

The size of t_n is limited by $HWIN$ traces, and t_{len} in time. Assuming a sampling interval $\Delta t = 4ms$, the Nyquist frequency is given by $f_{Nyq} = \frac{1}{2\Delta t} = 125Hz$. Ideally, one sample in the time window t_n should correspond to one Hz sample after DFT (Presterud, 2009). This implies that the time-window should contain 125 samples when using $\Delta t = 4ms$. Hence, the time-window length in time is given by $t_{len} = 125 * \Delta t = 125 * 4ms = 500ms$. Correspondingly a sampling interval of $\Delta t = 2ms$ will give a Nyquist frequency of $f_{Nyq} = 250Hz$ and an equally sized time-window as when using $\Delta t = 4ms$ because $t_{len} = 250 * 2ms = 500ms$.

3.3 τ-p to common-p method

Elboth and Hermansen (2009) presented a method for attenuating SI using TFDN on common-p gathers. This method serve as a reference method for the thesis. The different processing steps of the τ-p to common-p method have been described in the previous sections. This section provides a summary of the entire processing sequence, together with some additional information and considerations made when setting variables that control the results of the method.

Figure 3.4 presents a schematic illustration of how the τ-p to common-p method works. First a τ-p transform is performed on a set of SI contaminated shot-gathers. It is important to choose a moveout range, $DTmin$ and $DTmax$, which enclose the observed SI moveout. Typically ten shot gathers is sufficient for the algorithm to work. However, for illustrative purposes only four shot gather are presented in the figure. Once all four shot gathers have been transformed to the τ-p domain, the common-p traces are sorted from τ-p domain to common-p gathers. Assuming a non synchronous arrival time of SI, it is now possible to isolate the SI by applying TFDN using $HWIN = 4$. However, the user defined parameter $fac(t)$ contained in Eq. (3.9) need to be tested for to obtain optimal results. The user provide two values for $fac(t)$, $fac(start)$ and $fac(end)$. They represent the factor at the start and end time of where TFDN operate in the common-p gathers. The values between $fac(start)$ and $fac(end)$ are linearly extrapolated.

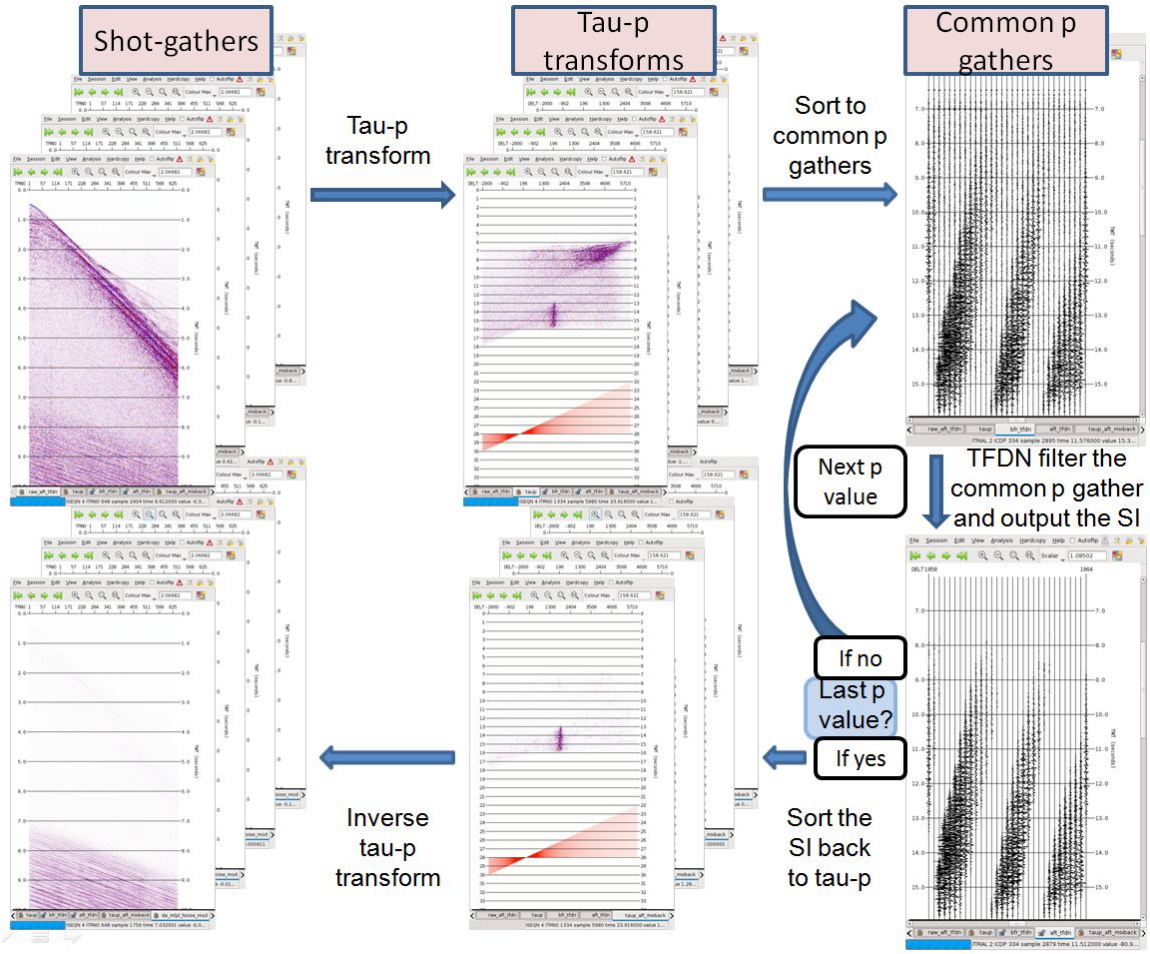

Figure 3.4: Illustration of how the "τ-p to common-p" algorithm works on four shot gathers.

Like mentioned in Chapter 3.1.1, a forward/inverse τ-p transform is not considered signal preserving. In order to minimize the effect on the desired signal TFDN continuously output the filtered SI. The common-p traces are sorted back to τ-p domain once all the common-p gathers have been filtered. Finally, the SI τ-p models are inversely transformed to obtain SI model in the

shot domain. The SI is then removed from the shot gathers by an adaptive subtraction in a least squares sense of the SI noise model. The final subtraction of the SI models are not presented in Figure 3.4.

4. VECTOR FIELD METHOD

This chapter explains the developed *Vector Field* (VF) method. VF is designed to automatically detect the moveout of SI in the shot domain. Some attempts have been made on automatic detection of moveout in the shot domain. Claerbout (1992) presented a method for detecting moveout in seismic data by plane wave destruction. It is based on finding explicit solutions to the one way wave equation with respect to the moveout in the shot gather. Fomel (2002) investigates the applications of plane wave destruction further when solving the equation as a finite-difference problem in the frequency domain.

This thesis presents how a SI moveout estimate can be found from a vector field estimate of a shot gather. As mentioned in the introduction, an expanded abstract has been published during the development of VF. The following description of VF method is based on what was published in the expanded abstract. However, some minor modifications and examples from testing are included. Development and testing of VF method have been carried out in MATLAB (MATLAB, 2010).

Once the moveout has been estimated, SI can be removed by two techniques. The first technique generates a τ-p mute based on the SI moveout estimate, while the second technique uses the line integral convolution (LIC) (Cabral and Leedom, 1993) and an estimate of vector fields to separate SI from reflection hyperbolas. The estimation of SI moveout in the shot gather is essential for both techniques. It is therefor included in the following description. Figure 4.1 presents a SI contaminated shot gather from the Lupin dataset which is a typical North Sea dataset. The shot gather is used in some of the following explanations.

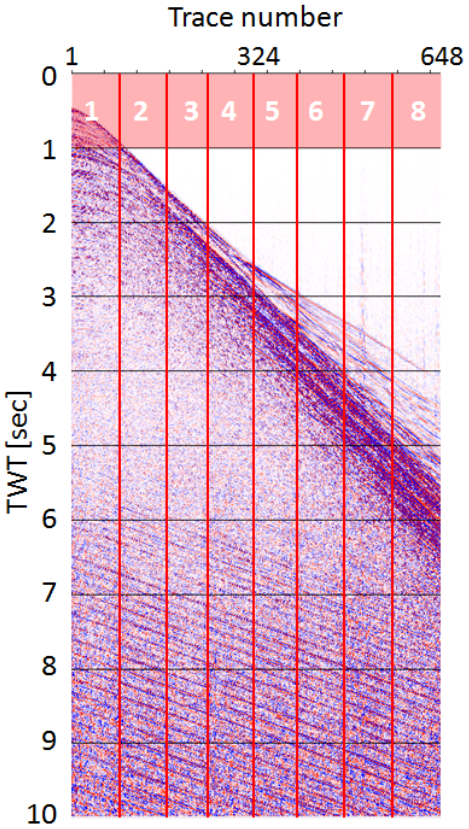

Figure 4.1: Shot gather with prominent SI from ahead, and 8 space windows indicated in red.

4.1 Vector field estimation

A calculated $M \times N$ vector field $\vec{V_0}$ represents the local moveout in a $M \times N$ shot gather. The vector field consists of two components, $\vec{V_0} = (V_x, V_t)^\top$. V_x represents the moveout in space direction and is always equal to 1 sample. V_t represents the local moveout in time direction, and is calculated by normalized cross-correlation in a sliding window in time and space.

4.1.1 Calculating V_t by normalized cross-correlation

Consider two neighbor traces t_1 and t_2 in a shot gather. Both represent discretely sampled functions with finite length limited by a sliding window $t_w(\hat{m})$ with center time sample $\hat{m}$.

For simplicity it is assumed that the vector field $\vec{V_0}$ is sampled at every J^{th} time sample in the shot gather. The size of the time window and the two time sections $t_1(t_w(\hat{m}))$ and $t_2(t_w(\hat{m}))$ is given by $K = \{\hat{m} - (J-1) : \hat{m} + (J-1)\} = 2 * J - 1$. The normalized cross-correlation factors of the two sections with sample lag τ applied to the first trace is calculated according to Eq. (4.1):

$$R_{t_1 t_2}(\tau) = \begin{cases} \dfrac{1}{K} \displaystyle\sum_{k=0}^{K-\tau-1} \dfrac{(t_{1,k+\tau} - \gamma_{t_1})({t_2}^*_{,k} - \gamma_{t_2})}{\sigma_{t_1}\sigma_{t_2}} & , \quad \tau \geq 0 \\ {R^*}_{t_1 t_2}(-\tau) & , \quad \tau < 0 \end{cases} \tag{4.1}$$

where the asterisk denote the complex conjugate, γ is the mean, σ is the standard deviation, and $k = 1, 2, ..., K$ denote the sample number within t_w.

The local moveout $V_t(m = \hat{m}, n)$ is then found by taking the sample lag τ giving the maximum normalized cross-correlation factor S between the time series:

$$V_t(m = \hat{m}, n) = \arg\max_{\tau}(R_{t_1,t_2}(\tau)) \tag{4.2}$$

Figure 4.2 (left) presents two identical signals, with a time lag of 7 samples applied to the second. The normalized cross-correlation is calculated and plotted (right) using $J = \hat{m} = 10$, which gives the time window range $\{\hat{m}-(J-1) : \hat{m}+(J-1)\} = 19$ samples. As expected, the maximum normalized cross-correlation factor S is found at time lag $\tau = 7$. This implies that the local moveout between the two traces in this time window is $V_t = 7$ samples. The normalized cross-correlation plot indicates the local moveout and the similarity factor S. Furthermore, it is indicated where V_t is placed in the time window, and how the final resultant vector $\vec{V_0}(10, 1)$ relates to V_t and V_x.

A similarity factor of $S = 1$ at lag $\tau = 7$ is indicative of a perfect match between the traces. S is later used to indicate whether the calculated local moveout is noise or the true local moveout.

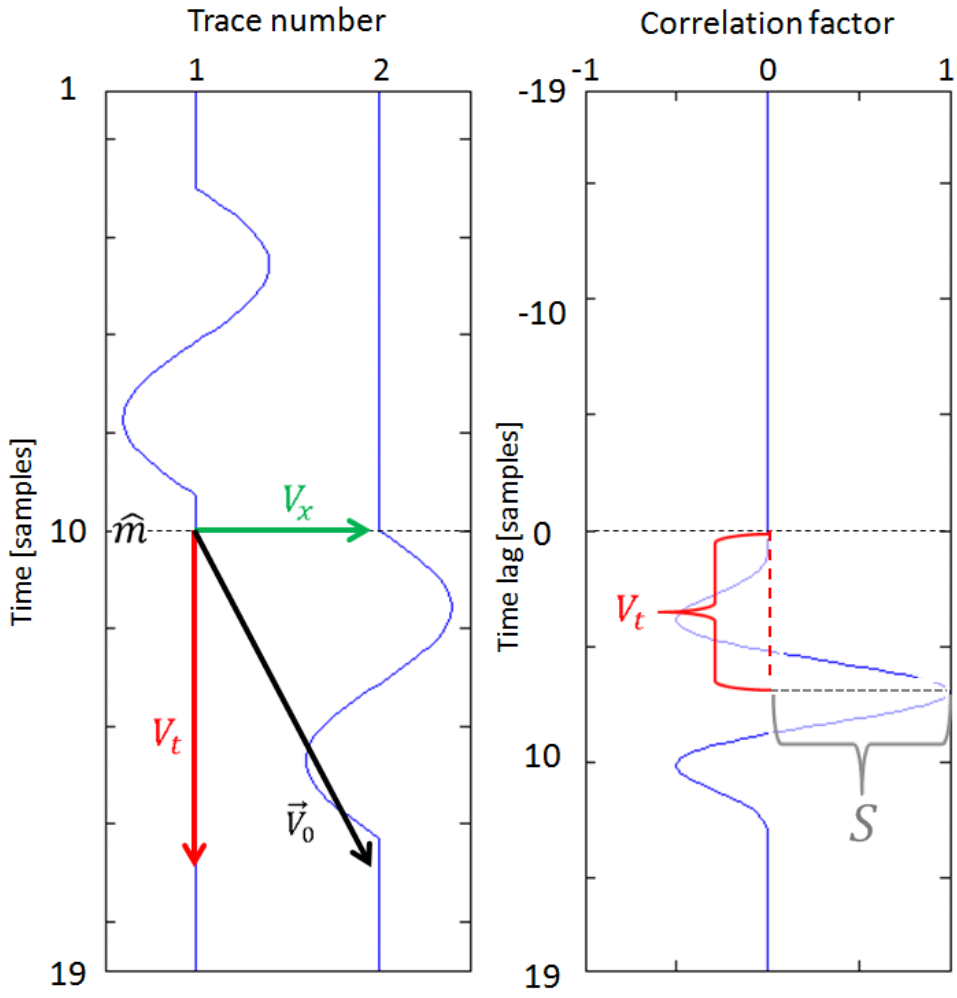

Figure 4.2: Two syntehtic traces (left), and the normalized cross-correlation with time lag applied to the first trace (right).

The time window t_w is moved up one trace at every calculation of the local moveout vector. The process is repeated until all traces at every J^{th} time sample in the shot gather have been sampled with $\vec{V}_0$. Figure 4.3 illustrates the move up of t_w on three synthetic traces with length of 30 samples. A sampling interval $J = 10$ is used when calculating the local moveout vector. This gives 4 sampled locations of $\vec{V}_0$.

Upper and lower moveout limitations on V_t

Eq. (2.4) showed that the maximum moveout in the shot domain is giving $p_{max} = \pm\frac{1}{v_w}$, where $v_w = 1480m/s$. The seismic cable used for recording the Lupin dataset consists of $N = 648$ receivers at a receiver spacing $\Delta x = 12.5m$. The total length of the cable is therefor $X = (N-1) * \Delta x = 647 * 12.5m = 8087.5m$. The maximum total moveout in time found in a shot gather is given by $t_{max} = p_{max} * X = \pm\frac{X}{v_w} = \pm 5.391s$. Furthermore, the maximum moveout in

number of samples for each trace is found by dividing t_{max} by the product of the total number of traces N and the sampling interval $\Delta t = 4ms$. This gives a theoretical maximum value for $V_{t,max} = \pm\frac{t_{max}}{N*\Delta t} = \pm\frac{5.391s}{648*4*10^{-3}s} = \pm 2.080 \approx \pm 2.1$ samples. Local exceptions may occur due to dipping geology. However, this is not taken into the following considerations.

The theoretical maximum is set as a threshold when V_t is calculated. If the computed local moveout V_t exceed these thresholds, it is discarded as noise.

4.1.2 Optimizing the vector field $\vec{V}_0$.

Three considerations are made when optimizing the vector field $\vec{V}_0$. First, the moveout resolution for each local moveout value V_t is considered. Second and third, the two parameters J and S are tested for.

Improving moveout resolution by interpolation

Figure 4.2 is considered for illustrating the meaning of *moveout resolution*. The figure presents the normalized cross correlation of two traces when $J = 10$ is used. The size of the time window is $\{\hat{m} - (J-1) : \hat{m} + (J-1)\} = 19$ samples. One sample in the time lag correspond to one sample of the traces. If a sampling interval of $\Delta t = 4ms$ was used on the traces (left), the potential round of error on the calculated moveout vector is given by:

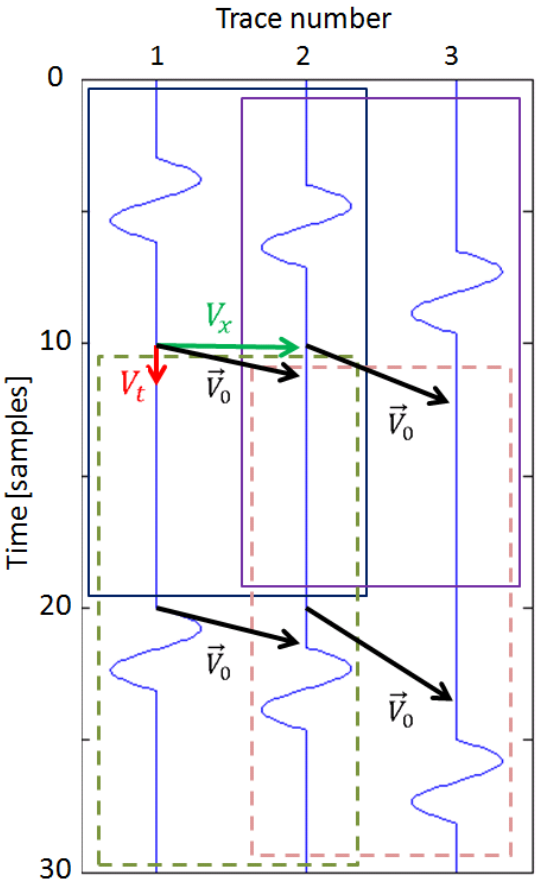

Figure 4.3: Three synthetic traces with 30 samples, sampled with $\vec{V}_0$ at every $J = 10$ time sample. The overlapping time windows are illustrated with solid rectangles (dark blue and purple) at $m = J = 10$, and with dashed rectangles (green and pink) at $m = 2 * J = 20$.

$$\delta p \approx \frac{\Delta t}{2} \approx \frac{4ms}{2} \approx 2ms \tag{4.3}$$

The round of error can be reduced by introducing a higher sampling interval. For this purpose, the traces are over sampled by a factor of 10. The new samples are interpolated from the existing ones by *Spline interpolation* in MATLAB. This gives a new sampling interval of the vector field $\hat{J} = 100$, and $\Delta t = 0.4ms$. According to Eq. (4.3) the new potential round of error of a vector

is therefor $\delta p \approx 0.2ms$, which is acceptable. In the following it is assumed that the traces have been interpolated by a factor of 10 when V_t has been calculated.

Testing of S and J

The sampling interval and similarity factor threshold, respectively J and S, have to be tested to optimize the vector field $\vec{V}_0$. Two plots are presented for such purpose. The first plot show the number of vectors as a function of moveout. This plot is useful for testing how variations of the similarity factor threshold S affects the number of vectors found at each moveout. Figure 4.4 presents four number plots when using a sampling interval $J = 10$ of $\vec{V}_0$ at varying similarity factor thresholds S. The vector fields have been calculated on the shot gather presented in Figure 4.1.

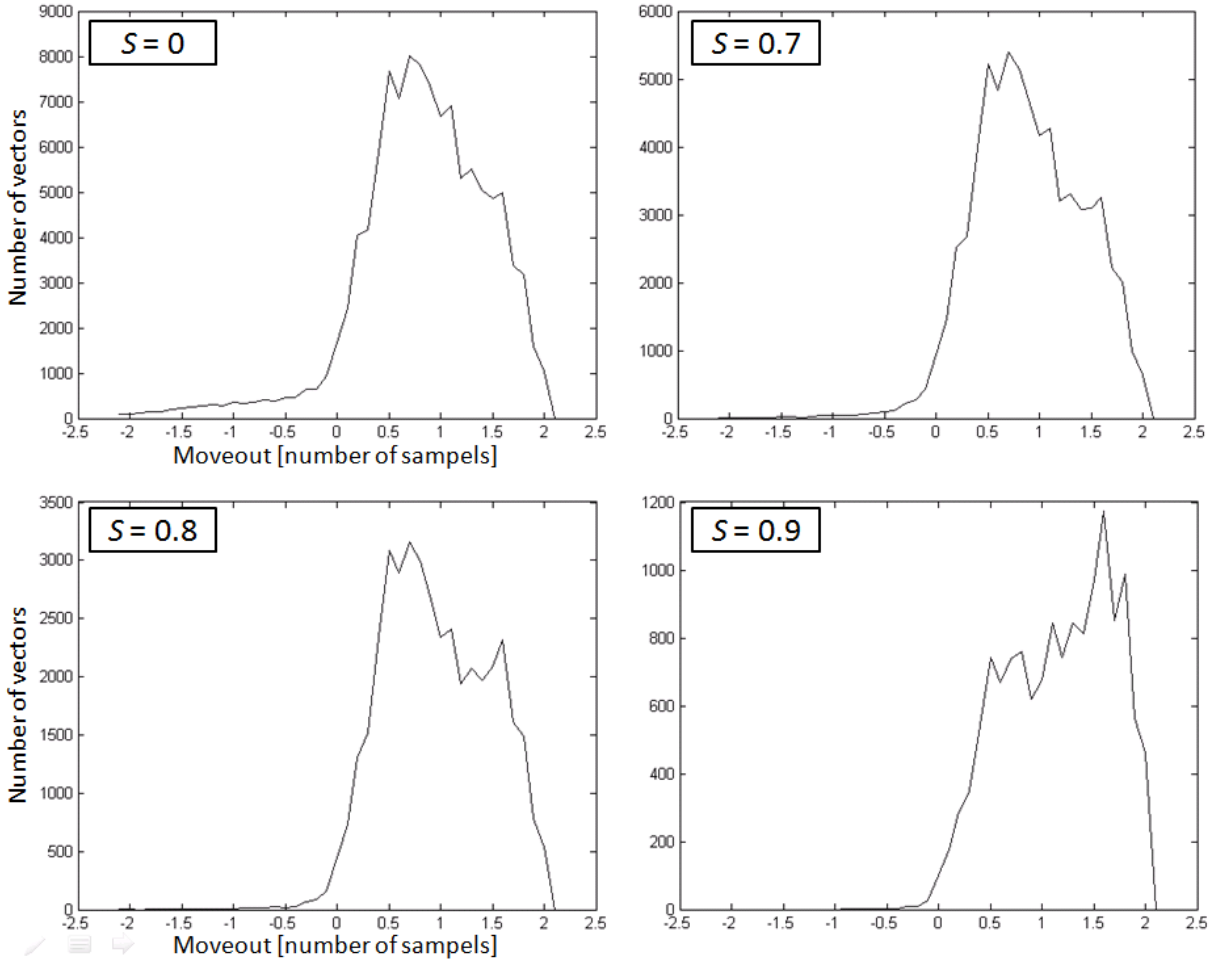

Figure 4.4: Number of vectors with respect to moveout when using $J = 10$ and varying the similarity factor threshold S.

All variations of S show a high number of vectors with moveout between 0 and 2 samples/trace. However, the shape of the curves vary considerably. It appears from the shot gather (See Figure 4.1) that there are no coherent events with negative dip. Such vectors are therefor considered

noise in $\vec{V}_0$. Most of these vectors are discarded when similarity thresholds $S = 0.7$ and $S = 0.8$ are used. Furthermore, it is observed from the shot gather that the moveout of the SI is approximately $\frac{1800ms}{648\text{traces}*4ms} \approx 0.7$ samples/trace. The curve is most prominent at the SI moveout when using $S = 0$, $S = 0.7$ and $S = 0.8$. However, since $S = 0$ include more negative moveout vectors, and $S = 0.8$ gives significantly fewer vectors then $S = 0.7$, similarity factor threshold $S = 0.7$ is considered the better.

The second plot presented in Figure 4.5 is made by splitting the considered shot gather into 8 equally sized space windows. The space windows are illustrated in red in Figure 4.1. Each consists of $\frac{N}{8} = \frac{648}{8} = 81$ traces. In each space window, the number of vectors is plotted as a function of moveout. This plot is good for illustrating how the moveout of the vectors vary in space.

Figure 4.5 presents four number of vectors versus space window plots at $S = 0.7$. The sampling interval J vary from every 5^{th} sample up to every 25^{th} before interpolation. Each space window plot shows a significant number of vectors with SI moveout ($\sim 0.7 samples/trace$). Furthermore, it can be observed that each plot presents a high occurrence of vectors with high moveout at space windows containing high trace numbers. This can be explained by the moveout of reflection hyperbolas, being low at near offset and high at far offset. Both SI and reflection data vectors are indicated in the space window plot with sampling interval $J = 10$.

Figure 4.5 shows that using both $J = 5$ and $J = 10$ give the least variation in number of vectors at SI moveout. The processing time of each shot gather is reduced by increasing J. Therefore, a sampling interval $J = 10$ is used in the following SI moveout estimation.

4.2 Identifying the moveout of SI

The SI moveout estimation by VF method in shot gathers is based on two main assumptions:

- A linear appearance of the SI
- A different moveout of SI compared to reflection hyperbolas

Chapter 2.1 presented some variations of SI moveout in the shot domain. One observation was that SI often appear close to linear. However, deviations occur when SI arrive at short distances from the side of the affected streamer. Figure 2.2 presented three calculated moveout curves when SI arrive at varying distance from the side of the receiver cable. The curves show that the moveout may be approximated to linear at distances above 40 km for that specific receiver length.

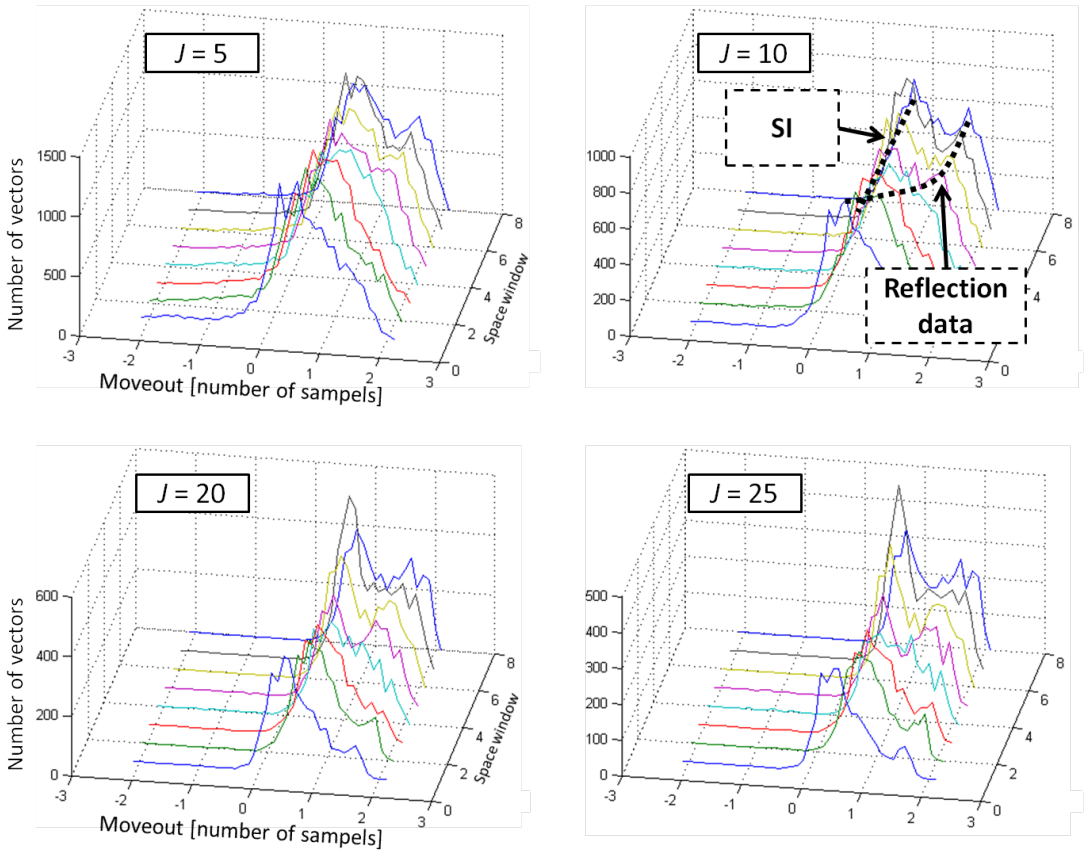

Figure 4.5: Four plots illustrating the number of vectors as a function of moveout with respect their space window location (see Figure 4.1). The sampling interval J is varied when using similarity factor $S = 0.7$.

Figure 2.2 also presented the moveout of SI arriving from abeam. In this case the moveout of the SI may overlap with the moveout of the reflection hyperbolas in the shot domain. The following description of VF method shows that this lead to problems when calculating the SI moveout.

4.2.1 Three plots designed for automatic detection of SI moveout in the shot domain

Three plots for SI moveout estimation in a marine shot gather are presented:

1. Normalized number of vectors with respect to moveout
2. Normalized sum of absolute amplitude with respect to moveout at sampled locations of $\vec{V}_0$
3. Standard deviation (STD) of relative number of vectors through space with respect to moveout

1: Number of vectors plot

The number of vectors plot was presented in the previous section for the purpose of testing S. However, the plot is also suitable for testing if many vectors occur with the same moveout in the shot gather, e.g. linear SI. This plot is normalized in order to generalize the use of it to other dataset. Figure 4.6 shows the normalized sum of the number of vectors with the same moveout for the shot gather presented in Figure 4.1. A high normalized number is present at SI moveout (cross).

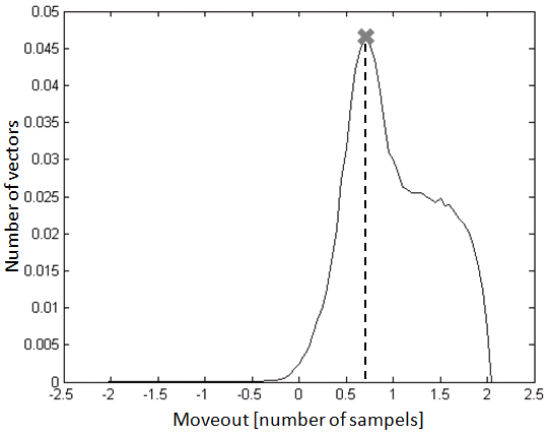

Figure 4.6: Normalized number of vectors as a function of moveout.

2: Amplitude plot

The amplitude of SI in a shot gather is often significant, and may mask the amplitudes of the underlying signal. An amplitude plot for SI moveout detection takes advantage of high SI amplitudes. By plotting the sum of the absolute amplitude for each moveout values of the distribution, $V_{t,i}$, at the sampled locations of $\vec{V}_0$ in the $M \times N$ shot gather, the total amplitude at each moveout value is visualized. The calculated sum of the amplitudes are normalized in order to generalize the use of the plot. Figure 4.7 illustrates an amplitude plot of the considered shot gather presented in Figure 4.1. A high amplitude is observed around the moveout representing the SI (cross).

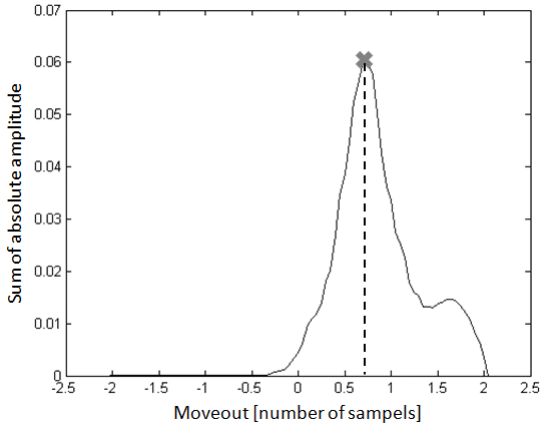

Figure 4.7: Normalized sum of absolute amplitudes at vector locations with common moveout in the shot gather.

3: STD plot

The STD plot is made by looking at the distribution of the moveout components V_t of $\vec{V}_0$ for each space window W presented in Figure 4.1. The assumption is that the vectors indicative of SI have a rather constant moveout in space and time while vectors indicative of reflection hyperbolas have more variations. In particular, V_t is smaller

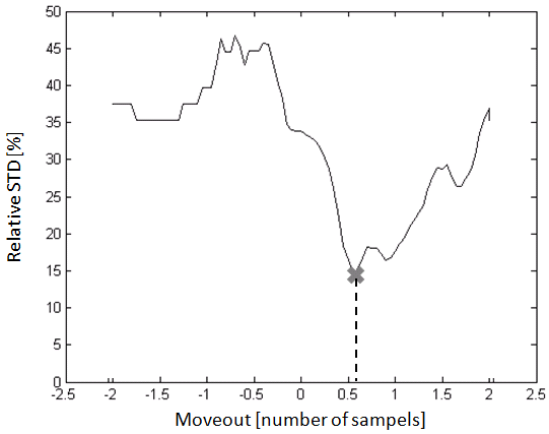

Figure 4.8: Standard deviation of relative number of vectors at common moveout thorugh space.

at near offset and increases with offset. Therefore, the SI moveout is expected to be the one with minimum relative STD. For each moveout value of the distribution, $V_{t,i}$, the STD $\sigma_{V_{t,i}}$ of the number of occurrences $n_{i,w}$ for $w = 1, 2, ..., W$, is calculated over the $W = 8$ (space windows) representations available. The relative STD is then normalized STD given by

$$\sigma_i = \frac{\sigma_{V_{t,i}}}{\max\limits_{w}(n_{i,w})} \times 100 \tag{4.4}$$

The minimum σ_i is achieved at moveout

$$p \equiv \arg\min_{V_{t,i}} \sigma_i \tag{4.5}$$

Figure 4.8 shows the STD plot when $\vec{V_0}$ is calculated on the shot gather presented in Figure 4.1 and using similarity factor threshold $S = 0.7$, sampling interval $J = 10$ and $W = 8$ space windows. As expected, the minimum occurs at moveout close to the SI moveout.

4.2.2 SI moveout estimation algorithm

Appendix A presents the flowchart of the algorithm used when estimating the moveout of SI in a shot gather. The SI moveout estimation is based on three consecutive approaches. Each approach is designed to output the moveout of SI if found. Finally, if neither approach one, two or three find SI, the shot gather is presumed to be SI free. All three approaches depend on the three previously presented plots. The three moveouts found at maximum of the number and amplitude plots, and minimum of the STD plot are sorted into an array referred to as $INDEXES$. Accordingly, $INDEXES(1) = index1$ corresponds to the moveout at maximum of number plot, $INDEXES(2) = index2$ to moveout at maximum of amplitude plot, and $INDEXES(3) = index3$ to the moveout at minimum of the STD plot.

Each approach is now described with respect to the flowchart. Six thresholds are mentioned, and testing of these are described in Section 4.2.3.

First approach

First approach looks at the variation of the three indexes found. The assumption is that a small variation of the three indexes is indicative of SI. Therefore, if the STD of the three indexes exceed the user defined threshold, $indexTHRS$, the second approach initiates. However, if the STD of the indexes is smaller or equal to $indexTHRS$, and the mean of the indexes is within the user defined moveout threshold $moutTHRS$, the moveout of the SI is set to the mean of

$INDEXES$:

$$SImoveout = \frac{index1 + index2 + index3}{3} \tag{4.6}$$

Second approach

The second approach looks for the *two indexes* with the lowest STD. Three tests are performed on the mean of these indexes to determine the moveout of SI. First, it is tested if the STD of the *two indexes* are lower or equal to $indexTHRS$. Secondly, it is tested if the plot producing the worse index has a higher/lower value then the respective "plot threshold" at moveout equal to the mean of the *two indexes*. Finally, it is tested if the mean of the two indexes are within the allowed moveout range $moutTHRS$. If all three tests pass, the SI moveout is set to mean of the *two indexes*. However, the third approach is initiated if one or more tests fail.

Third approach

The third approach consists of three main tests for SI moveout detection. Indexes from each plot are tested in the two remaining plots with respect to the corresponding plot thresholds. The order of the tested indexes are determined by the considered significance of each plot for SI moveout detection.

First, $index1$ at the maximum of the number plot is tested with respect to the user defined threshold $numbTHRS$. If the value is higher then the threshold, the two other plots are tested with the same index and their respective thresholds, $ampTHRS$ and $stdTHRS$. Finally, it is tested if $index1$ is within $moutTHRS$. If all tests pass, the SI moveout is presumed to be $index1$. However, if one test fails, the process is repeated by using $index2$ and finally $index3$. The shot gather is presumed SI free if neither of the indexes present an acceptable SI moveout.

4.2.3 Threshold determination for identifying SI

The previously mentioned thresholds need to be set in order for the SI moveout detection to work. Two of the thresholds are set by reasoning. These are $indexTHRS$ and $moutTHRS$. $indexTHRS$ determines the allowed standard deviation between the moveout found in the plots. Using $indexTHRS = 0.2$ samples allow a variation of 0.2 samples/trace between the considered indexes. This corresponds to $0.8ms$ in $\Delta t = 4ms$ data, which is four times the potential V_t round of error (see Eq. (4.3)) after interpolation. This is considered acceptable.

$moutTHRS$ determines the allowed maximum moveout of SI in the considered shot gather. Both of the methods presented for final SI removal in Section 4.3 rely on different moveout

between the SI and the reflection hyperbolas. Introducing a threshold with respect to moveout eliminates the possibility of overlapping moveout. A moveout threshold of $moutTHRS = 1$ sample/trace is introduced for this purpose.

Finally, the three specific thresholds with respect to values at SI moveout in the plots are determined.

Identify SI i number of shots, and determine the plot thresholds from these

The three thresholds; $numbTHRS$, $stdTHRS$ and $ampTHRS$, determine the upper/lower limits of acceptable values at SI moveout in the plots. They are determined by comparing the values at SI moveout in the three plots for a set of SI contaminated shot gathers. First, 24 SI contaminated shot gathers are chosen from the test dataset. Each shot gather presents SI with varying moveout and amplitude that should be detected when using VF method. The SI moveout is manually identified in the shot gathers. All three plots are made for each shot gather and values at SI moveout are manually picked. The results from each plot are presented in Table 4.1.

Table 4.1: Values from amplitude, number and STD plot at SI moveout for 24 SI contaminated reference shots.

Shot	1	3	4	5	6	7	8	9
Moveout	0,65	0,65	0,65	0,65	0,65	0,7	0,7	0,7
Amplitude	0,019	0,0686	0,0615	0,0648	0,057	0,0466	0,0449	0,0359
Number	0,0338	0,0311	0,0398	0,4444	0,0476	0,0454	0,0376	0,0336
STD	17,31	21,32	15,87	11,8023	10,3	13,5305	15,145	16,1209
Shot	31	32	43	44	45	46	52	73
Moveout	0,7	0,7	0,7	0,7	0,7	0,7	0,75	0,75
Amplitude	**0,0159**	0,0206	0,0181	0,0187	0,0324	0,0188	0,0172	0,0553
Number	0,0306	0,0291	0,0366	0,0395	0,0454	0,0426	0,0349	0,0379
STD	20,6	14,4375	17,583	13,5876	14,4252	19,3809	20,9999	14,4761
Shot	78	120	132	218	674	677	678	680
Moveout	0,75	0,75	0,75	0,76	0,27	0,27	0,27	0,27
Amplitude	0,0318	0,0273	0,0265	0,026	0,0614	0,0511	0,0689	0,056
Number	0,0337	0,0263	0,0239	**0,0232**	0,0367	0,0366	0,0438	0,0378
STD	19,168	19,8568	19,9327	15,9089	27	25,4	**28,1**	27,5
Min amplitude	0,0159							
Min number	0,0232							
Max STD	28,1							

A minimum in the values from the amplitude plots is observed at shot 31. According to the value found, the minimum amplitude plot threshold is set to $ampTHRS = 0.0159$. The mini-

mum from the number plots is found at shot 218, giving a minimum number plot threshold of $numbTHRS = 0.0232$. Finally, a maximum from the STD plots is found at shot 678, giving the maximum STD plot threshold $stdTHRS = 28.1$.

4.3 Two methods for removing the SI

Two methods are presented for removing the SI from the contaminated shot gathers. The first method is the main focus of this thesis, while the second is a more experimental approach. Both rely on SI moveout detection from $\vec{V}_0$. Vectors representing SI moveout have a small variation Δp through the shot gather. The SI moveout range for each shot gather is therefore set to $p \pm \Delta p$, with $\Delta p = 0.12$ samples/trace. This corresponds to a total moveout of $\pm\Delta\hat{p} = \pm 300ms$ in time through the shot gather.

4.3.1 Generating τ-p mutes

The first SI removal method consists of generating τ-p mutes in MATLAB by using the SI moveout estimate. Each mute consists of a lower and upper mute line defined by a set of unique parameters. These are best explained by using an example.

VF method applied to the SI contaminated shot gather in Figure 4.1 presents a SI moveout of $p = 0.75$ samples/trace. The shot gather is sampled with $\Delta t = 4ms$ and contain $N = 648$ traces. The total moveout range of the SI in time through the shot gather will therefore correspond to $\hat{p} \pm \Delta\hat{p} = (p * \Delta t * N) \pm \Delta\hat{p} = (0.75 * 4ms * 648) \pm 300ms = 1944ms \pm 300ms$.

First, the lower mute line is applied in τ-p domain to remove everything with moveout lower then what is defined. Then, the upper mute line is applied to remove everything at moveout higher then what is defined. In this way, the mute lines isolate the SI in τ-p domain. The upper and lower mute line for shot 7 in Figure 4.1 are presented in Table 4.2.

Table 4.2: Lower and upper mute line designed by VF method for isolating the SI in Figure 4.1 in τ-p domain.

Lower mute line	**Upper mute line**
OPTN,ISEQN,DELT	OPTN,ISEQN,DELT
7,1,6000,6000,6000,6000>	7,1,0,0,0,0>
4000,1644,1644,6000,6000>	4000,0,0,2244,2244>
10000,1644,1644,6000,6000>	10000,0,0,2244,2244

The first line in Table 4.2 is the same for both mute lines. It simply states that the mute belong to a certain shot, $ISEQN$, and that the lines are defined by a given moveout $DELT$. The second

line starts with the number 7. This means that the mute lines belong to shot number 7. Five numbers follow the shot number. These, together with the numbers in the two last lines, follow a specific system. They define the time location of the mute, and the moveout range where everything is preserved. The system can be expressed as $(time[ms], \hat{p}_{min}, \hat{p}_{min}, \hat{p}_{max}, \hat{p}_{min})$. Everything outside the moveout range $\{\hat{p}_{min} : \hat{p}_{max}\}$ is muted. Figure 4.9 illustrates shot 7 in τ-p domain (A). It shows how the SI is isolated (B) according to the mute parameters $\hat{p}_{min}$ and $\hat{p}_{max}$.

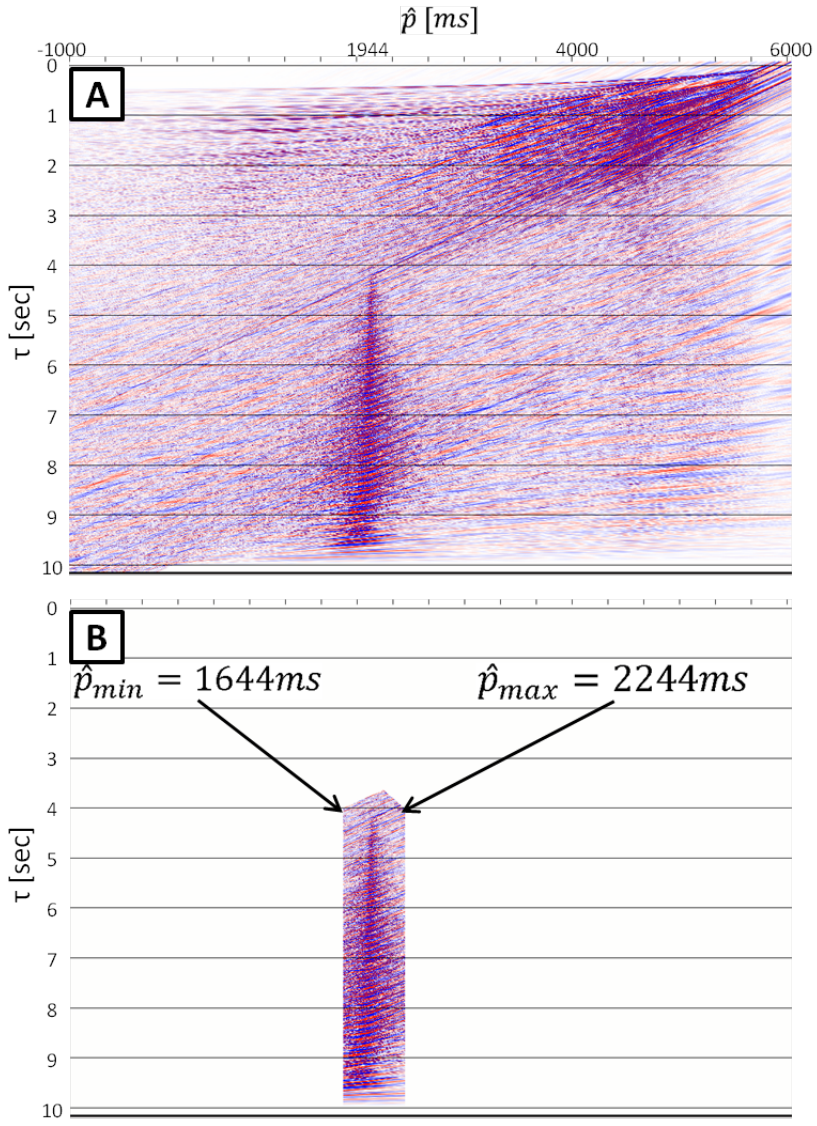

Figure 4.9: A: Linear τ-p transform of shot 7 in Figure 4.1, using $DTmin = -1000ms$ and $DTmax = 6000ms$. B: Shows how the SI is isolated using the mute parameters $\hat{p}_{min}$ and $\hat{p}_{max}$.

The first five numbers of both mute lines show that nothing is preserved. However, the second five numbers of the two mute lines start isolating the SI. First, the lower mute line starts at $4000ms$ and goes down to $10000ms$. Everything from $\hat{p}_{min} - \Delta\hat{p} = 1944ms - 300ms = 1644ms$ up to $DTmax$ is preserved. Second, the upper mute line start at $4000ms$ and goes down to $10000ms$. Everything from $DTmin$ to $\hat{p}_{min} + \Delta\hat{p} = 1944ms + 300ms = 2244ms$ is

preserved. Finally, the mute lines have isolated the SI, and the τ-p SI model can be inversely transformed and subtracted from the original shot gather.

Each mute starts with isolating the SI at $4000ms$ in the τ-p gather. This specific time is chosen as a constant because the SI amplitude is very low at lower arrival times in the test dataset.

Arrival time estimation

Now, a short description of how the VF method can estimate the arrival time of the SI is presented. This has not been implemented in VF method when generating the mutes, but may be used in future development. First, all vectors with moveout in the interval of the SI, $\hat{p} \pm \Delta\hat{p}$, are put in a SI vector field $\vec{V}_0^{SI}$. For each sample of the first trace $(t'\ 1)^\top$, the distance (in samples) to all vectors $(t_i\ x_i)^\top$ of the SI vector field $\vec{V}_0^{SI}$ is calculated by:

$$d_{tot}(t') = \sum_i d_i \tag{4.7}$$

where $d_i = \sqrt{(x_i - 1)^2 + (t_i - t')^2}$. Thereby, an estimate of the central arrival time is obtained at minimum distance

$$\hat{\tau} \equiv \arg\min_{t'} d_{tot} \tag{4.8}$$

The distance from each sample $(t'\ 1)^\top$ to all SI vectors are calculated for the shot gather presented in Figure 4.10 (left), and plotted (right). The central arrival time $\hat{\tau}$ of the SI is indicated by black crosses.

4.3.2 Line integral convolution (LIC)

The second method to remove SI is a method referred to as line integral convolution (Cabral and Leedom, 1993). The line integral convolution (LIC) is an imaging technique that was developed to use texture advection to densely visualize vector fields and render images with a large amount of details. Compared with simpler integration-like techniques, where one follows the flow vector at each point to produce a line, it has the advantage of producing a whole image at every step. The LIC technique has been adapted for SI removal purposes, taking advantage of the fact that SI is coherent.

The input SI vector field has to be as densely sampled as the input shot gather. Missing vectors in $\vec{V}_0^{SI}$ are therefor estimated by spline interpolating over the existing vectors in both time and space direction. This is done in two iterations. If the interpolated samples at each iteration are within the SI range $p \pm \Delta p$, they are averaged. However, the vector sample is discarded if it lies outside the SI moveout range. The final missing vectors after two iterations of interpolation in

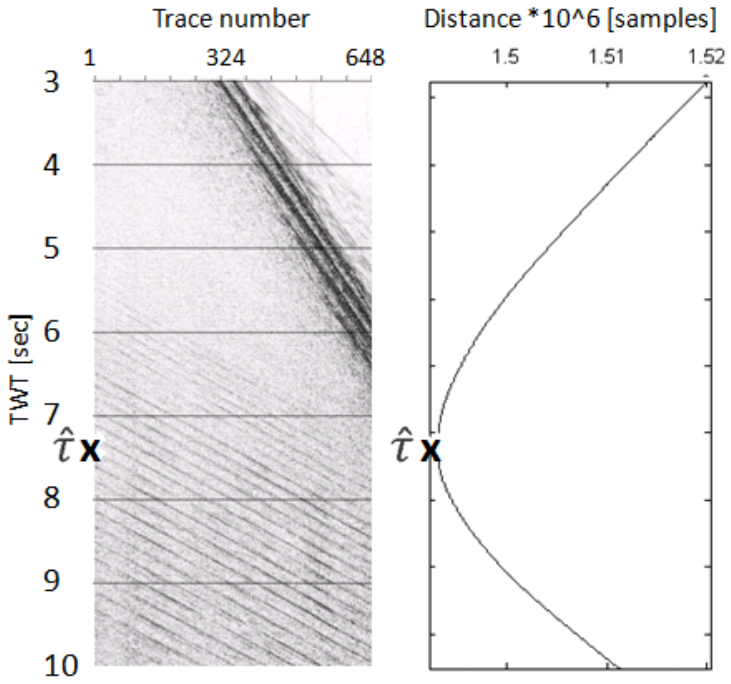

Figure 4.10: SI contaminated shot gather (left) with corresponding distance plot (right). The central arrival time is found at $\hat{\tau}$ and is indicated with a black cross.

space and time are averaged by the surrounding vectors.

For every sample of the input shot gather $D(t, x)$, a local streamline $\vec{r}(s)$ that starts at this center sample is calculated in the forward and backward directions for $2L + 1$ samples, following the input vector field $\vec{V}_0^{SI}$. The output value in $D1(t, x)$ is then the average value of all the amplitudes along this streamline. This relation can be expressed as

$$D1(t,x) = \frac{1}{2L+1} \sum_{-L}^{L} D(\vec{r}(s)) \tag{4.9}$$

Since SI is coherent along the line integral, it adds up constructively. Conversely, the reflection hyperbolas are not coherent over the same line integral and should therefore stack out. LIC filters the input shot gather along local streamlines defined by $\vec{V}_0^{SI}$ to generate a SI model $D1$ in shot domain. This model is then subtracted from the input shot gather D to produce a SI attenuated shot gather.

5. RESULTS

This chapter shows some of the results obtained when the Lupin dataset is processed by the reference τ-p to common-p method, and the two SI removal combinations presented for VF method. Obtained results are commented, while discussion is presented in the following chapter.

Table 5.1: Three sequences of SI contaminated shot gathers from the Lupin dataset.

Sequence	First sequence	Second sequence	Third sequence
Shots	Shot 1-220	Shot 630-750	Shot 751-910
Direction	Abeam	Abeam/aside	Abeam/aside and astern

The Lupin dataset consists of 910 shot gathers of which approximately 55% are considered heavily contaminated by SI. The shot gathers can be subdivided into three sequences depending on the arrival direction of the SI. Each sequence are presented in Table 5.1. Six shot gathers are chosen to illustrate the variety of obtained results by τ-p to common-p and VF method combined with τ-p muting; two from each of the three sequences. These are briefly described in the following list:

7. Presented in Figure 5.2(A). Contain high amplitude linear SI from abeam.

78. Presented in Figure 5.2(D). Contain high amplitude linear SI from abeam.

641. Presented in Figure 5.2(G). Contain low amplitude hyperbolic SI from abeam/aside.

680. Presented in Figure 5.3(A). Contain relatively high amplitude SI from abeam/aside. The SI appear linear at first 400 traces, then curved.

829. Presented in Figure 5.3(D). Contain moderate amplitude hyperbolic SI from abeam/aside and moderate amplitude linear SI from astern.

909. Presented in Figure 5.3(G). Contain moderate to high amplitude hyperbolic SI from abeam/aside and low amplitude linear SI from astern.

First, all 910 shot gathers are processed using the reference τ-p to common-p method, and VF method with τ-p muting. Optimal parameters have been tested for each method. All shots are processed in one sequence by each method and their respective parameters. They are processed in one sequence without changing parameters to ensure more comparable results.

Some residual SI is observed in the shot gathers after VF method with τ-p muting. A combination of the two methods are tested as an attempt of removing the residual SI. Results from all three variations of methods are presented as before, after, and difference plots on the six shot gathers and the stack. Root Mean Square (RMS) values are calculated on before, after, and difference plot of the six shot gathers for each method.

Finally, VF method is combinded with LIC for SI removal. Due to a long processing time, only shot 7 and 909 are processed by VF method in combination with LIC. Instead, the LIC length L is varied to see how this affects the results.

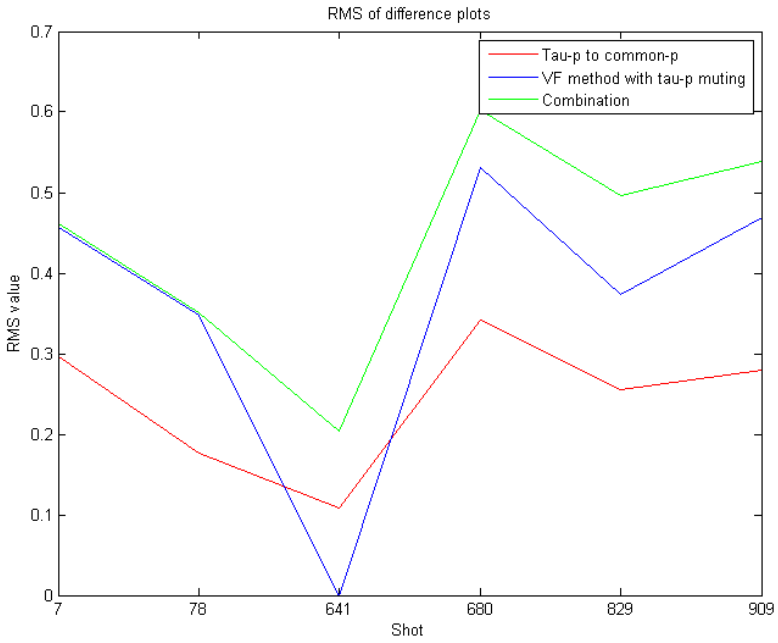

Figure 5.1: Red: RMS plot of difference plots on six shots after τ-p to common-p method. Blue: RMS plot of difference plots on six shot gathers after VF method combined with τ-p muting. Green: RMS plot of difference plots on six shot gathers after VF method with τ-p muting is followed by τ-p to common-p method.

RMS calculations

The RMS value of a $M \times N$ shot gather D is calculated according to Eq. (5):

$$RMS = \sqrt{\frac{\sum_{m=1}^{M} \sum_{n=1}^{N} D(m,n)^2}{MN}}, \tag{5.1}$$

where $m = 1, 2, 3, .., M$, $n = 1, 2, 3, ..., N$ and $D(m, n)$ represents the $M \times N$ dataset. The RMS values are calculated on before, after and difference plots of the six shot gathers from the

Table 5.2: RMS values on before, after and difference plots when τ-p to common-p, VF with τ-p muting, and a combination of the two have been applied on all six shot gathers.

Method	Shot	Before	After	Difference
τ-p to common-p	7	1,5785	1,515	0,296
	78	1,3781	1,3425	0,1762
	641	1,9571	1,9385	0,1085
	680	2,1344	2,0538	0,3418
	829	2,1124	2,0624	0,2556
	909	2,0457	1,9798	0,2793
VF with τ-p muting	7	1,5785	1,5108	0,4572
	78	1,3781	1,3336	0,3474
	641	1,9571	1,9571	0
	680	2,1344	2,0672	0,5311
	829	2,1124	2,079	0,3736
	909	2,0457	1,9914	0,4684
Combining methods	7	1,5785	1,5015	0,4626
	78	1,3781	1,3278	0,3501
	641	1,9571	1,9245	0,2037
	680	2,1344	2,0142	0,6016
	829	2,1124	2,0268	0,4961
	909	2,0457	1,9398	0,5386

three combinations of methods and presented in Table 5.2. Furthermore, are the RMS values from the six difference plots from all three combinations of methods plotted in Figure 5.1.

5.1 τ-p to common-p method

First, all 910 shots are processed in one sequence by using the reference τ-p to common-p method in CGG Veritas' processing software Uniseis. Before, after and difference plots are presented for six of the shot gathers as well as parts of the stack. The parameters used in TFDN are presented in Table 5.3.

Table 5.3: TFDN parameters used in τ-p to common-p method.

Parameter	**Value**
$f_{min}[Hz]$	0
$f_{max}[Hz]$	125
HWIN	50
$t_{len}[ms]$	500
fac_{start}	5.5
fac_{end}	1.8

Figure 5.2 and 5.3 present the results on the six shot gathers, while Figure 5.4 shows the results on the stack. Two squares are superimposed on the stack. A zoom into these sections are

presented in Figure 5.5. RMS values for all six shots have been presented in Table 5.2, while the RMS values from the difference plots of the six shots are plotted in Figure 5.1 (red).

5.1.1 Comments on the results from τ-p to common-p method

The after plot of shot 7 and 78 in Figure 5.2(B) and (E) show that there are some residual SI left after τ-p to common-p method. This is circled in both figures. After plots of shot 641 and 680 from second sequence show varying results. These are presented in Figure 5.2(H) and 5.3(B). The difference plot of shot 641 (I) shows that little SI has been removed compared to shot 680 (C). However, the amplitude of the SI is significantly lower in shot 641 compared to 680. The RMS values for shot 641 and 680 in Table 5.2 may verify these observations, showing that the RMS value of shot 641 is lower then shot 680 before τ-p to common-p method. Shot 829 and 909 in Figure 5.3(E) and (H) from the final sequence show that SI from astern has been sufficiently removed, while some SI from abeam/aside is still present. The residual SI is circled in both figures.

The difference plots of the two sections from the stacks in Figure 5.5(E) and (F) show that some coherent SI has been removed. Three squares are superimposed to indicate the SI in the stacks.

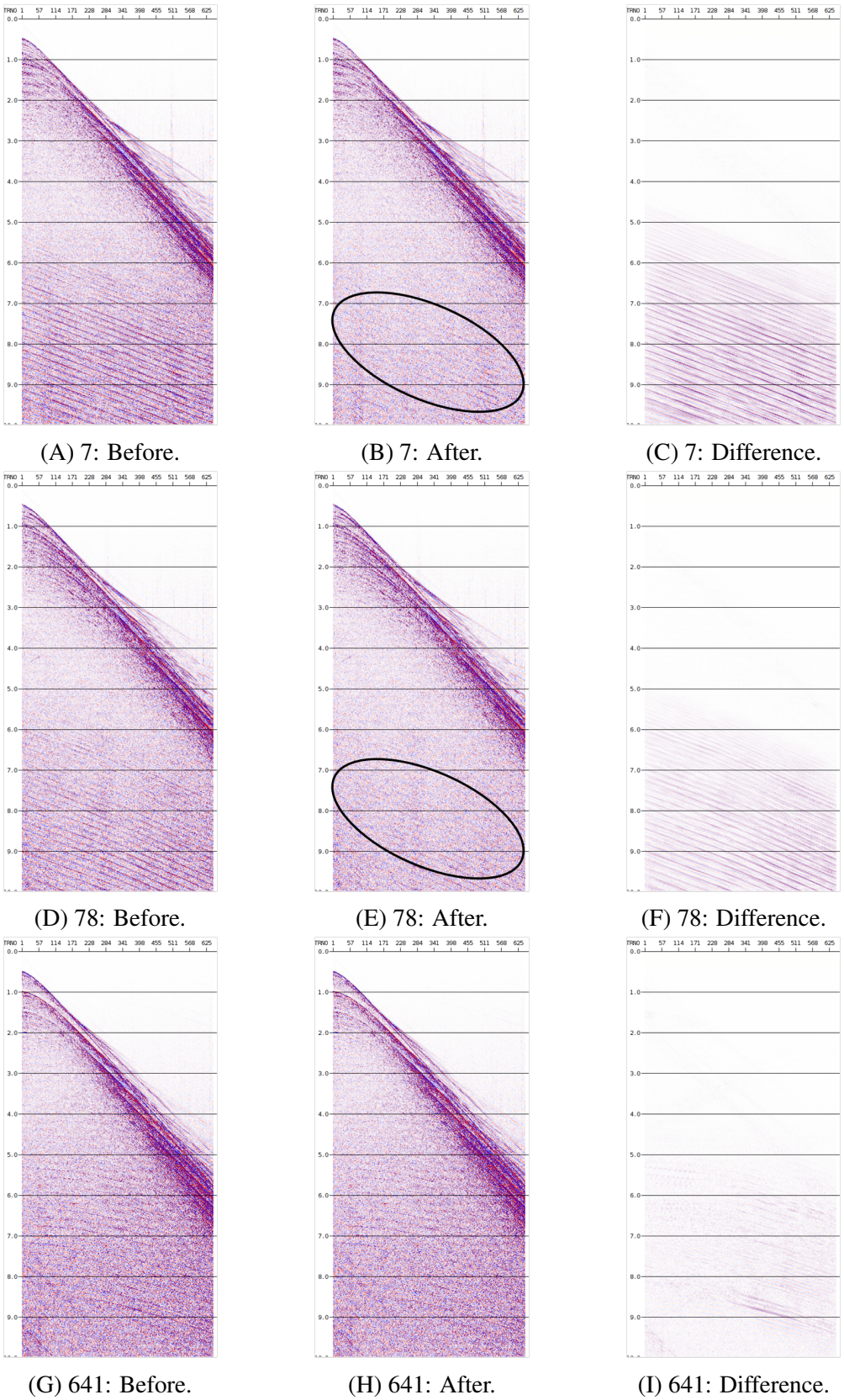

(A) 7: Before. (B) 7: After. (C) 7: Difference.

(D) 78: Before. (E) 78: After. (F) 78: Difference.

(G) 641: Before. (H) 641: After. (I) 641: Difference.

Figure 5.2: Before (left column), after (middle column) and difference plot (right column) for shot 7, 78 and 641 when applying τ-p to common-p method.

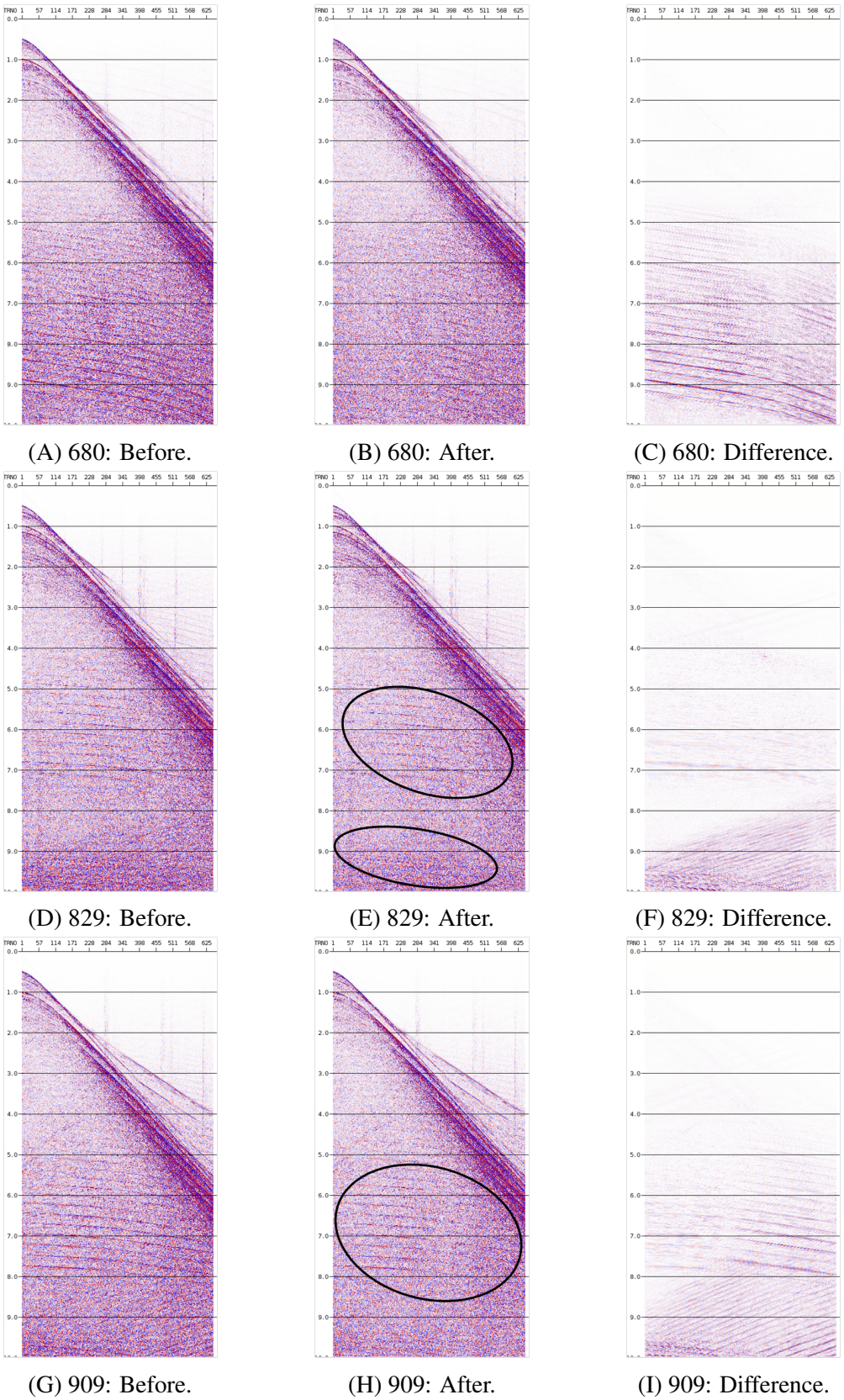

(A) 680: Before. (B) 680: After. (C) 680: Difference.

(D) 829: Before. (E) 829: After. (F) 829: Difference.

(G) 909: Before. (H) 909: After. (I) 909: Difference.

Figure 5.3: Before (left column), after (middle column) and difference plot (right column) for shot 680, 829 and 909 after applying τ-p to common-p method.

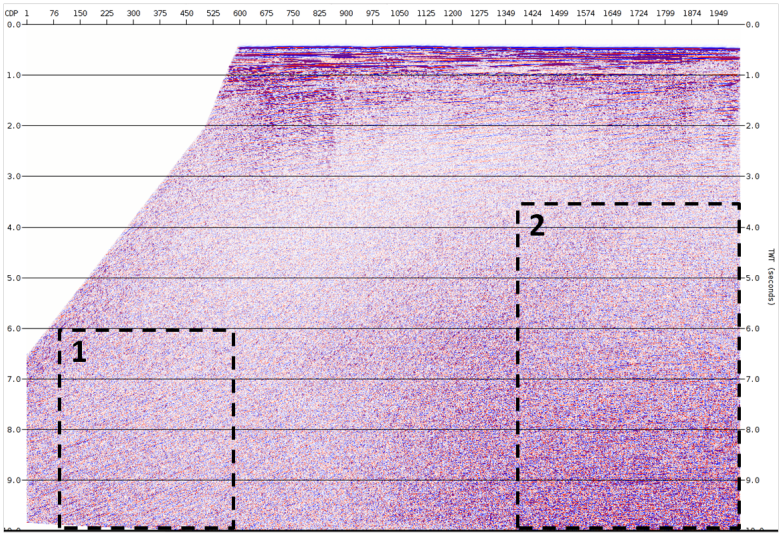

(A) Stack before τ-p to common-p method.

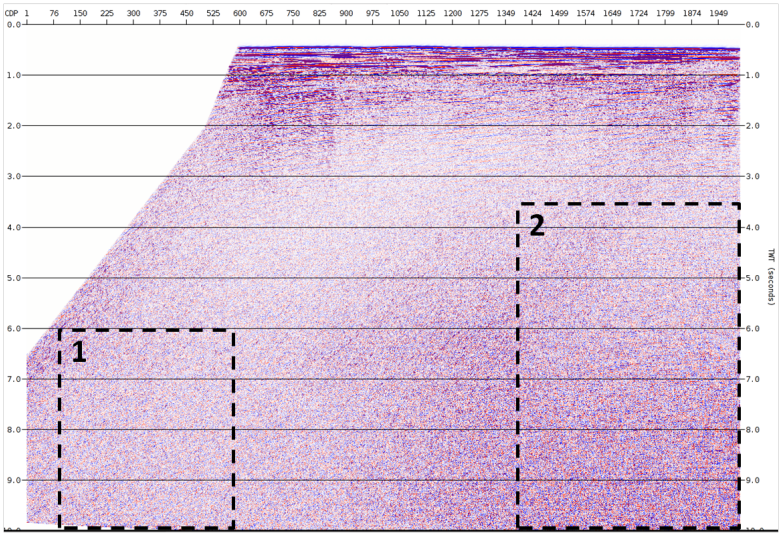

(B) Stack after τ-p to common-p method.

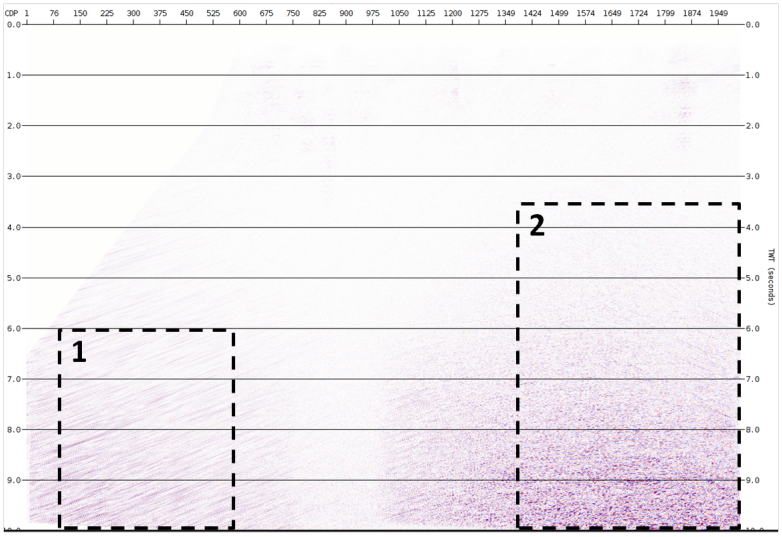

(C) Difference after τ-p to common-p method.

Figure 5.4: Before, after and difference of stack when τ-p to common-p method is applied to the dataset.

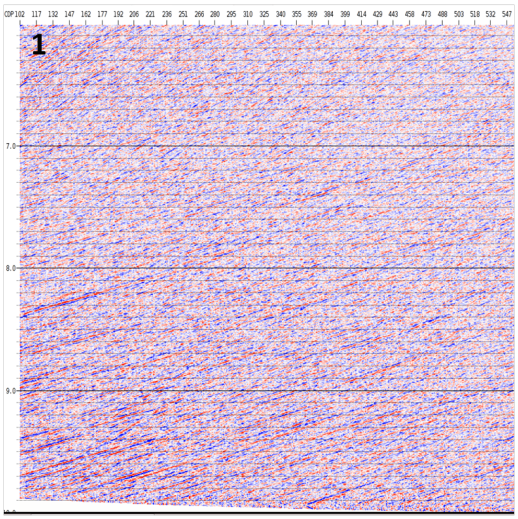

(A) 1: Stack before τ-p to common-p.

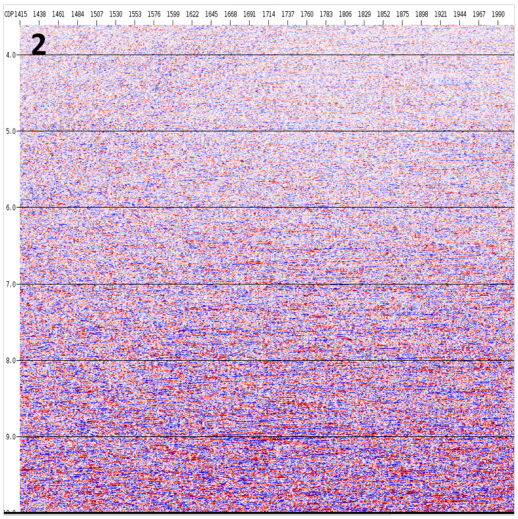

(B) 2: Stack before τ-p to common-p.

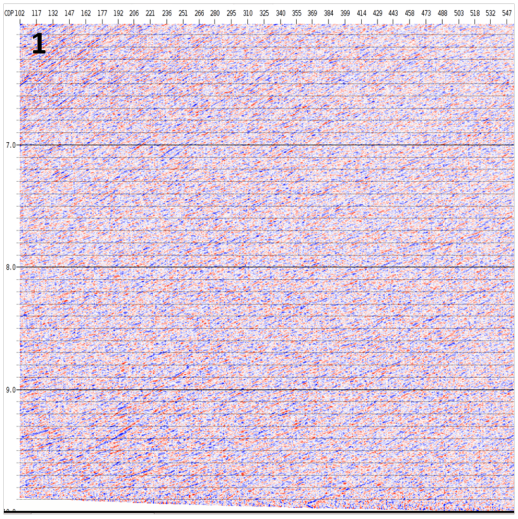

(C) 1: Stack after τ-p to common-p.

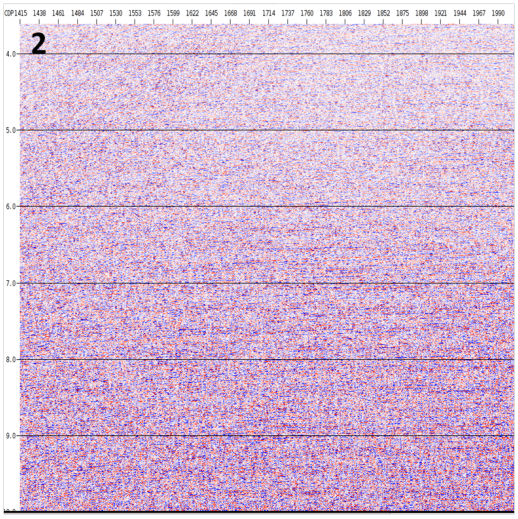

(D) 2: Stack after τ-p to common-p.

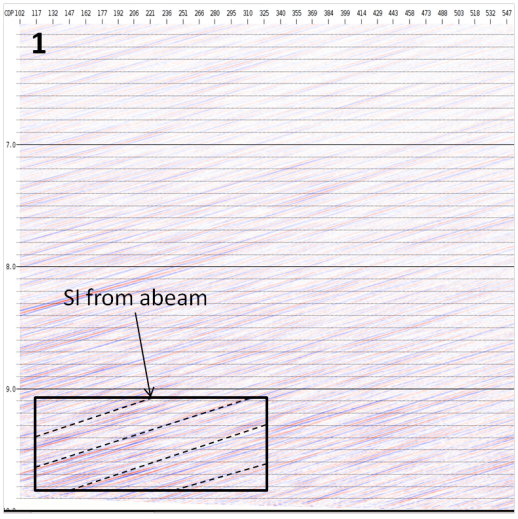

(E) 1: Difference τ-p to common-p.

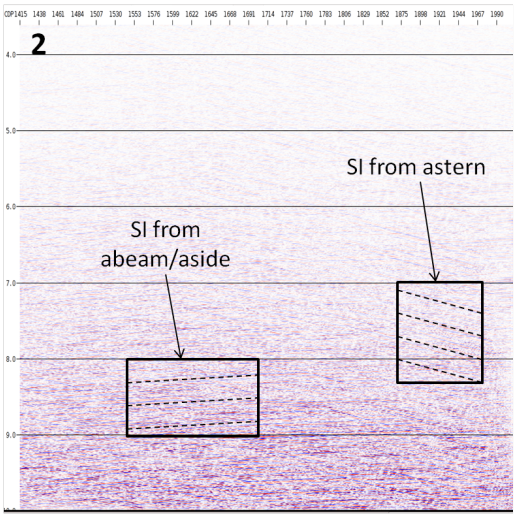

(F) 2: Difference after τ-p to common-p.

Figure 5.5: Before, after and difference of section 1 (left column) and 2 (right column) indicated in Figure 5.4 when τ-p to common-p method is applied to the dataset.

5.2 VF method with τ-p muting

In this section VF method with τ-p muting is tested. All 910 shots are processed by VF method in MATLAB, with τ-p mutes as output. The parameters used in VF method are presented in Table 5.4. Finally, the shots are τ-p transformed and muted in CGG Veritas' processing software Uniseis according to the generated mutes. Before, after and difference plots of the six considered shot gathers are presented in Figure 5.6 and 5.7. Calculated RMS values for each plot after VF method with τ-p muting are shown in in Table 5.2, and RMS values for the difference plots are shown in Figure 5.1 (blue). Results on the stack is presented in Figure 5.8. A zoom into the squares indicated on the stacks are presented in Figure 5.9.

Table 5.4: Parameters used in VF method.

Parameter	**Value**
S	0.7
J	10
$intfac$	10
Min/max mout	$\pm$ 2.1 samples/traces
$\Delta\hat{p}$	$\pm$ 300 ms
$indexTHRS$	0.2
$numbTHRS$	0.0232
$ampTHRS$	0.0159
$stdTHRS$	21.1

5.2.1 Comments on results from VF method with τ-p muting

The six shot gathers presented in Figure 5.6 and 5.7 show varying results with VF method combined with τ-p muting. After plot of shot 7 and 78 in Figure 5.6(B) and (E) show that more linear SI has been removed then by using the reference τ-p to common-p method (see Figure 5.2(B) and (E)). The RMS plot of the difference plot in Figure 5.1 substantiates this observation, showing that VF method with τ-p muting (blue) has removed more SI from these shots then the reference τ-p to common-p method (red).

Comparing shot 641 and 680 in Figure 5.6(H) and 5.7(B) show great differences after VF method with τ-p muting. Difference plot of shot 641 in Figure 5.6(I) shows that VF has not identified any SI, and therefore not removed any. This can also be observed in the RMS plot in Figure 5.1, showing that no data has been removed. The difference plot of shot 680 in Figure 5.7(C) shows that the near offset linear SI has been removed and the more hyperbolic SI at far offset still remains. The remaining hyperbolic SI for shot 680 is circled in both after (B) and difference plot (C).

Comparing the difference plot of shot 680 after VF method with τ-p muting to the difference plot after the reference τ-p to common-p method (see Figure 5.3(C)) shows that more near offset linear SI has been removed, while less far offset hyperbolic SI. The RMS plot of the difference plot of shot 680 in Figure 5.1 show that more data has been removed by VF method with τ-p muting then the reference τ-p to common-p method.

Difference plots of the final two shot gathers in Figure 5.7(F) and (I) show that only SI from abeam/aside have been removed. Furthermore, it is observed that only the middle part of the hyperbolic SI in shot 829 (F) has been removed, while the whole curve of the hyperbolic SI in shot gather 909 (I) is removed. The remaining SI from astern in both shots, and abeam/aside at near offset in shot 829, is circled in the after plot of both shots (see Figure 5.7(E) and (H)). The difference plots of these shots after the reference τ-p to common-p method in Figure 5.3(F) and (I) show that more SI from astern was removed compared to using VF method with τ-p muting. However, the RMS plot in Figure 5.1 shows that VF method with τ-p muting removed more data, specially SI from abeam/astern.

Difference plots of the sections on the stack (see Figure 5.9(E) and (F)) show similar features as presented for the τ-p to common-p method in Figure 5.5(E) and (F). However, the second section (F) shows that no SI from astern has been removed. The SI from abeam in first section (E) and abeam/astern (F) in second section of the stack are indicated in superimposed squares.

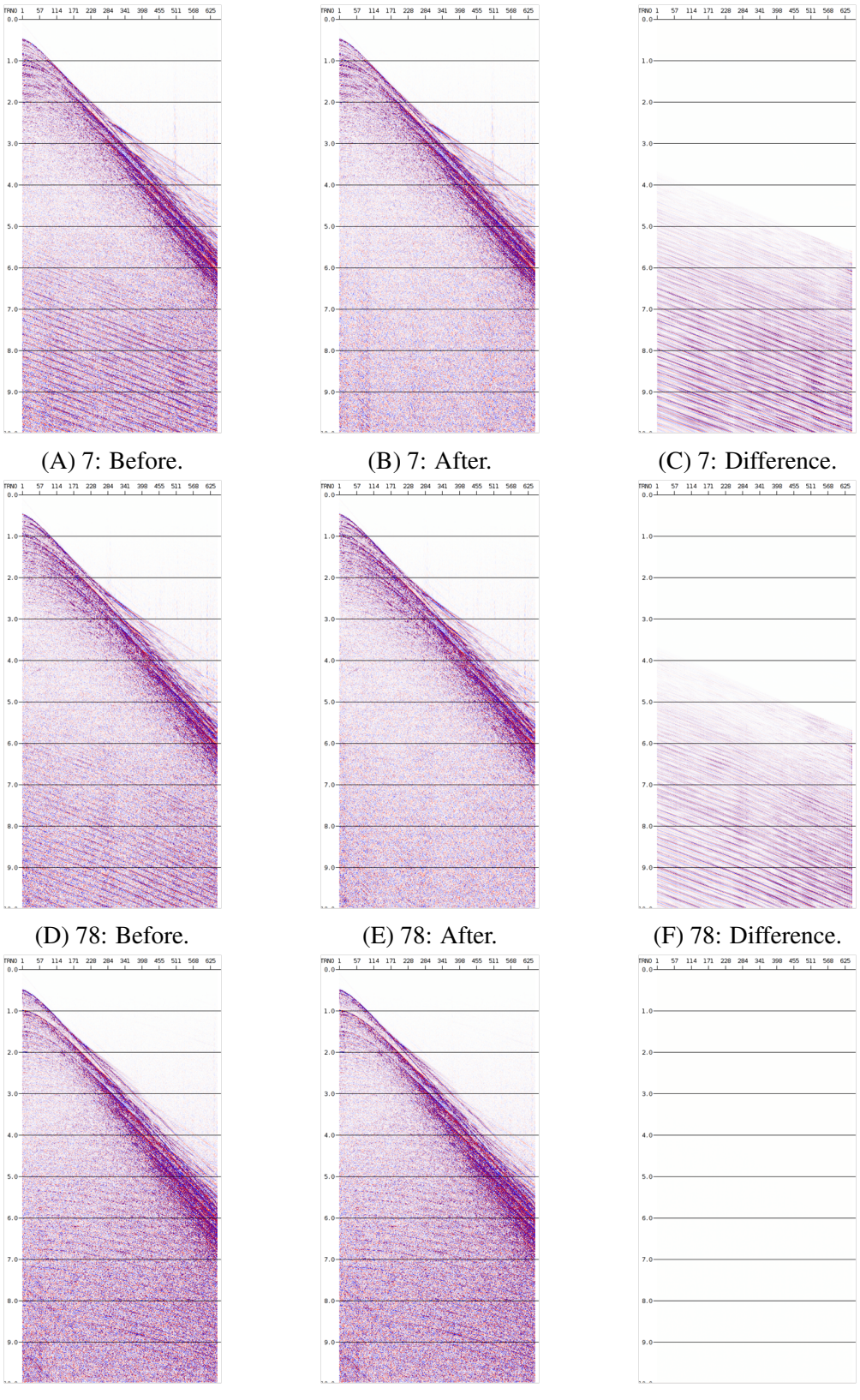

(A) 7: Before. (B) 7: After. (C) 7: Difference.

(D) 78: Before. (E) 78: After. (F) 78: Difference.

(G) 641: Before. (H) 641: After. (I) 641: Difference.

Figure 5.6: Before (left column), after (middle column) and difference plot (right column) for shot 7, 78 and 641 after applying the VF method and τ-p muting.

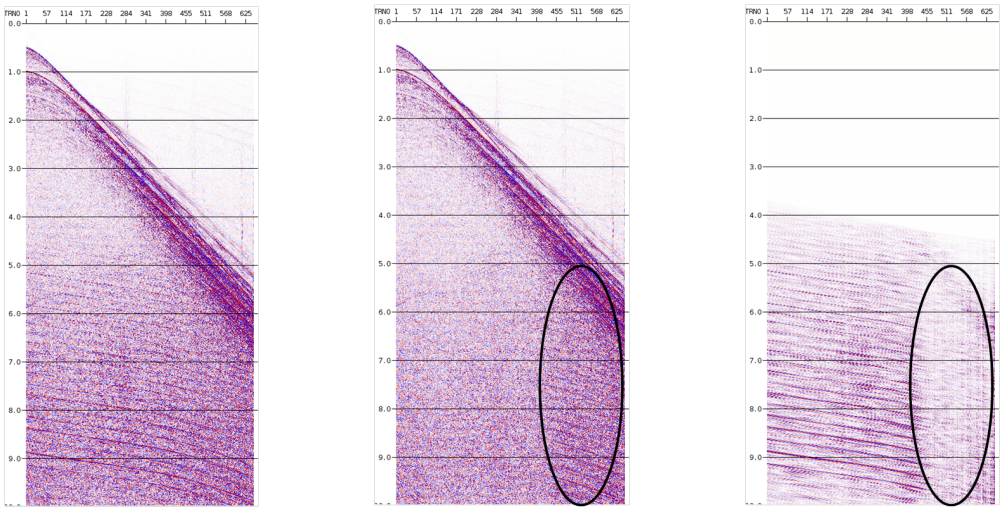

(A) 680: Before. (B) 680: After. (C) 680: Difference.

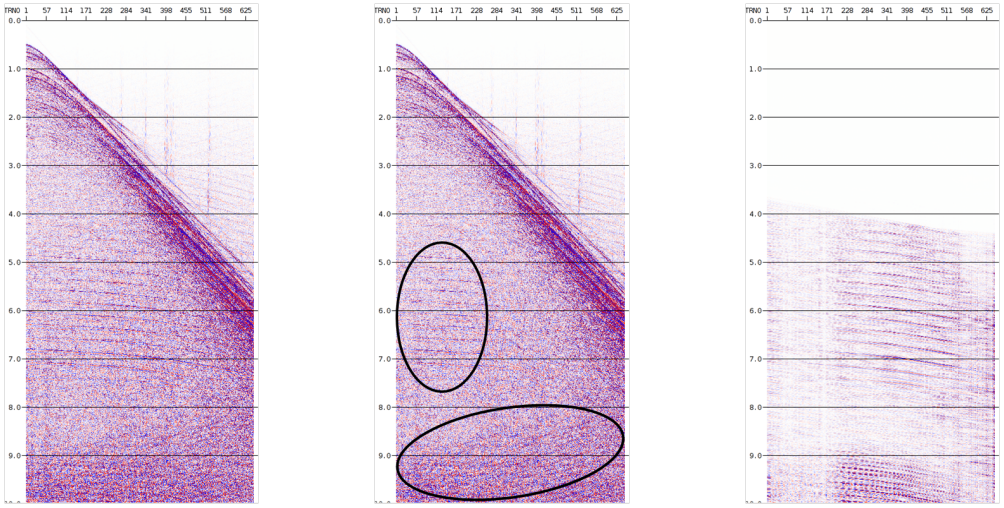

(D) 829: Before. (E) 829: After. (F) 829: Difference.

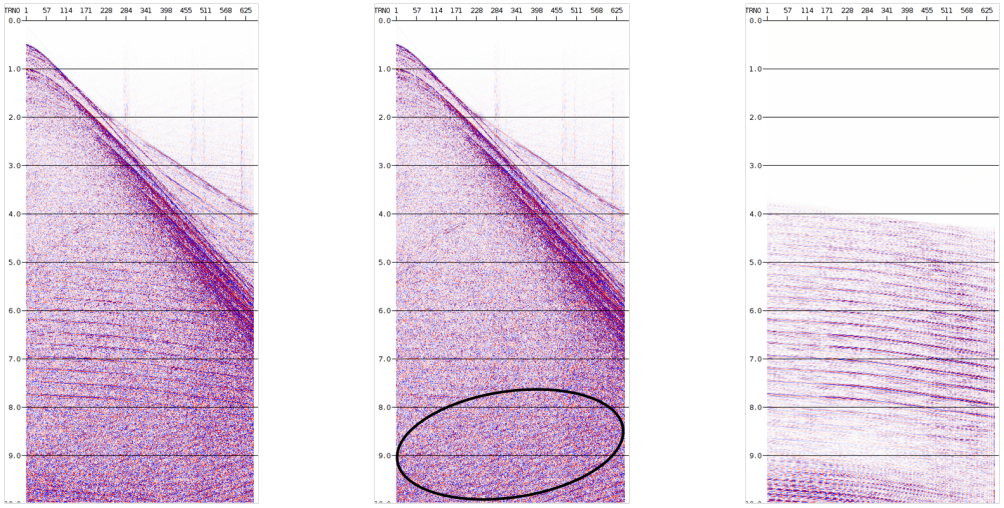

(G) 909: Before. (H) 909: After. (I) 909: Difference.

Figure 5.7: Before (left column), after (middle column) and difference plot (right column) for shot 680, 829 and 909 after applying the VF method and τ-p muting.

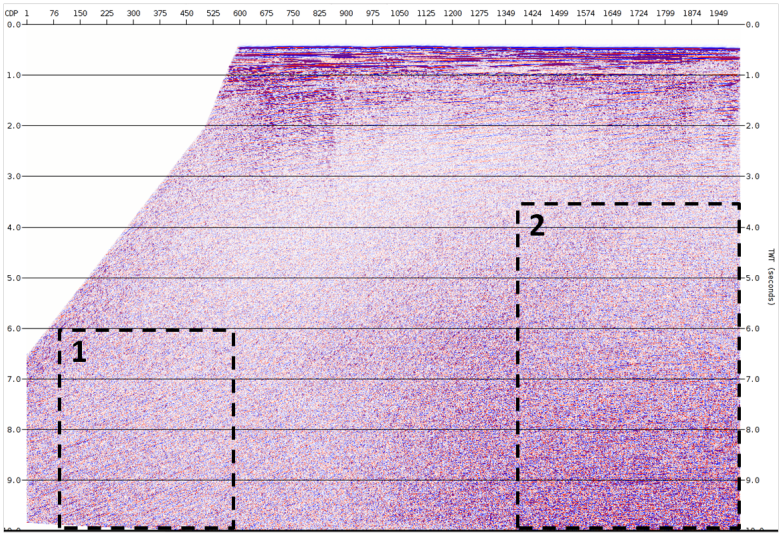

(A) Stack before VF method.

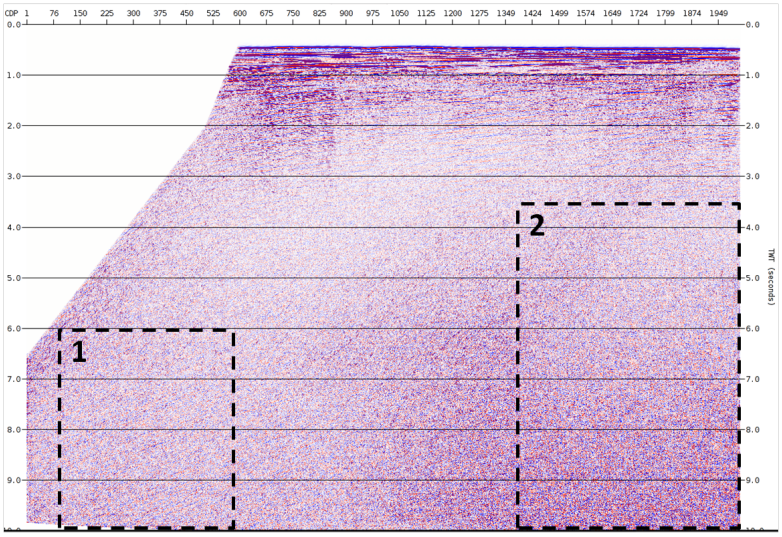

(B) Stack after VF method.

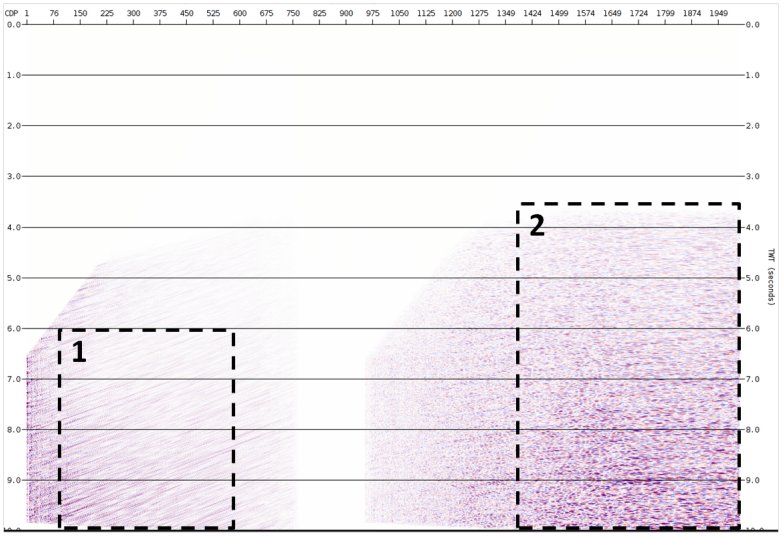

(C) Difference after VF method.

Figure 5.8: Before, after and difference of stack when VF method and τ-p muting is applied to the dataset.

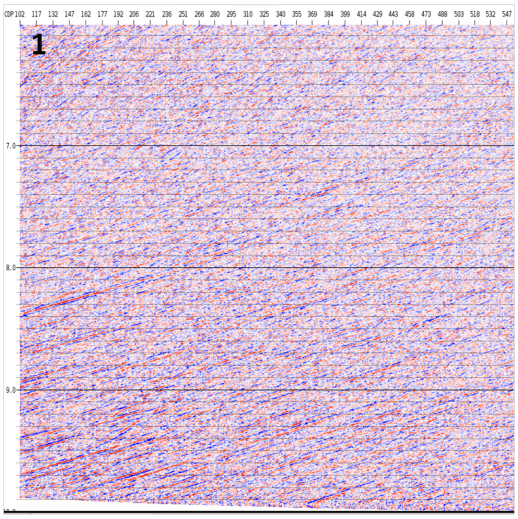

(A) 1: Before VF method.

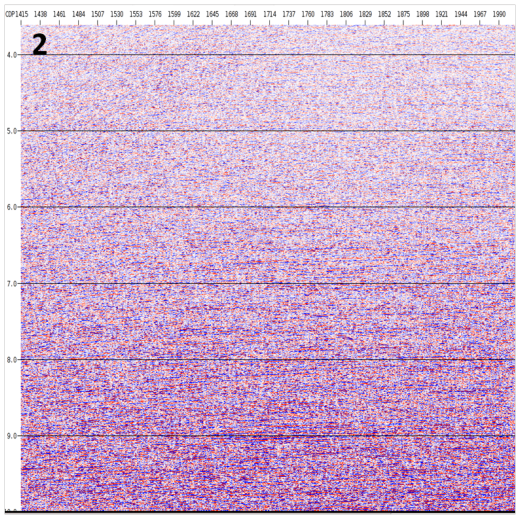

(B) 2: Before VF method.

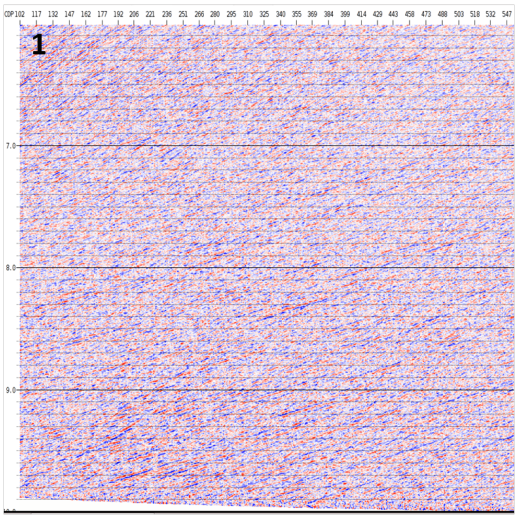

(C) 1: After VF method.

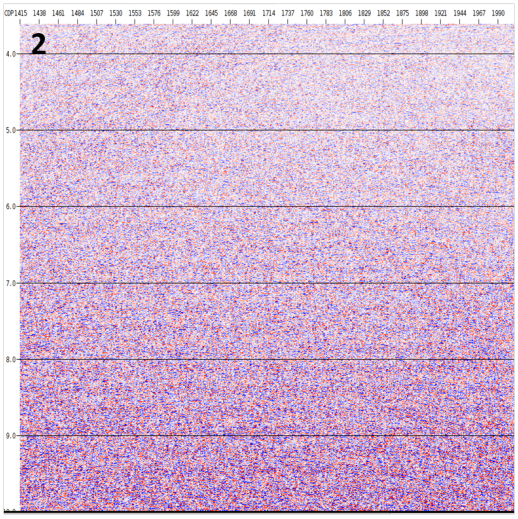

(D) 2: After VF method.

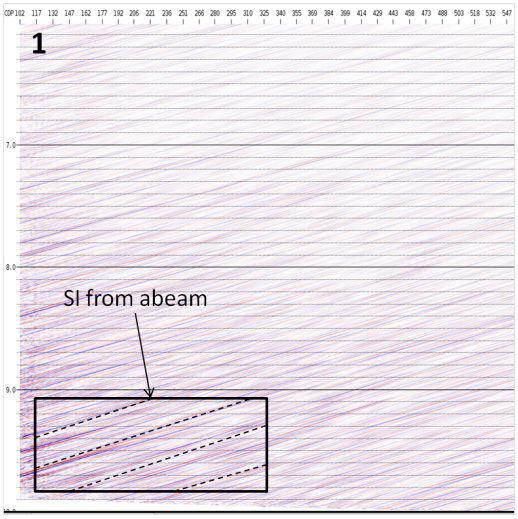

(E) 1: Difference after VF method.

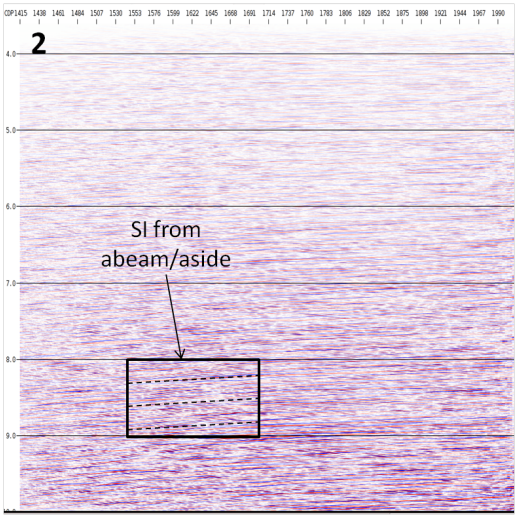

(F) 2: Difference after VF method.

Figure 5.9: Before, after and difference of section 1 (left column) and 2 (right column) indicated in Figure 5.8 when the VF method combined with τ-p muting is applied to the dataset.

5.3 First VF with τ-p muting, then τ-p to common-p method.

As an experimental approach, a combination of VF method with τ-p muting and τ-p to common-p method is tested. First, the dataset is processed by VF method with τ-p muting according to the parameters presented in Table 5.4. Residual SI is observed in some of the shot gathers. As an attempt of removing this, the dataset is processed further by the reference τ-p to common-p method according to the parameters presented for TFDN in Table 5.3.

Before, after and difference plots are presented for the six chosen shot gathers in Figure 5.11 and 5.12. RMS values have been been calculated in before, after and difference for all six shots when VF method with τ-p muting is followed by τ-p to common-p method. These are presented in presented in Table 5.2, and the RMS values from the difference plots have been plotted in Figure 5.1 (green).

Results on the stack are presented in Figure 5.13 and 5.14. Difference plot illustrating the effect of the final τ-p to common-p method is added in all figures.

5.3.1 f-k plots of shot 909

f-k plots are good for visualizing waves with different moveout and amplitude in shot domain. Therefore, the f-k plot of the unprocessed shot 909 with SI from abeam/aside and astern is presented in Figure 5.10 (A). The reflection data, two occurrences of SI, and the swell noise is circled in the figure. Furthermore, does the figure show the f-k plot of the corresponding shot after τ-p to common-p (B), after VF with τ-p muting (C), and after VF method with τ-p muting follow by τ-p to common-p method (D). Each f-k plot shows which data remains after each method. These results are commented in the following subsection, and furthermore discussed in the next chapter.

5.3.2 Comments on results when combining methods

The fourth column in Figure 5.11 and 5.12 show the effect of the final τ-p to common-p step on the shot gathers. Three observations are made. First, it is observed that no data is removed by τ-p to common-p method on shot 7 and 78 in Figure 5.11(D) and (H) when VF method with τ-p muting have successfully removed the SI. The RMS plot in Figure 5.1 of the difference plots substantiate these observations, showing that no extra data has been removed by the final τ-p to common-p step (green), compared to only using the VF method with τ-p muting.

Secondly, it is observed that more SI have been removed from shot 641 in Figure 5.11(L) when VF method with τ-p muting is followed by τ-p to common-p method, compared to only using

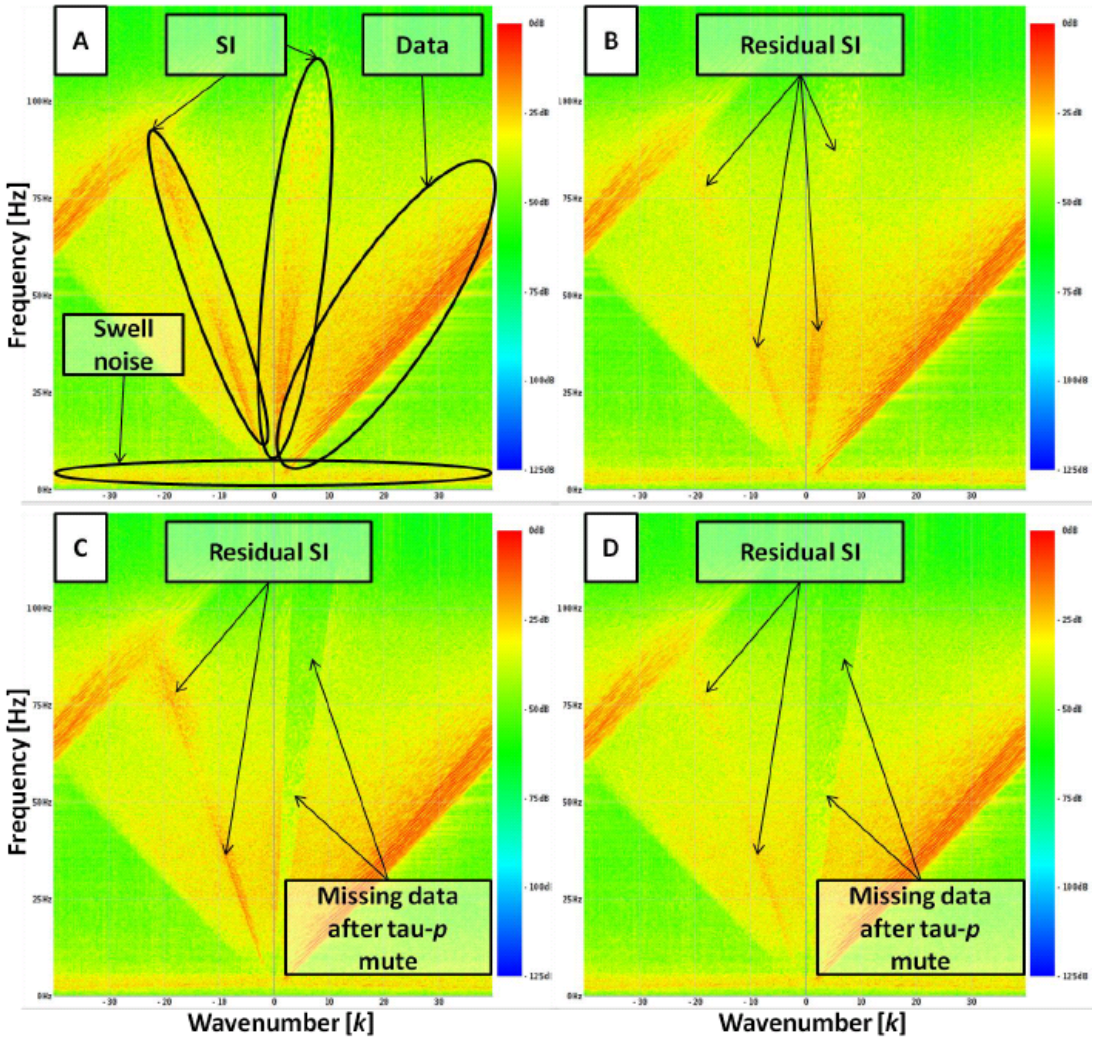

Figure 5.10: A: f-k transform of shot 909 presented in Figure 5.7(G). B: f-k transform of shot 909 after τ-p to common-p method. C: f-k transform of shot 909 after VF method with τ-p muting. D: f-k transform of shot 909 after VF method with τ-p muting is followed by τ-p to common-p method.

τ-p to common-p method in Figure 5.2(I). This is an interesting observation due to the fact that VF method combined with τ-p muting was not able to identify any SI in the respective shot (see Figure 5.6(I)). Therefore, one should expect to see similar results as when simply using the reference τ-p to common-p method. The RMS plot in Figure 5.1 verify the observation, showing that a combination of the two methods remove significantly more SI from shot 641 compared to using only using the reference τ-p to common-p method. Somehow, VF method with τ-p muting compliment the reference τ-p to common-p method. This observation is discussed further in the discussion chapter.

Results on shot 680 and 909 show another way these methods compliment each other. Shot 648 in Figure 5.12(D) shows that τ-p to common-p method remove the far offset hyperbolic SI (circled) which VF method with τ-p muting is unable to remove in Figure 5.7(C). Also, τ-p to common-p method is able to remove remaining SI from abeam/aside and astern in shot

829 and 909 in Figure 5.12(H) and (L) compared to only using VF method with τ-p muting in Figure 5.7(F) and (I). This SI is indicated by circles in both figures. Investigating the f-k plots of shot 909 in Figure 5.10 (B) shows that residual SI exists after the reference τ-p to common-p method. Specially the SI from abeam/aside. Furthermore, it is observed that VF method with τ-p muting successfully removes the SI from abeam/aside (C), and fail to remove the SI from astern. The final f-k plot illustrating the effect when combining the methods (D) shows that the SI from abeam/aside has been successfully muted by VF method with τ-p muting, while the SI from astern is attenuated by the final τ-p to common-p method.

The RMS plot in Figure 5.1 substantiates the observation that the final τ-p to common-p method has been able to remove some of residual SI which VF method combined with τ-p muting could not remove. It shows that more data has been removed from both shot gathers.

The two difference plots of the sections of the stack in Figure 5.14(E) and (F) show that more SI have been removed by using a combination of the two methods compared to simply using τ-p to common-p in Figure 5.5(E) and (F) or VF method with τ-p muting in Figure 5.9(E) and (F). The plot illustrating the effect of the final τ-p to common-p method in Figure 5.14(G) and (H) show that some extra coherent SI have been removed from both shot gather. Specially the SI from astern i the second section (H). This SI is indicated in the superimposed square.

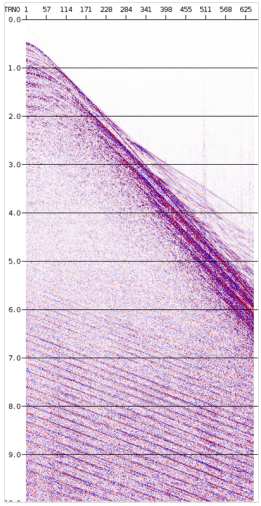

(A) 7: Before.

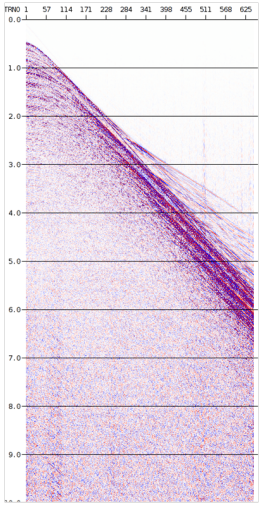

(B) 7: After.

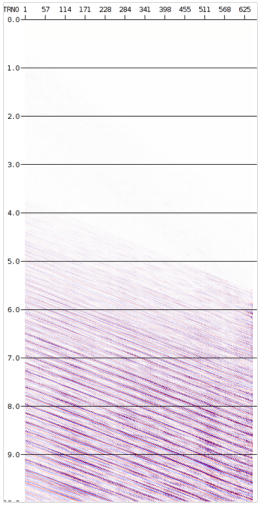

(C) 7: Difference.

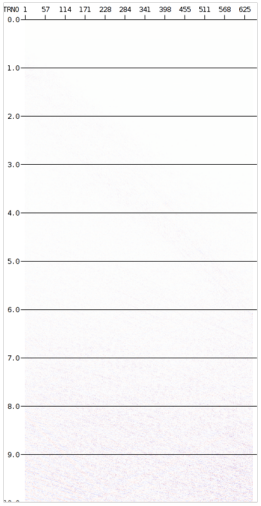

(D) 7: Effect of final step.

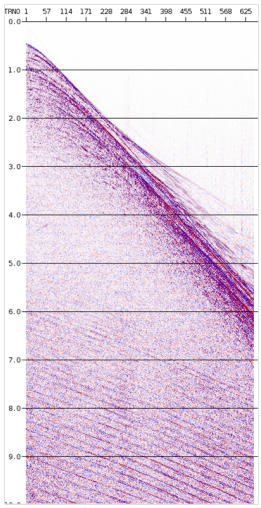

(E) 78: Before.

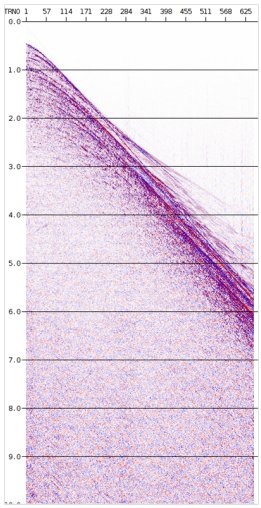

(F) 78: After.

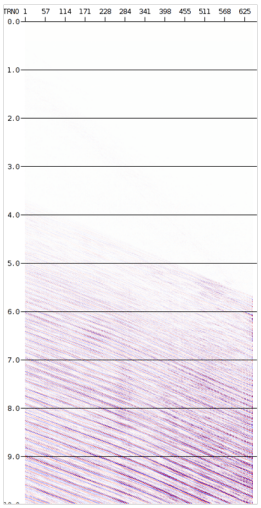

(G) 78: Difference.

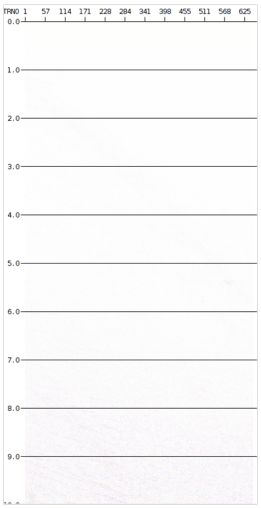

(H) 78: Effect of final step.

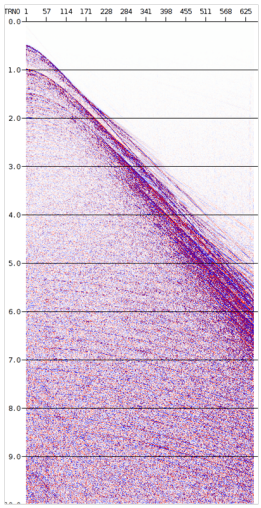

(I) 641: Before.

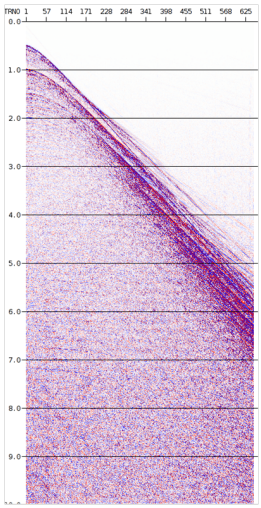

(J) 641: After.

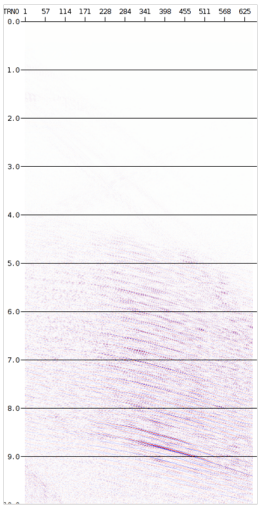

(K) 641: Difference.

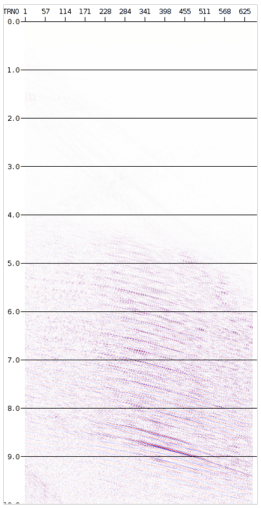

(L) 641: Effect of final step.

Figure 5.11: Before (first column), after (second column) and difference plot (third column) for shot 7, 78 and 641 after applying the VF method and τ-p muting followed by the τ-p to common-p method. Fourth column show the effect of the final τ-p to common-p method on the shot gathers.

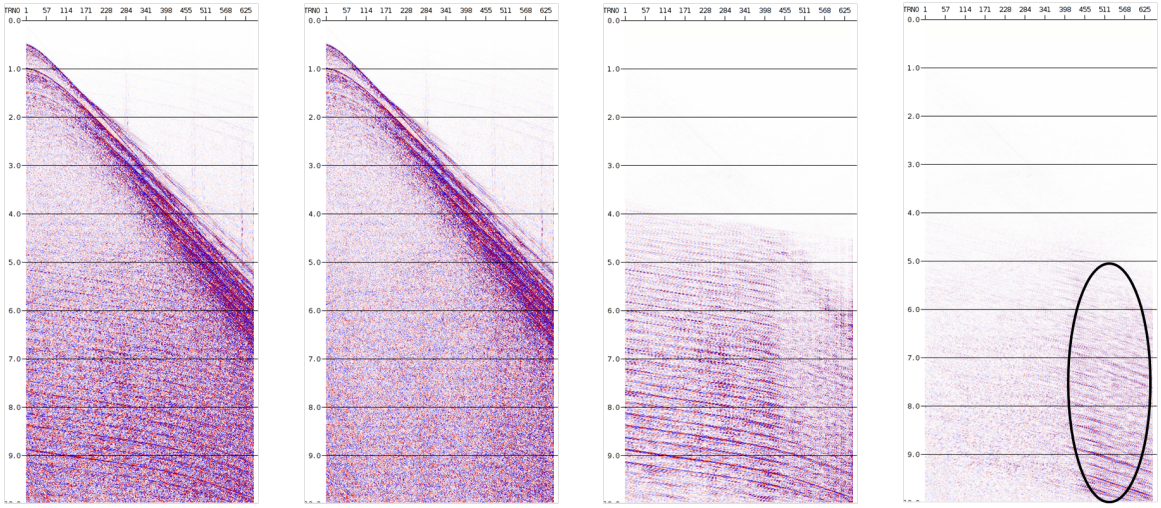

(A) 680: Before. (B) 680: After. (C) 680: Difference. (D) 680: Effect of final step.

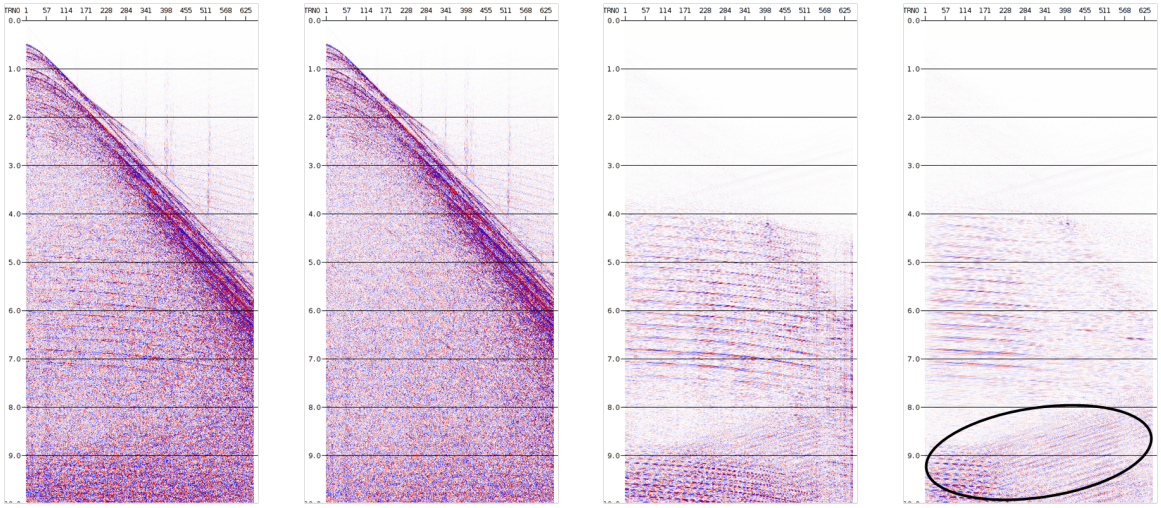

(E) 829: Before. (F) 829: After. (G) 829: Difference. (H) 829: Effect of final step.

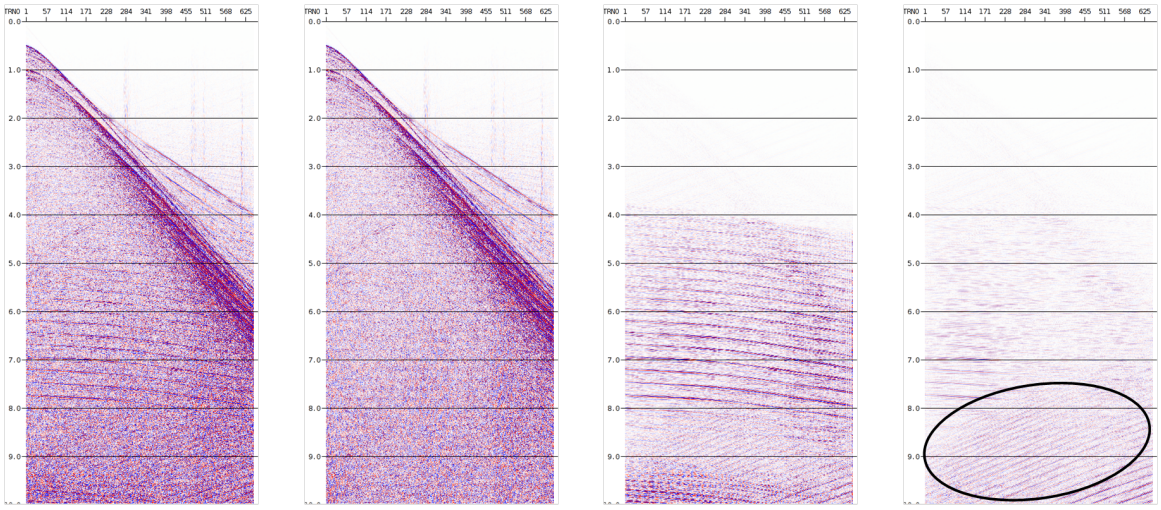

(I) 909: Before. (J) 909: After. (K) 909: Difference. (L) 909: Effect of final step.

Figure 5.12: Before (first column), after (second column) and difference plot (third column) for shot 680, 829 and 909 after applying the VF method and τ-p muting followed by the τ-p to common-p method. Fourth column show the effect of the final τ-p to common-p method on the shot gathers.

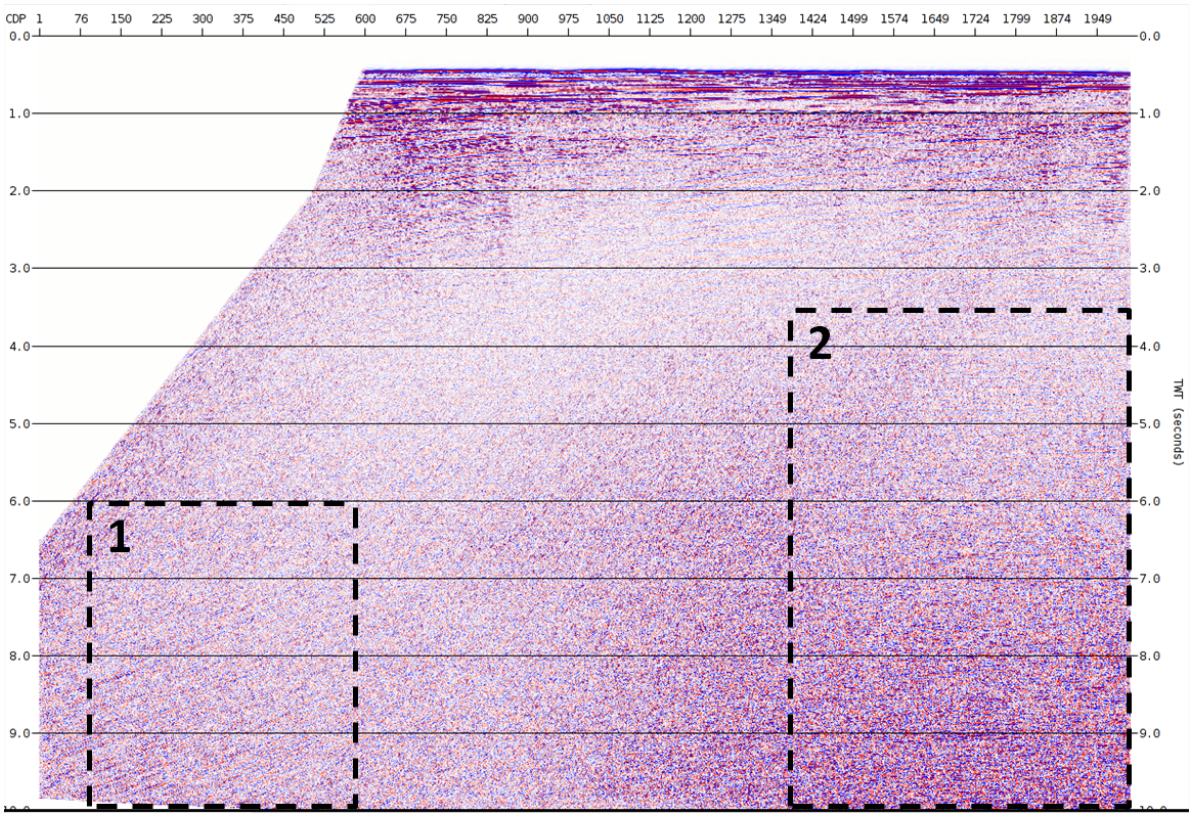

(A) Stack before applying VF and τ-p to common-p method.

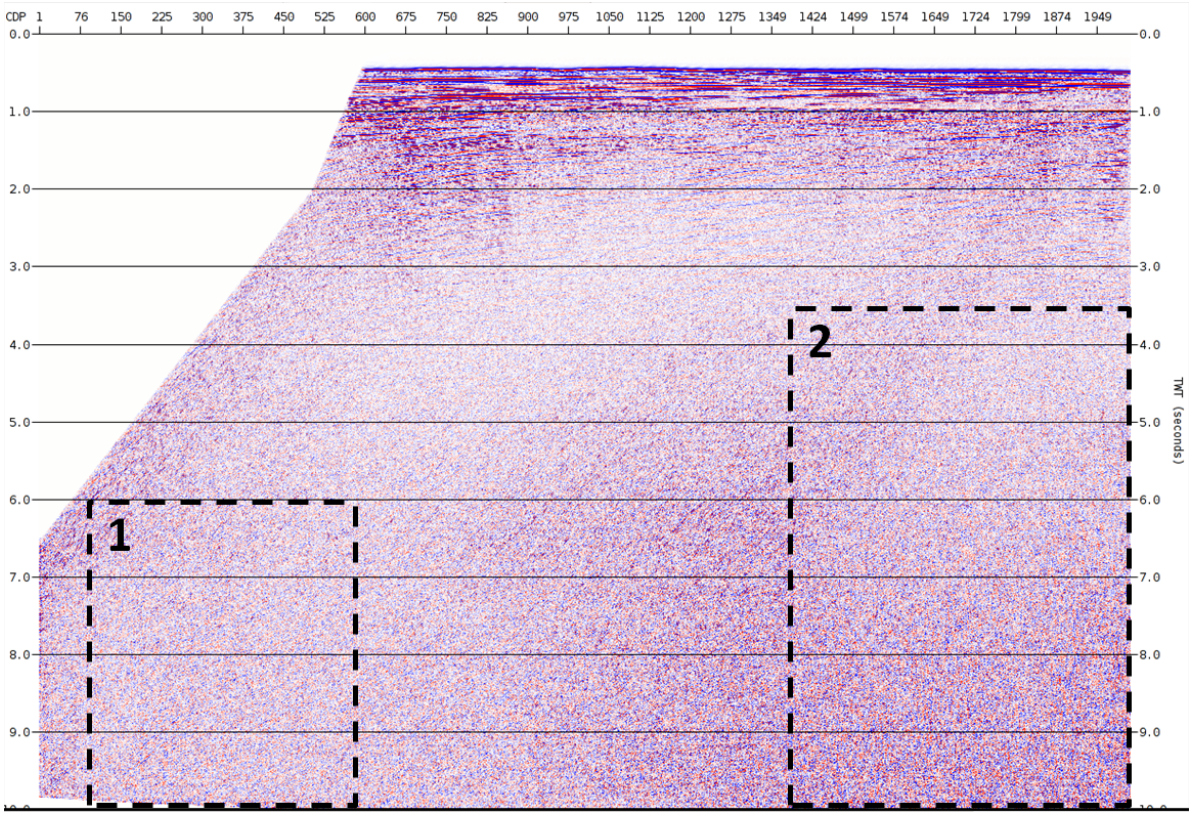

(B) Result after VF followed by τ-p to common-p method.

Figure 5.13: First part (second part continue on next page) of figure illustrating the effect on the stack when applying VF method followed by τ-p to common-p method on the dataset.

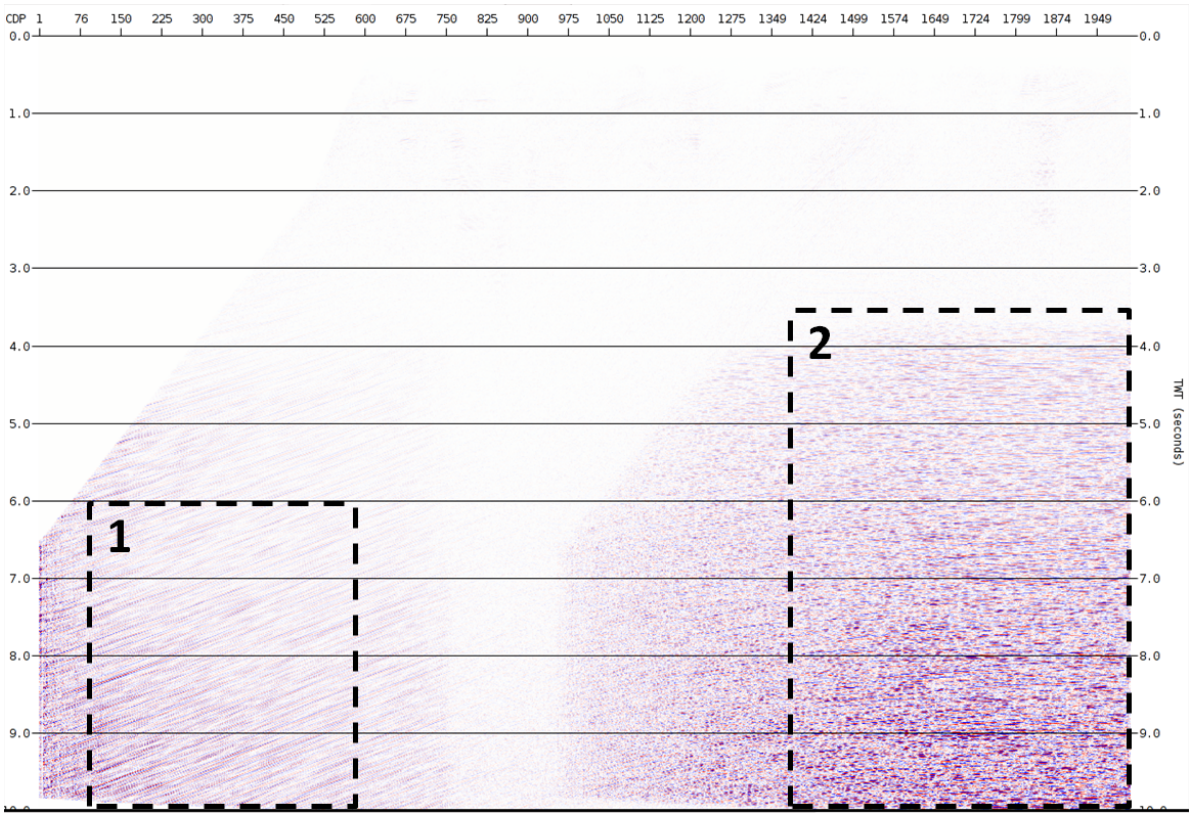

(C) Difference plot after VF followed by τ-p to common-p method.

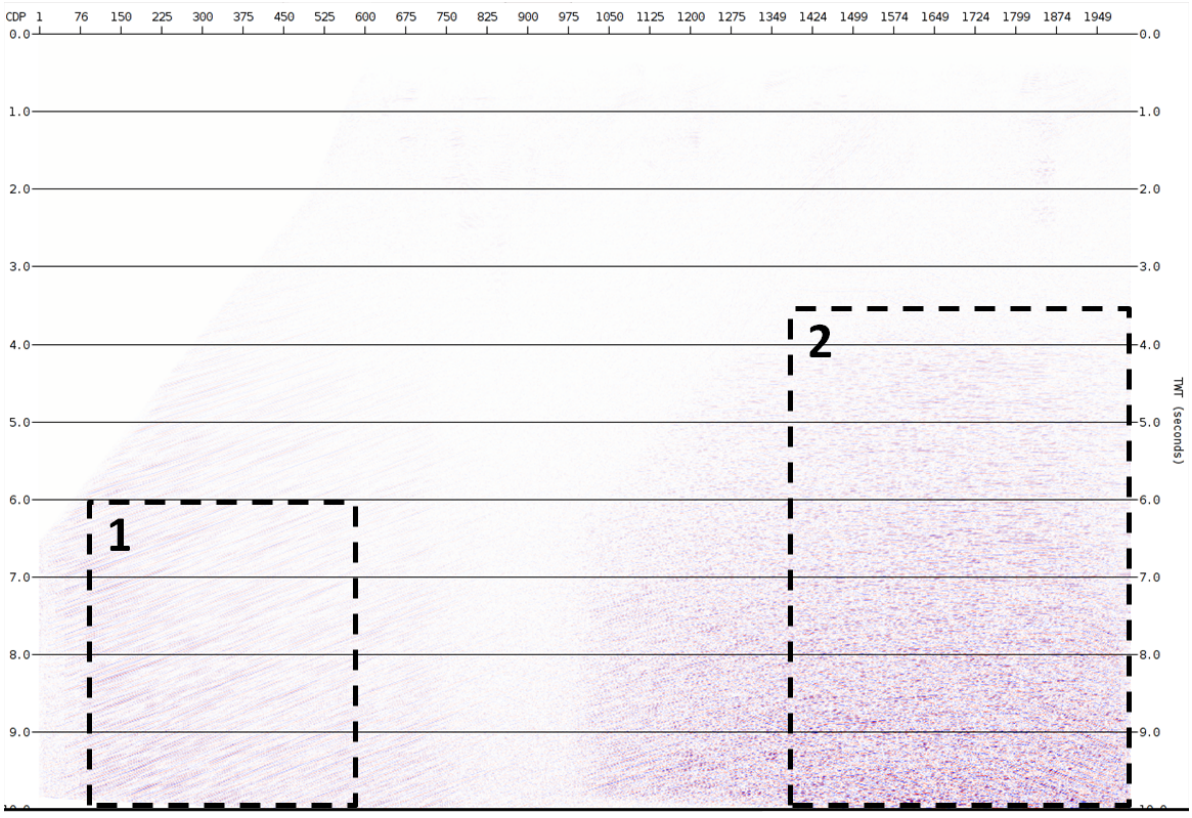

(D) Difference plot showing the effect of the final τ-p to common-p method.

Figure 5.13: Last part (first part on previous page) of figure illustrating the effect on the stack when applying VF method followed by τ-p to common-p method on the dataset.

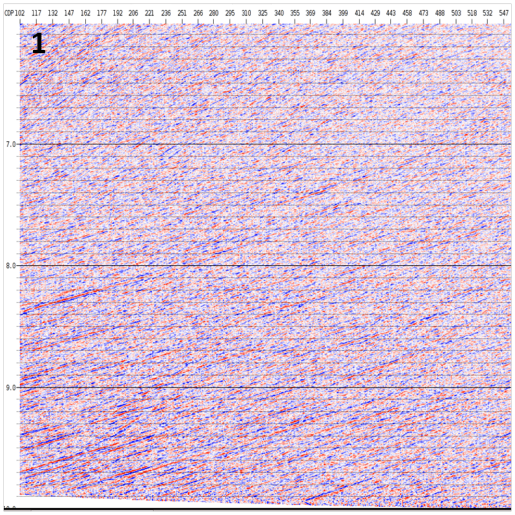

(A) 1: Before VF + τ-p to common-p method.

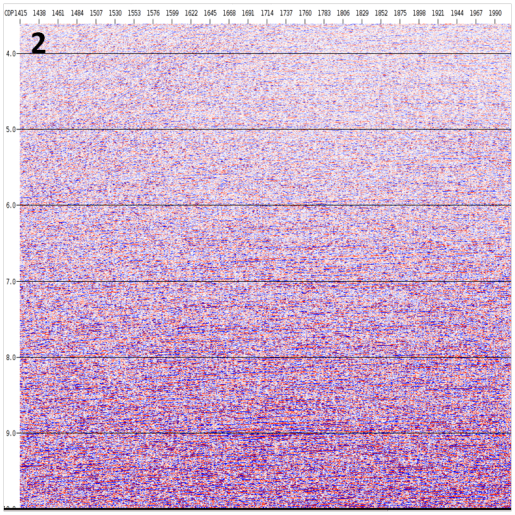

(B) 2: Before VF + τ-p to common-p method.

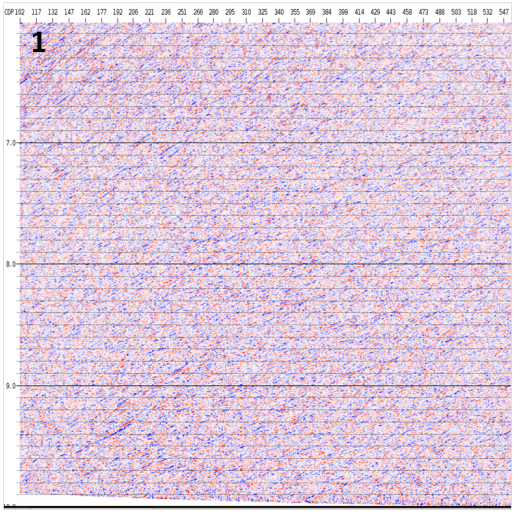

(C) 1: After VF + τ-p to common-p method.

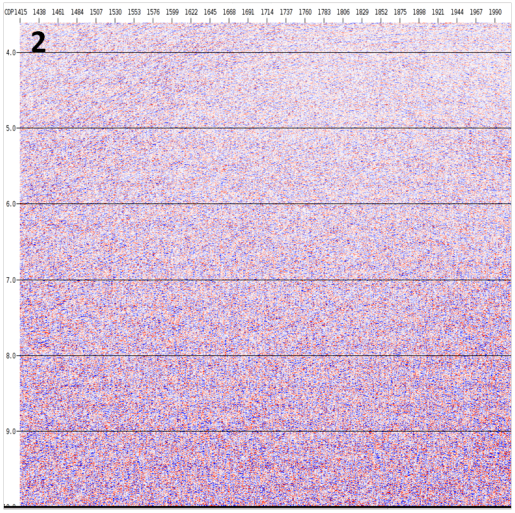

(D) 2: After VF + τ-p to common-p method.

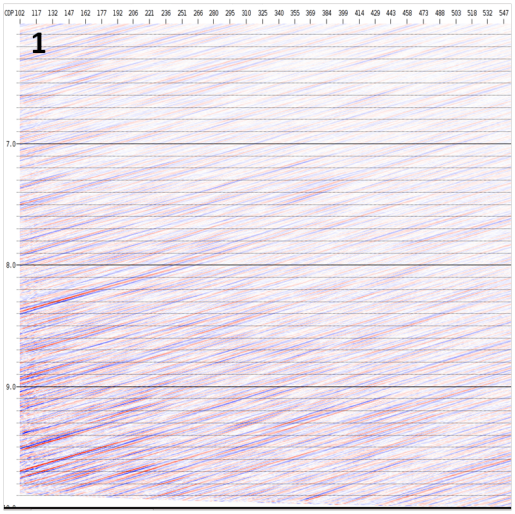

(E) 1: Difference after VF + τ-p to common-p method.

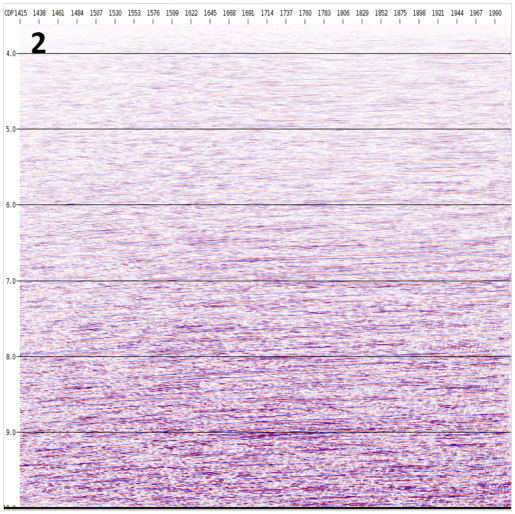

(F) 2: Difference after VF + τ-p to common-p method.

Figure 5.14: Before, after and difference of section 1 (left column) and 2 (right column) indicated in Figure 5.13 when VF followed by τ-p to common-p method is applied to the dataset (Figure continues on next page).

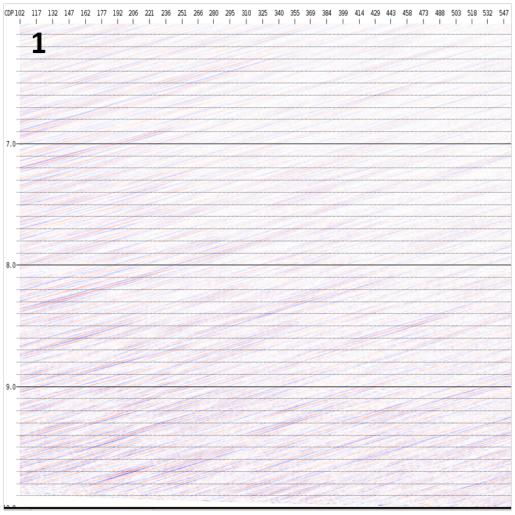

(G) 1: Effect of τ-p to common-p method.

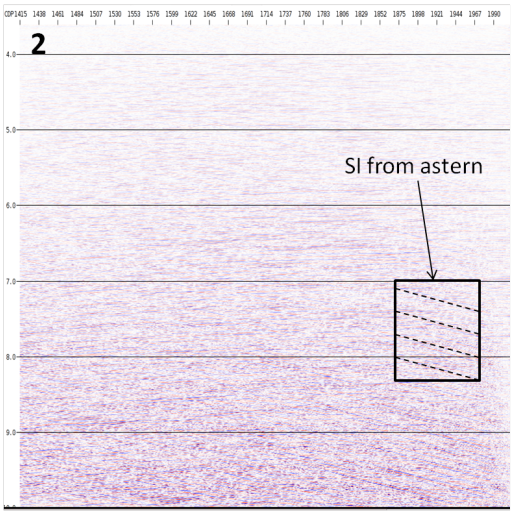

(H) 2: Effect of τ-p to common-p method.

Figure 5.14: (Rest of figure on previous page) Effect of τ-p to common-p method on section 1 (left) and 2 (right) indicated in Figure 5.13.

5.4 VF method with Line Integral Convolution

Finally, VF method is tested in combination with Line Integral Convolution (LIC). LIC requires a long processing time for each shot gather. Only two shot gathers are therefore processed by VF method in combination with LIC. These are shot 7 from first sequence and 909 from third sequence in Table 5.1. Shot 7 contain high amplitude linear SI from abeam, while shot 909 contain high amplitude hyperbolic SI from abeam/aside, and low amplitude linear SI from astern.

Results are presented in Figure 5.15 and 5.16. They show four columns. First column represents before VF method with LIC, and second and third column represent two versions of the after plot. The difference between the second and third column is an applied mute line which serve as an upper limit for LIC in the third column. This mute line is also shown in the difference plot in fourth column. Thereby, the whole difference plot in fourth column belong to the after plot in second column, while everything below the mute line in the difference plot belong to the whole after plot in third column.

Furthermore, does each figure contain three rows. Three different LIC lengths L are tested to see how the results vary, starting with 2 in first row, 10 in second row, and 30 in third row. As mentioned, the LIC length L determines the length of the local streamline, which is $2L+1$.

5.4.1 Comments on results when using VF method with LIC

First, three observations are made on the shot gathers with respect to processing time. These are presented in Table 5.5. It can be seen from the table that the processing time for each shot increases significantly when increasing the LIC length L.

Table 5.5: Processing time of shot 7 and 909 with VF method combined with LIC when varying the LIC length L at 2, 10 and 30.

LIC length L	2	10	30
Processing time	5:45 min	9 min	22:30 min

Second, it is observed that the amount of SI removed increases by increasing the LIC length. The difference plots in Figure 5.15(D) and 5.16(D) show that much data is removed from both shot gathers when using $L = 2$. This is also seen as a clear border illustrating a significant amplitude difference around the applied LIC mute line in the after plot of both shots in Figure 5.15(C) and 5.16(C).

Furthermore, can it be seen from the difference plot for shot 909 in Figure 5.16(D) that the linear SI from astern is removed when using $L = 2$, and kept untouched when increasing L to 10 (H) and 30 (L).

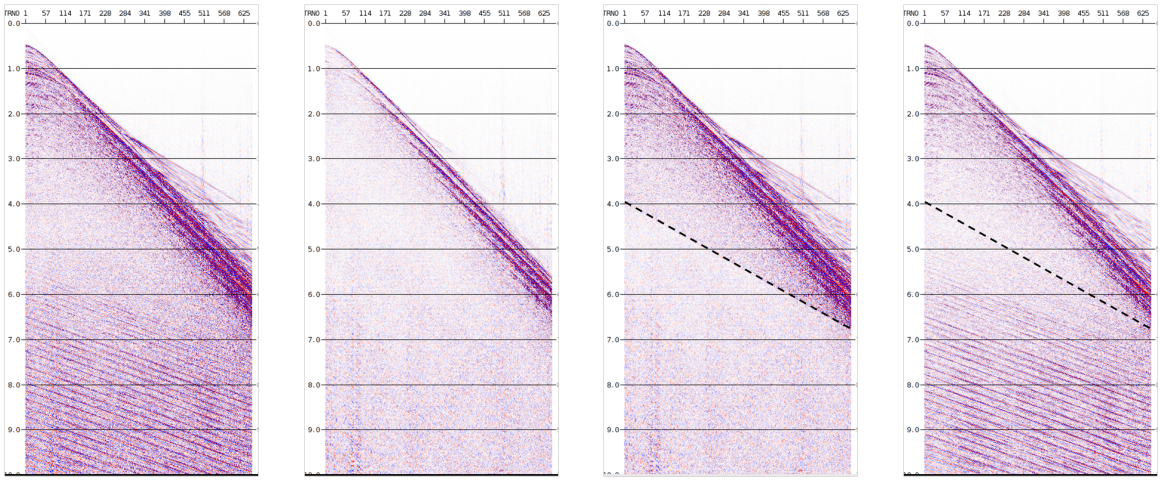

(A) Shot 7, L=2: Before. (B) After. (C) After w\muteline. (D) Difference.

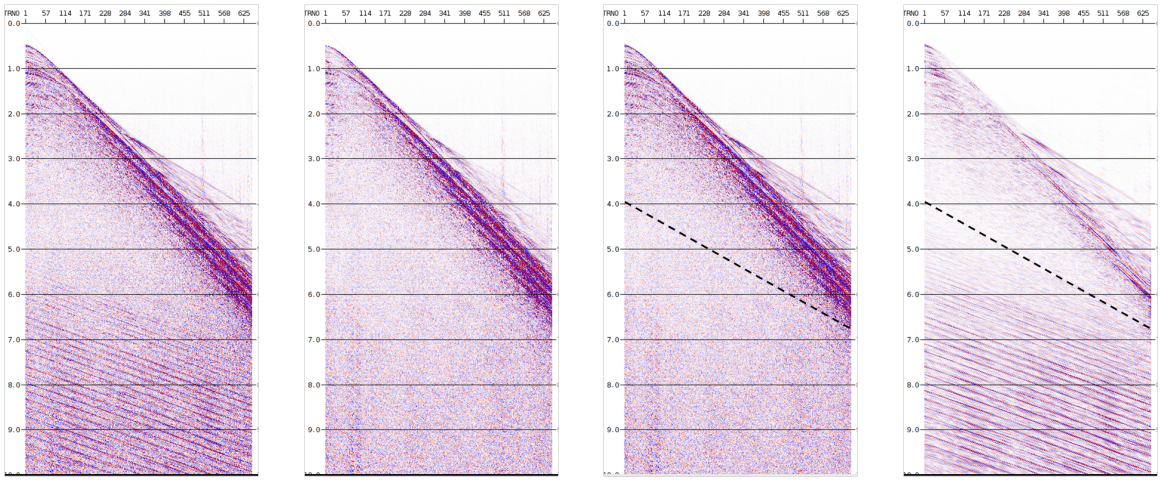

(E) Shot 7, L=10: Before. (F) After. (G) After w\muteline. (H) Difference.

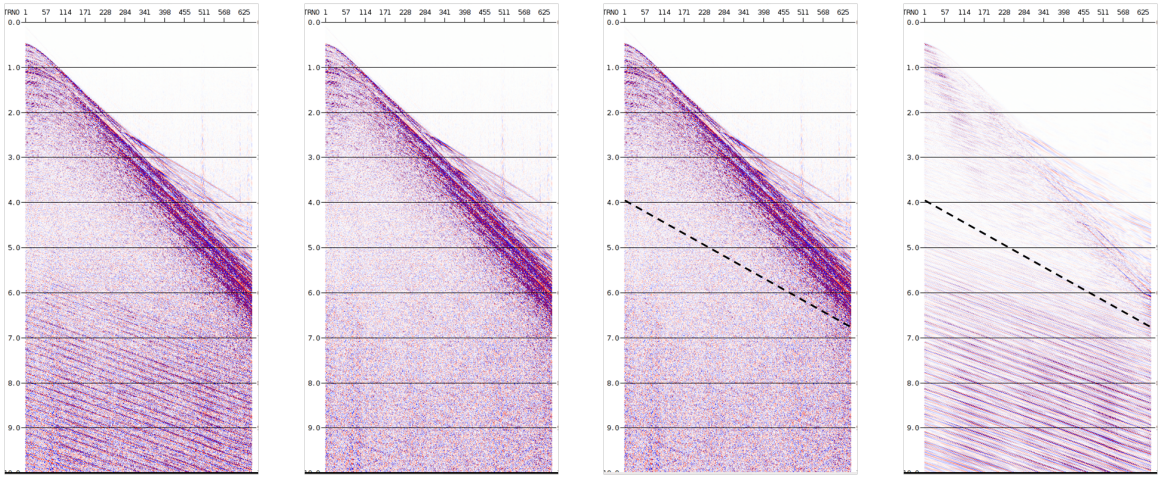

(I) Shot 7, L=30: Before. (J) After. (K) After w\muteline. (L) Difference.

Figure 5.15: Before (first column), after (second column), after with applied mute line (third column) and difference (fourth column) when applying VF with LIC method on shot 7 and varying LIC length L from 2 (first row), 10 (second row) and 30 (third row). The whole difference plot in fourth column belong to the after plot in second column, while everything below the superimposed mute line belong to the after plot in third column.

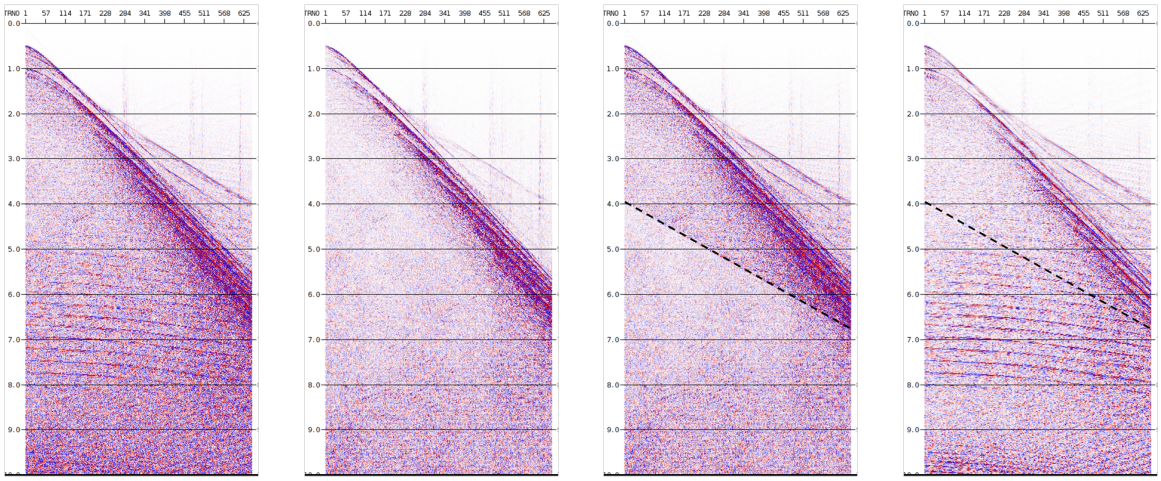

(A) Shot 909, L=2: Before. (B) After. (C) After w\muteline. (D) Difference.

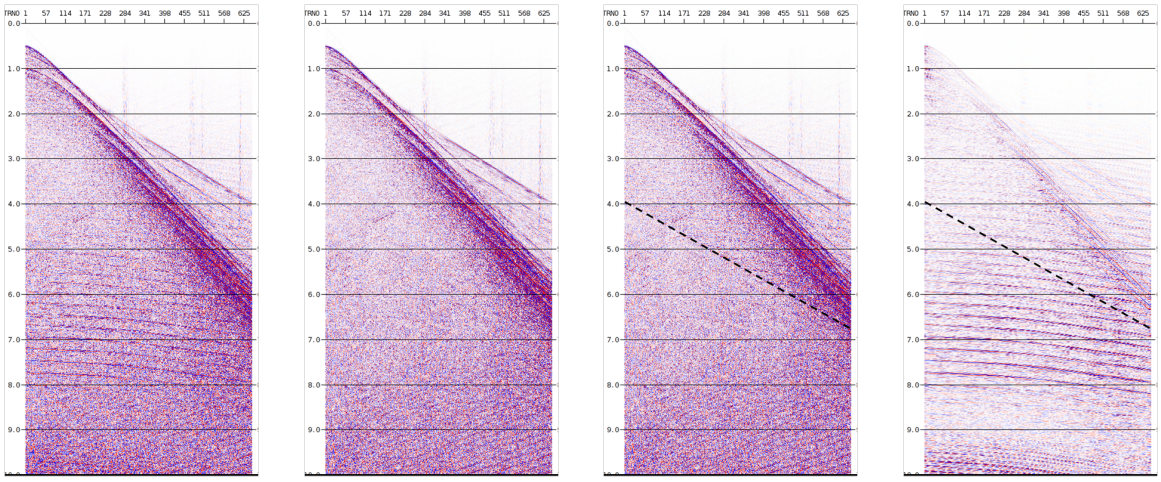

(E) Shot 909, L=10: Before. (F) After. (G) After w\muteline. (H) Difference.

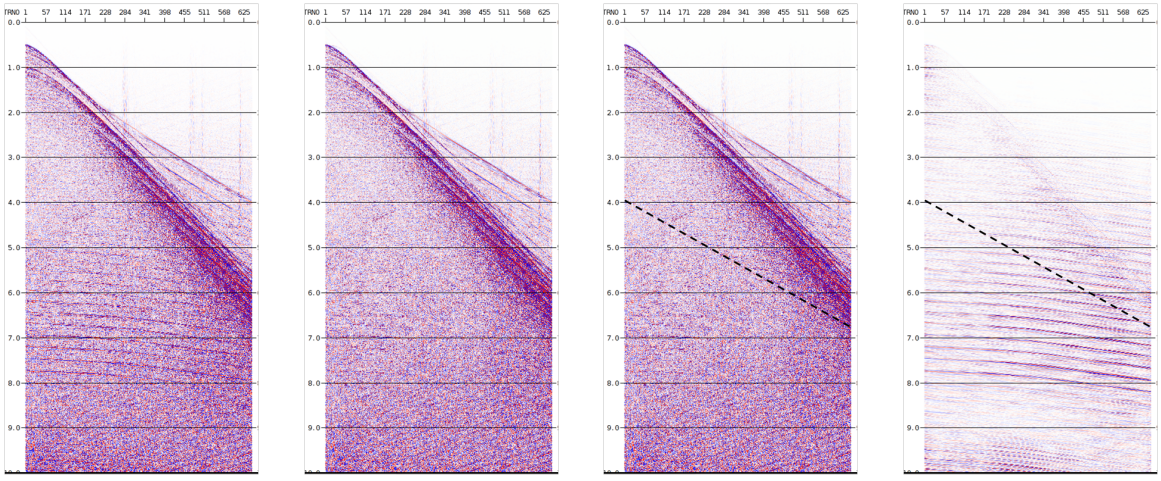

(I) Shot 909, L=30: Before. (J) After. (K) After w\muteline. (L) Difference.

Figure 5.16: Before (first column), after (second column), after with applied mute line (third column) and difference (fourth column) when applying VF with LIC method on shot 909 and varying LIC length L from 2 (first row), 10 (second row) and 30 (third row). The whole difference plot in fourth column belong to the after plot in second column, while everything below the superimposed mute line belong to the after plot in third column.

6. DISCUSSION AND CONCLUSION

This chapter presents a comparison and discussion of the result from the SI removal methods presented in the previous chapter. The goal is to clarify which factors that control the outcome of each method. Such factors might be moveout, arrival time, amplitude and shape of the SI in the shot domain.

Three sections are included in this chapter. The first section contains four subsections. The first subsection presents a discussion and comparison of obtained results on the six shot gathers when using the reference τ-p to common-p method, and the developed VF method with τ-p muting. Then, results by the two methods on the stacks are discussed in second subsection with respect to what was observed on the shot gathers. Third subsection presents a discussion of the results from combining the two methods. Finally, the results on the two shot gathers by VF method with LIC are discussed in fourth subsection.

Second section presents potential improvements for each method. These have mainly been discovered during testing and development. Finally, all the main observations from the thesis work is summarized to form the basis for the final conclusion in third section.

6.1 Discussion of results

Shot gathers

As mentioned, all SI removal methods which are based on randomization of SI through sorting/transforming the data fail if the arrival time is synchronous in consecutive shot gathers. Random noise attenuation tools such as TFDN and f-x PF consider the SI as a coherent signal and preserve it if this is the case.

The first sequence of shot gathers (see Table 5.1) contain SI from abeam. A number of these experience a synchronized arrival time of the SI. This may explain the poor results on shot 7 and 78 in Figure 5.2(B) and (E) after τ-p to common-p method. The number of $HWIN$ amplitudes compared in each window of TFDN have been set to 50. TFDN uses a Lower Quartile estimate (LQT) multiplied with $fac(t)$ as a threshold when identifying SI. As Presterud

(2009) mentioned, this would require 25% SI free amplitude samples in $HWIN$. Generally, this is not the case for the first sequence of shot gathers. Two possible solutions are presented to compensate for this problem:

1. Increase number of amplitude samples ($HWIN$) compared in each time window of TFDN

2. Decrease $fac(t)$

The goal by increasing $HWIN$ is to increase the ratio of SI free amplitude samples. However, this leads to two complications. First, it will increase the processing time significantly. Second, it is not fair to assume that the geology remains linear over large distances. An increase in $HWIN$ means that amplitude samples are compared over a higher number of common-p traces, and thereby a longer distance in space. Assuming a changing geology over this distance, TFDN may actually recognize some real data as random noise and remove it. $HWIN = 50$ amplitude samples was tested and found optimal with respect to both processing time and results. The second solution is to lower the time dependent factor $fac(t)$. This imply a harsher TFDN which remove lower amplitudes. However, it is observed that more reflection data is removed by lowering $fac(t)$. This is therefore not desirable.

Unlike the τ-p to common-p method, VF method is not affected by a synchronized arrival time of the SI. This is because VF method works on singular shot gathers instead of sequences. SI moveout estimation by VF is based on looking at statistical parameters for vectors with common moveout. This means that it depends on a fairly linear moveout of the SI. This is generally the case for all SI in the first sequence of shot gathers. Furthermore, is is observed in shot 7 and 78 that the amplitude of the SI is fairly high and consistent through space. These are both factors that contribute in SI moveout estimation by VF. Results on shot 7 and 78 (see Figure 5.6(B) and (E)) show that all SI have successfully been removed by VF in combination with τ-p muting.

The second sequence of shot gathers contain SI that arrives predominately from abeam/aside. The SI has a curved shape, and the amplitude varies from low at the first shot gathers to fairly high at the last. τ-p to common-p method show poor results on shot 641 in Figure 5.2(H), while significantly improved on 680 in 5.3(B). The amplitude of the SI in shot 641 is low. Furthermore, will the curvature of the SI ensure that the SI does not map to a small area in τ-p domain (few p traces with high amplitude), but rather smear out on more p traces with lower amplitudes. This, in combination with a fairly synchronized arrival time of the SI in the surrounding shot gathers, may be why so bad results are observed at shot 641 by τ-p to common-p method.

VF method does not discover any SI in shot 641 in Figure 5.6(I). Investigation shows that only the maximum of the amplitude plot (see Figure 6.1 (top)) is within the allowed SI moveout

range shown in Table 5.4. Third approach of the SI moveout estimation algorithm presented in Chapter 4.2.2 is therefor used. By further investigating the two remaining plots in Figure 6.1 it is discovered that the number plot (middle) has an accepted value at the moveout from the amplitude plot. However, the STD plot (bottom) shows that the relative standard deviation of the number of vectors with the specific moveout is higher then the supplied threshold $stdTHRS$. This is because of the high curvature of the SI. Shot 641 is therefor presumed noise free by VF method, and no data is removed.

Shot 680 shows a higher SI amplitude. It appears linear in the first 400 traces, while more curved at the last. The high amplitude and relatively linear appearance ensure that both τ-p to common-p and VF method are successful at identifying and removing some SI in Figure 5.3(B) and 5.7(B). However, it is observed from the difference plot in Figure 5.7(C) that VF method has identified the moveout of the linear part of the SI, and generated the τ-p mute accordingly. The curved SI at the far offset traces is therefor not removed by VF. One option could be to increase the allowed moveout range $\Delta\hat{p}$ of the SI. This may include more of the curved SI in the τ-p mute, but also remove more data.

The final two shot gathers from third sequence (see Figure 5.7(D) and (G)) show two types of SI, both from abeam/aside and astern. The SI from astern has low amplitude and is partly masked by the SI from abeam/aside. Both the peak of the amplitude and number of vectors plot in VF are therefore located at the moveout of the SI from abeam/aside. This is why VF method has identified the SI from abeam/aside, and not the SI from astern. The SI from astern appears more linear in both shot gathers then the SI from abeam/aside. This gives a low spread of the SI in the τ-p domain, and is why τ-p to common-p method shows best results on this

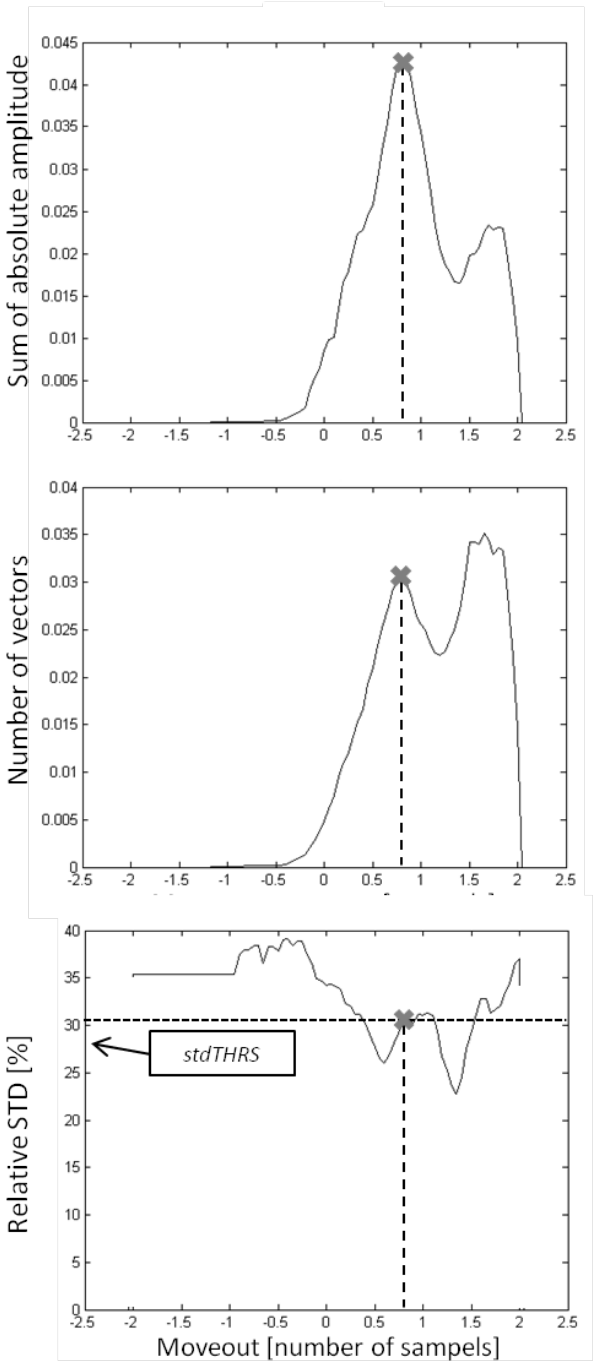

Figure 6.1: Maximum of amplitude plot (top) indicated with a cross. Middle and bottom plot show number and STD plot with crosses at corresponding moveout.

SI. The RMS plot in Figure 5.1 shows that more data has been removed by VF method in combination with τ-p muting, then using τ-p to common-p method. VF method with τ-p muting isolate and remove some of the SI from abeam/aside well compared to the reference τ-p to common-p method.

A general observation is made on the f-k plots after each method of shot 909 in Figure 5.10. It is apparent from the f-k plot that τ-p to common-p method (B) does not remove SI from the shot in the same way as VF method with τ-p muting (C) does. The f-k plots show that VF method with τ-p muting simply removes the given data with a specific moveout, rather then attenuating some high amplitudes like τ-p to common-p method does. The missing data and SI after VF method with τ-p muting is clearly seen in the f-k plot. This missing data may contribute as a possible source of error when the RMS values are calculated at the difference plots after each method.

Stacks

Results on the stacks after τ-p to common-p and VF method with τ-p muting in Figure 5.4(B) and 5.8(B) show some similar features. Both methods have removed much of the linear SI from abeam in first section. This is apparent from the difference plot of section 1 from the stacks in Figure 5.5(E) and 5.9(E), where both show a high spatial consistency of the removed SI from abeam.

The difference plot of the stack shows that VF method with τ-p muting does not affect SI free shot gathers. This is apparent from the CDP's in the middle region of the stack, around CDP 800. These CDP's does not contain traces from shot gathers with SI. By comparing the results of the difference plots in Figure 5.4(C) and 5.8(C) it can be seen that τ-p to common-p method have removed data in this region. This may therefor be an indication that the user defined threshold $fac(t)$ used in TFDN have been set to harshly, allowing TFDN to remove some reflection data from the common-p gathers.

The right part of the stacks contain traces from shot gathers in sequence two and three in Table 5.1. These are first affected by SI from abeam/aside, and finally from abeam/aside and astern. The zoomed parts of section two on the stack in Figure 5.5(F) and 5.9(F) show that τ-p to common-p and VF method with τ-p muting have removed much of the SI from abeam/aside. This SI can be seen as the low dip spatially coherent events indicated in the superimposed squares. However, from the difference plots it seems like VF method with τ-p muting has removed more of this type of SI then τ-p to common-p method. RMS plots in Figure 5.1 of the two shot gathers from this sequence may substantiate this observation, showing higher RMS values for the difference plots after VF with τ-p muting (blue) then the reference τ-p to common-p method (red). However, as observed in the f-k plots in Figure 5.10 for shot 909

after VF method with τ-p muting (C) and τ-p to common-p method (B), it may also be that this amplitude difference is simply related to the missing data after the τ-p mute.

VF method with τ-p muting was unable to detect the low amplitude SI from astern in the last sequence of shot gathers. However, due to the linearity of this SI, the reference τ-p to common-p method was more successful at removing this SI. This is apparent from the difference plot of section two of the stack in Figure 5.5(F), illustrating some of this SI from astern in the superimposed square to the right.

Combining the methods

Combining VF and τ-p muting with τ-p to common-p method show several interesting results. It is observed that VF with τ-p muting and τ-p to common-p method may compliment each other in two ways.

Like previously mentioned, it can be seen that τ-p to common-p method fail to remove SI if the arrival time of the SI is synchronized in the considered consecutive shot gathers. This effect can be minimized by applying VF method with τ-p muting first. This is because VF method remove SI from many of the shot gathers, and thereby make the appearance of the remaining SI more random. Studying shot 641 in Figure 5.11(I) and the RMS plot of the difference plots in Figure 5.1 verify this observation. Originally, neither VF method with τ-p muting or τ-p to common-p method managed to obtain any successful results on this shot gather. VF method did not identify any SI and did therefore not remove any. Furthermore, was the arrival time of the SI too synchronized for τ-p to common-p method. However, from Figure 5.11(L) it can be seen that the amount of SI that has been removed after τ-p to common-p method is significantly improved after VF method with τ-p muting have been applied on the surrounding shot gathers. The RMS plot in Figure 5.1 (green) substantiates this presumption, showing that the amount of data removed has increased by using a combination of the methods, even though no SI was removed by the first VF method with τ-p muting.

Shot 680, 829 and 909 in Figure 5.12(A), (E) and (I) illustrate another way these methods compliment each other. VF method manage to identify and remove some SI from these shots. However, the difference plots in Figure 5.7(C), (F) and (I) show that only parts of the SI have been removed by VF method with τ-p muting from the shot gathers. The SI from astern has not been removed from shot 829 and 909, and the difference plot of shot 680 and 829 show that only parts of the SI from abeam/astern has been removed. The effect of the final τ-p to common-p after VF method with τ-p muting shown in Figure 5.12(D), (H) and (L) on the these shot gathers show that τ-p to common-p method is able to significantly improve the model of the subtracted SI. The residual SI after VF method with τ-p muting from abeam/aside in shot 680 and 829 is sufficiently removed by τ-p to common-p method. Furthermore, is the SI from astern removed from shot 829 and 909 by the final τ-p to common-p method. Also here does the RMS plot in

Figure 5.1 show that more data have been removed when combining the methods. This verify the observation that some residual SI after VF method with τ-p muting can be removed by finally applying the reference τ-p to common-p method.

The difference plot of the stack in Figure 5.13(C) verify what was observed on the shot gathers and RMS plot. More SI has been removed from the stack then using either VF or τ-p to common-p method. The final effect of τ-p to common-p method on section two of the stack in Figure 5.14(H) show that coherent SI from abeam/aside and astern have been removed from the stack.

VF method with LIC

VF method combined with LIC for SI removal was tested on shot 7 and 909. The LIC length L was varied between 2, 10 and 30 to see how the results were affected.

It is apparent from the difference plots in fourth column of Figure 5.15 and 5.16 that more SI is removed compared to reflection data when increasing L. This is considered a reasonable observation if assumed that the vector field $\vec{V}_0^{SI}$ have been sampled with vectors which represent the correct moveout of the SI. If this is the case, the SI should sum up constructively along the streamlines, while other data with different moveout should "stack" out as noise. An increase in L implies an increase in the $2L + 1$ samples long streamline. This should therefore mean a better average estimate of the subtracted center amplitude sample of the streamline.

All difference plots show that some of the high amplitude shallow reflection hyperbolas have been removed. These high amplitudes contaminate the calculated subtracted averages, making LIC subtract higher amplitudes then it should. This effect can be minimized by increasing L further. However, this lead to two problems. First, it would imply a less localized average estimate of the subtracted center sample of the streamline. This may give negative results since the amplitude of the SI is rarely uniform through the shot gathers. Second, it increases the processing time for each shot gather significantly. Testing have shown that optimal results are obtained when using $L = 30$.

A mute line has been introduced in the after plots in third column of both figures. This mute line has been introduced as an attempt to minimize the effect by LIC on the high amplitude shallow reflection signal. The final obtained SI model is therefore muted above this mute line, and subtracted from the original SI contaminated shot gather. However, by doing this it is assumed that the SI is not present at arrival times lower then the applied mute line. From the after and difference plot in Figure 5.16(K) and (L) it can be seen that this is not the case. SI is present above the mute line. However, one may argue that the amplitude of the SI is sufficiently low compared to the shallow reflection data, and thereby allowing the signal processor to neglect this SI.

6.2 Potential improvements

This section presents some potential improvements for the tested SI removal methods. The potential improvements have been discovered during the development and testing of the methods.

τ-p to common-p method

As observed in some of the shot gathers, τ-p to common-p method struggle to remove low amplitude hyperbolic SI. It was observed that this type of curved SI smears out in the τ-p domain, and therefore gives the SI a lower amplitude in the common-p traces. These amplitudes are difficult for TFDN to identify and remove. Applying a hyperbolic or parabolic Radon transform on these shot gathers may reduce the spread in τ-p domain, and therefore improve the output after TFDN. A hyperbolic or parabolic Radon transform is therefore proposed for such SI.

VF method

Two potential improvements are proposed for SI moveout detection by VF method. The first potential improvement concerns implementing the method in CGG Veritas' processing software Uniseis. Until now, development of VF method has taken place MATLAB. MATLAB is good at plotting and testing different parameters. However, the different processing steps in MATLAB are significantly slower compared to equivalent processing steps in Uniseis. Implementing the method in Uniseis would therefore allow more efficient testing of parameters and thresholds with respect to processing time.

The next potential improvement concerns allowing VF method to work in 3-D. Generally, VF method works on a singular shot gather and calculates the moveout of the SI from this. However, it is fair to assume that the SI can be expected to have a spatial coherency through all seismic cables for a given marine seismic vessel at a given recording interval. Testing for SI by VF method and comparing results from each cable can potentially improve the SI detection, and further improve the moveout estimate.

VF method with τ-p muting

f-k and RMS plots showed that VF method with τ-p muting removed more data then the reference τ-p to common-p method. A short discussion was presented on whether this was due to the fact that more data with a given moveout was removed by the τ-p muting, or simply because more SI was removed. Missing data and SI was easily observed in the f-k plot. A possible way of investigating/compensating for this observation is now presented.

First, consider a sequence of shot gathers. Some of the shot gathers contain SI while others are SI free. All shot gathers are processed by VF method with τ-p muting. Missing data/SI can be observed in f-k domain if it is assumed that SI has been removed from some of the shot gathers. The processed sequence of shot gathers are then transformed/sorted to either common offset or common-p domain where reflection data is expected to appear coherent. Missing data from shot gathers after VF method with τ-p muting may then be recovered by interpolating over the unprocessed SI free data. An estimate of removed data versus SI can therefore be obtained.

The next potential improvement concerns processing time when combining VF with τ-p muting, with the reference τ-p to common-p method. Good results were observed when the these methods were combined. This was specially the case on shot gathers where the reference τ-p to common-p method had failed due to a synchronized or semi synchronized arrival time of the SI. In future development, it might be interesting to investigate whether equally good results from combining the methods can be obtained if VF method with τ-p muting is applied on every second or third shot gather. Still, this will contribute on "randomizing" the arrival time of the SI in the consecutive shot gathers while also reducing the processing time significantly.

VF method with LIC

Results from VF method in combination with LIC showed that some high amplitude shallow reflection data was removed. One possibility for avoiding this is to introduce some sort of weighted average instead of simple average when calculating the subtracted center value of the streamline. Amplitudes that deviate more then a certain percentage from the mean of the amplitude samples in the streamline can be damped when calculating the average. This may minimize their effect on the final output. This will however require substantial testing. Furthermore, may high amplitudes such as swell noise complicate the testing further.

Another potential improvement for VF method with LIC concerns an iterative approach for SI removal. The general idea is to create a vector field from velocity data which represents the moveout of the reflection data in the shot domain. LIC may then be applied in an iterative approach to build up models of both the reflection data and the SI by using their respective vector fields. Finally, the SI model may be subtracted from the original shot gather, and SI free data is obtained. This approach may potentially reduce LIC's effect on the shallow reflection hyperbolas as shown in the results.

6.3 Conclusion

Recent years have shown an increase in the marine seismic activity, specially in the Norwegian continental shelf (NCS) region. The possibility for acquiring seismic data in this region strongly depends on the seasonal weather conditions. Due to strong winter storms, seismic data is only acquired during the summer months. A high seismic activity in these months often lead to SI in the seismic data. This lead to an increasing demand for efficient SI removal methods.

Sorting of seismic data to obtain a random appearance of SI and then remove the SI by random noise attenuation methods have proven efficient. Specially, the tested reference τ-p to common-p method. It shows that little user interaction is necessary. However, some problems related to this method exist. First, this method experience problems when the arrival time of the SI is synchronized or semi synchronized in a series of consecutive shot gathers. Second, results from this method show that hyperbolic low amplitude SI is difficult to remove. Third, the method is fairly slow because of the huge amounts of data being transformed/sorted prior to the SI removal.

τ-p muting is a standard way of removing coherent noise from seismic data. The method require only one shot gather, unlike the reference τ-p to common-p method. However, attributes such as moveout and arrival time of the SI have to be identified in order to isolate the SI in τ-p domain. These attributes may change in consecutive shot gathers, making the process of designing accurate τ-p filters a long and tedious job. This often lead to inaccurate generalized mutes designed to work for a set of shot gathers.

Testing and results by the developed VF method show that it is possible to identify attributes such as moveout and arrival time of the SI. These attributes are identified by using a vector field estimate of the local moveout in the considered shot gather. Unlike τ-p to common-p method, only shot gathers where SI is identified are processed further. Thereby, VF method does not touch SI free shot gathers, and may therefore be considered a time saving method. However, results have shown that examples occur when high curvature SI has not been identified in the considered shot gather, and thereby not removed.

An interesting observation was made when applying VF method with τ-p muting to the shot gather, then followed by the reference τ-p to common-p method. The goal was to remove residual SI after VF method with τ-p muting. Results on some shot gathers and RMS plots showed that the methods compliment each other in several ways. It was observed that VF method with τ-p muting may contribute on randomizing the arrival time of the SI in common-p domain, and thereby improve the results of the final τ-p to common-p method. Furthermore, was is observed that residual SI after VF method with τ-p muting, e.g. some hyperbolic parts and also low amplitude SI from other directions, could be removed completely by applying the final reference τ-p to common-p method. A combination of the two mathods is therefore recommended for

future SI removal purposes. Specially, in cases where SI arrive semi synchronous in a series of consecutive shot gathers.

VF method in combination with LIC for SI removal requires a long processing time for each shot gather compared to combining VF method with τ-p muting. Results show that shallow reflection data is removed by LIC because of its high amplitude. Because of the long processing time and relatively poor results on the reflection data, LIC is not considered an efficient way of removing SI compared to both VF method with τ-p muting and the reference τ-p to common-p method. Specially not when the VF method with τ-p muting is combined with the reference τ-p to common-p method.

Bibliography

K. Akbulut, O. K. Saeland, P. Farmer and T. Curtis. *Suppression of seismic interference noise on gulf of mexico data*. *SEG Technical Program Expanded Abstracts*, pp. 527–529, 1984.

J. Brittan, L. Pidsley, D. Cavalin, A. Ryder and G. Turner. *Optimizing the removal of seismic interference noise*. *The Leading Edge*, **27**(2): 166–175, 2008.

B. Cabral and L. C. Leedom. *Imaging vector fields using line integral convolution*. In *Proceedings of the 20th annual conference on Computer graphics and interactive techniques*, pp. 263–270. ACM, 1993.

R. W. Calvert, G. J. H. Schoelcher and H. J. Blankespoor. *Evaluation of a controlled seismic boat interference experiment a final report shell international petroleum maatschappij the hague report ep-60410*, 1984. Unpublished Handout.

L. L. Canales. *Random noise reduction*. *SEG Technical Program Expanded Abstracts*, **3**(1): 525–527, 1984.

J. F. Claerbout. *Earth soundings analysis: Processing versus inversion*, volume 6. Blackwell Scientific Publications Cambridge, Massachusetts, USA, p 94-98, 1992.

T. Elboth and D. Hermansen. *Attenuation of noise in marine seismic data*. *SEG Technical Program Expanded Abstracts*, **28**(1): 3312–3316, 2009.

T. Elboth, H. H. Qaisrani and T. Hertweck. *De-noising seismic data in the time-frequency domain*. *SEG Technical Program Expanded Abstracts*, **27**(1): 2622–2626, 2008.

S. Fomel. *Applications of plane-wave destruction filters*. *Geophysics*, **67**(6): 1946–1960, 2002.

L. J. Gelius and T. A. Johansen. *Petroleum Geophysics*. UniGEO AS, Bergen, 2010.

N. Gulunay. *Two different algorithms for seismic interference noise attenuation*. *The Leading Edge*, **27**(2): 176–181, 2008.

N. Gulunay and D. Pattberg. *Seismic crew interference and prestack random noise attenuation on 3-d marine seismic data*. In *63rd Conference of Eur. Assn. Geosci. Eng*. 2001a.

N. Gulunay and D. Pattberg. *Seismic interference noise removal*. *SEG Technical Program Expanded Abstracts*, **20**(1): 1989–1992, 2001b.

N. Gulunay, M. Magesan and S. Baldock. *Seismic interference noise attenuation*. *SEG Technical Program Expanded Abstracts*, **23**(1): 1973–1976, 2004.

W. Huaien, L. Guangxin, C. E. Hinz and F. F. C. Snyder. *Attenuation of marine coherent noise*. *SEG Technical Program Expanded Abstracts*, **8**(1): 1112–1114, 1989.

R. L. Kirlin and W. J. Done. *Suppression of coherent noise in seismic data*. March 20 1990. US Patent 4,910,716.

K. Larner, R. Chambers, M. Yang, W. Lynn and W. Wai. *Coherent noise in marine seismic data*. *Geophysics*, **48**(7): 854–886, 1983.

J. Lie. *Seismic interference, filtering methods and revised noise limits*. In *Oceanology'88 Proceedings of an international conference*. 1988.

S. Maroof and C. Gravely. *Aliasing and tau-p: Presented at the 54th ann. Internat. Mtg., Sot. Explor. Geo hys., Atlanta*, 1984.

MATLAB. *Version 7.10.0 (R2010a)*. The MathWorks Inc., Natick, Massachusetts, 2010.

I. V. Presterud. *Time frequency de-noising of seismic data*. Master thesis in geophysics, University of Oslo, Department of Geosciences, 2009.

J. Radon. *On the determination of functions from their integral values along certain manifolds*. *Medical Imaging, IEEE Transactions on*, **5**(4): 170–176, 1986.

Schlumberger. *Oilfield glosarry*. http://www.glossary.oilfield.slb.com/en/Terms.aspx?LookIn=termMarch 2013.

A. A. Vassiliou and P. Garossino. *Time-frequency processing and analysis of seismic data using very short-time fourier transforms*. December 15 1998. US Patent 5,850,622.

M. C. Yu. *Seismic interference noise elimination*. February 22 2011. US Patent App. 13/031,970.

A. Appendix: SI moveout detection flowcharts

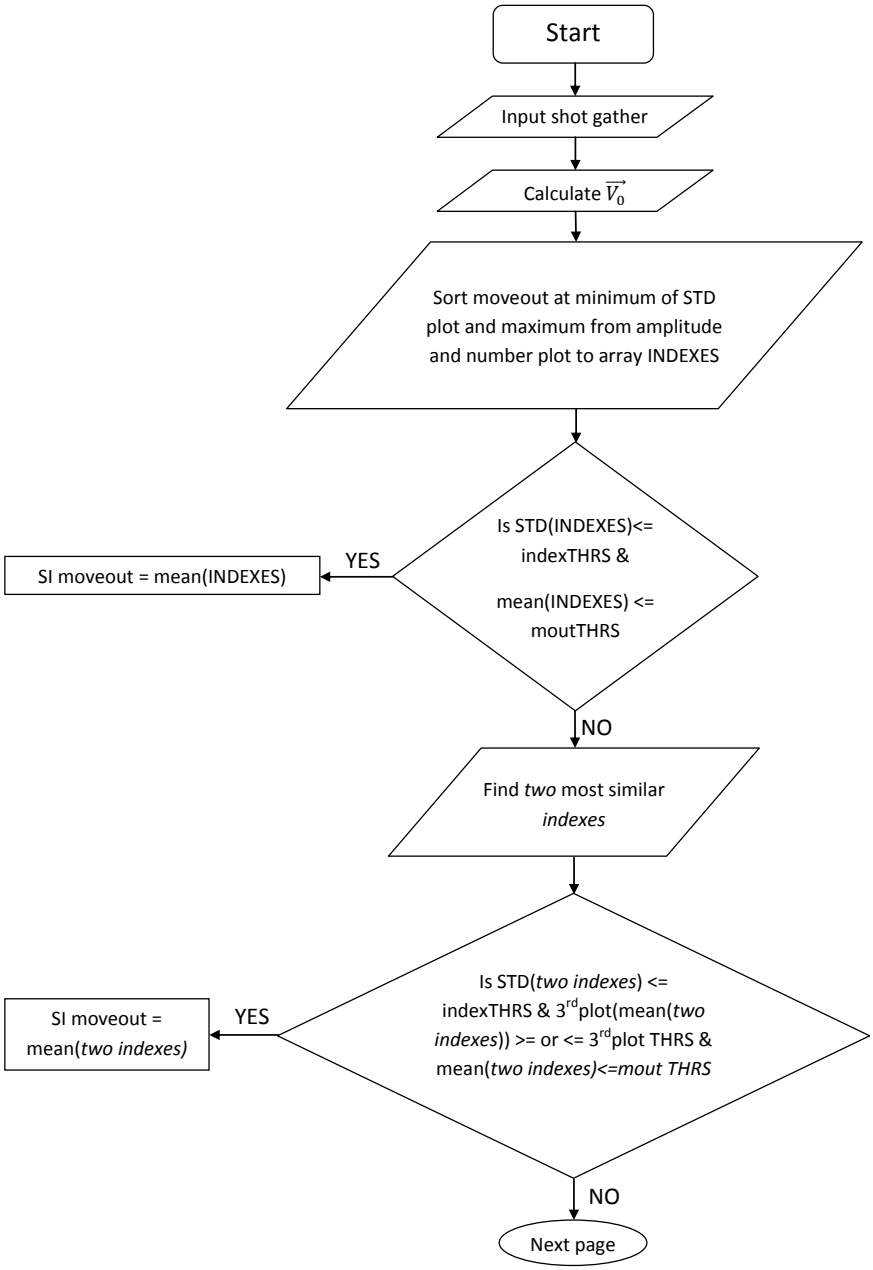

Figure A.1: Flowchart illustrating first two approaches of automatic SI moveout detection

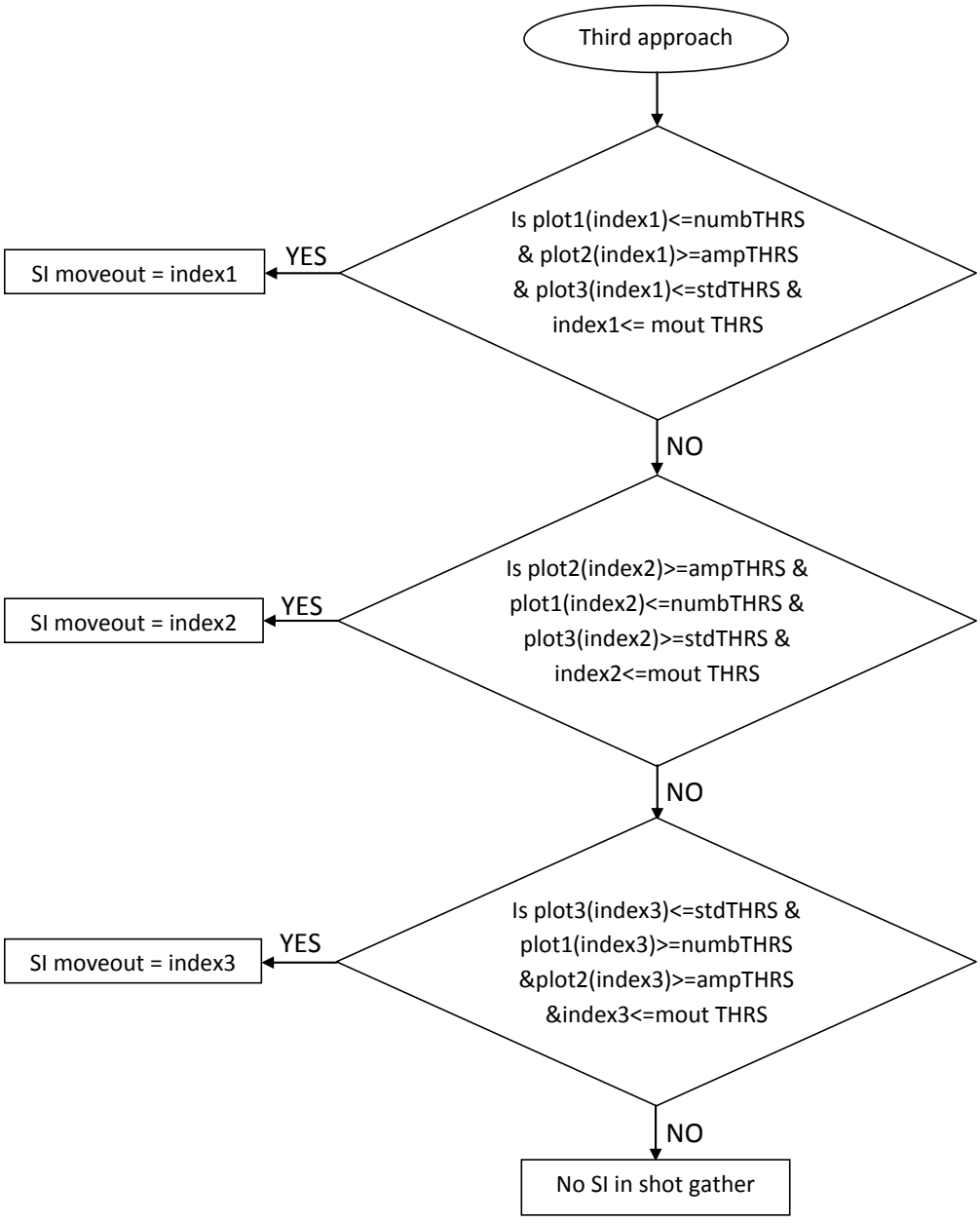

Figure A.2: Flowchart illustrating last approach of automatic SI moveout detection